

**Development of a Microstructured Reactor
for Heterogeneously Catalyzed Gas Phase Reactions
and its Application in the Oxidative Dehydrogenation of Propane**

vorgelegt von
Diplom-Ingenieur
Oliver Schwarz
aus Pinneberg

Von der Fakultät II - Mathematik und Naturwissenschaften
der Technischen Universität Berlin
zur Erlangung des akademischen Grades
Doktor der Ingenieurwissenschaften
Dr.-Ing.

genehmigte Dissertation

Promotionsausschuss:

Vorsitzender: Prof. Dr. rer. nat. Andreas Grohmann

Berichter: Prof. Dr. rer. nat. Reinhard Schomäcker

Berichter: PD Dr. Evgenii V. Kondratenko (Leibniz-Institut für Katalyse e.V.)

Berichter: Prof. Dr.-Ing. Thomas Turek (Technische Universität Clausthal)

Tag der wissenschaftlichen Aussprache: 10.12.2008

Berlin 2008

D 83

Acknowledgements

At this point I am glad to take the opportunity to express my gratitude to everyone who contributed directly or indirectly to the successful completion of this work. Foremost, I wish to thank my supervisor Prof. Dr. R. Schomäcker for letting me work in his lab and supporting me in many ways during the last three years. I would also like to thank PD Dr. E.V. Kondratenko for the excellent scientific co-operation, fruitful discussions, and for acting as a referee on my thesis. Special thanks to Prof. Dr. Th. Turek of TU Clausthal for providing the external report and Prof. Dr. A. Grohmann for his role as chairman of the examination board.

This work would not have been possible without the help of Atotech Deutschland GmbH. I would like to express my gratitude to Dr. G. Schäfer for the professional and trustful collaboration. I also wish to thank Dr. W. Richtering and Dr. R. Herber for coordinating the research project between Atotech and TU Berlin. Moreover, I wish to thank M. Hardenberg, H. Hübner, and P.-Q. Duong for their experimental work.

I am also grateful to the workgroup of Prof. Schomäcker for their help and support, interesting discussions, and for providing a pleasant working atmosphere. In particular, I would like to mention my colleagues Arne Dinse, Dr. Benjamin Frank, Juan Milano, Jonas Dimroth, Dr. Hary Soerijanto, Dr. Devender Singh Negi, Torsten Otremba, and Sonja Jost. Many thanks to Gabi Vetter, Christa Löhr, and Prof. em. Dr. P. Hugo, too, for helping wherever they could.

Without the qualified support of the technical staff at the Institute of Chemistry, it would not have been possible to complete the installation of a new experimental set-up in the high quality achieved. I would like to express my respect for their excellent craftsmanship: Rolf Kunert, Michael Knuth, Detlef Klabunde, Axel Schiele, Detlef Grimm, and Ralf Reichert.

Scientific co-operations greatly improved the present study. Special thanks to Dr. D. Habel, Dr. O. Görke, Dr. O. Ovsitser, and Prof. Dr. Ch. Hess for experimental help and fruitful discussions.

In addition, I am grateful to the State of Berlin for funding my PhD thesis by providing a NaFöG scholarship. I also wish to thank Sabine Hörske for administrating all aspects of the scholarship.

Most importantly, I am obliged to thank my caring parents Erika and Peter for their constant loving and invaluable support during the last three years and all my life before. The same is true for my girl-friend Sibylle, who was always there for me and supported me in all difficult situations. Without their help, I would not have been able to achieve anything close to the point where I stand today. Last but not least, I wish to thank all family and friends for their support and encouragement, contributing in many ways to make this part of my life a memorable experience.

Abstract

The potential of micro reaction technology and chemical micro processing for substantially improving the efficiency of chemical process development and production processes has long been promoted in the literature. Apart from the commonly cited advantages of this innovative technology, such as increased mass and heat transfer properties, there are two major drawbacks to microstructured reactors: The relatively high costs for their fabrication and the absence of a coherent concept to significantly increase their limited through-put.

Therefore, the main objective of the present study was the development of a scalable, flexible, low-cost manufacturing concept for microstructured reactors applicable for a wide range of heterogeneously catalyzed gas phase reactions. In particular, the development of a reliable bonding-method for fabricating the reactor modules and the optimization of techniques for depositing stable and selective catalyst coatings on the micro channel surfaces were investigated. As a sensitive test reaction, the oxidative dehydrogenation of propane (ODP) to propene was chosen to evaluate the performance of the microstructured reactors for fast and strongly exothermic heterogeneously catalyzed gas phase reactions.

Two sets of $\text{VO}_x/\gamma\text{-Al}_2\text{O}_3$ catalyst were prepared from wet saturation impregnation and ball-milling in order to elucidate the influence of the preparation method on physico-chemical and catalytic properties of the obtained materials. In addition, a specific catalyst preparation method was developed for generating catalytic materials that are suitable for coating microstructures. These catalysts were deposited as thin layers on the channel surfaces of the microstructured reactors by spray-coating, using chemical binders (organic and inorganic) in order to stabilize the ceramic catalyst material on the metallic substrate. Due to the various preparation methods, binder systems, and channel geometries that were examined, a highly flexible toolbox for manufacturing low-cost microstructured reactors has been developed.

The obtained modules were characterized with respect to stability, hydrodynamic, thermal, and catalytic behavior. Both, reactors and catalytic coatings turned out to be sufficiently stable under all applied reaction conditions. It was shown that microstructured reactors exhibit only minor backmixing, resulting in relatively narrow residence time distributions. Furthermore, it could be experimentally and theoretically verified that isothermal reaction conditions can be achieved over a wide range of temperatures and propane conversion degrees. It was also shown that the full kinetic potential of the applied catalysts can be exploited, due to the ability of microstructured reactors to prevent mass transfer limitations. Furthermore, it was revealed that a distributed oxygen feed in the ODP is not beneficial for increasing propene selectivity, since oxygen reaction orders appear to be very similar for propane dehydrogenation and propene deep oxidation.

Zusammenfassung

Das Potential der Mikroreaktions- und Mikroverfahrenstechnik zur Steigerung der Effizienz chemischer Entwicklungs- und Produktionsprozesse wurde lange in der Literatur diskutiert. Abgesehen von den Vorteilen dieser innovativen Technologie (wie verbesserter Stoff- und Wärmetransport), existieren zwei bedeutende Nachteile von mikrostrukturierten Reaktoren: Die relativ hohen Kosten für ihre Herstellung und das Fehlen eines kohärenten Konzepts, um deren begrenzten Durchsätze signifikant zu steigern.

Ziel der vorliegenden Arbeit war es, ein skalierbares, flexibles und preisgünstiges Herstellungskonzept für Mikrostrukturreaktoren zu entwickeln, die für einen weiten Bereich heterogen katalysierter Gasphasenreaktionen einsetzbar sind. Insbesondere wurden ein verlässliches Fügeverfahren zur Herstellung der Reaktormodule und die Optimierung der Aufbringung stabiler Katalysatorbeschichtungen auf die Mikrokanäle untersucht. Als Testreaktion wurde die oxidative Dehydrierung von Propan (ODP) gewählt, um die Einsatzfähigkeit mikrostrukturierter Reaktoren für schnelle und stark exotherme heterogen katalysierte Gasphasenreaktionen zu bewerten.

Es wurden zwei Reihen von $\text{VO}_x/\gamma\text{-Al}_2\text{O}_3$ Katalysatoren durch nasschemische Präparation und unter Verwendung einer Kugelmühle hergestellt, um den Einfluss der Präparationsmethode auf die physiko-chemischen und katalytischen Eigenschaften der erhaltenen Materialien aufzuklären. Zusätzlich wurde eine spezifische Präparationsmethode zur Herstellung von Katalysatoren entwickelt, die zur Beschichtung von Mikrostrukturen geeignet sind. Diese Materialien wurden als dünne Schichten auf die Kanäle der Reaktoren mit Hilfe der Sprühtechnik aufgetragen und die Haftung des keramischen Katalysatormaterials auf den metallischen Substraten durch chemische Binder sichergestellt. Auf Basis der verschiedenen Präparationsmethoden, Bindersysteme und Kanalgeometrien die untersucht wurden, konnte ein flexibles Konzept für die Herstellung von Mikrostrukturreaktoren entwickelt werden.

Die erhaltenen Module wurden in Hinblick auf Stabilität, hydrodynamisches, thermisches und katalytisches Verhalten charakterisiert. Die Reaktoren und katalytischen Beschichtungen stellten sich unter allen Reaktionsbedingungen als ausreichend stabil heraus. Es wurde gezeigt, dass mikrostrukturierte Reaktoren nur zu geringer Rückvermischung neigen, was sich in relativ engen Verweilzeitverteilungen zeigt. Weiterhin konnte experimentell und theoretisch verifiziert werden, dass isotherme Reaktionsbedingungen über einen weiten Bereich von Temperaturen und Propansätzen erreichbar sind. Ebenso wurde gezeigt, dass unter Einsatz von Mikrostrukturreaktoren das volle kinetische Potential der eingesetzten Katalysatoren ausgeschöpft werden kann. Weiterhin zeigte sich, dass eine verteilte Sauerstoffzufuhr die Propenselektivität nicht positiv beeinflusst, da die Reaktionsordnungen des Sauerstoffs bezüglich der Propanpartial- und der Propentotaloxidation sehr ähnlich sind.

Table of Contents

Abstract.....	i
Zusammenfassung.....	ii
Table of Contents	iii
List of Figures.....	v
List of Tables	viii
Symbols and Abbreviations	ix
1 Introduction and Objectives.....	1
2 Fundamentals and State of the Art	3
2.1 Micro Reaction Technology.....	3
2.1.1 Definitions and Components	3
2.1.2 Advantages and Disadvantages.....	6
2.1.2.1 Engineering Aspects	6
2.1.2.2 Organizational Aspects	10
2.1.3 Fabrication Methods	11
2.1.3.1 Micro Structuring Techniques.....	11
2.1.3.2 Assembly Techniques.....	13
2.1.3.3 Internal Surface Functionalization	13
2.1.4 Micro Systems for Chemical Production Processes	14
2.2 Oxidative Dehydrogenation of Propane.....	16
3 Experimental Methods.....	19
3.1 Catalyst Preparation	19
3.2 Catalyst Characterization	20
3.3 Catalytic Performance Tests	22
3.3.1 Gas Dosage and Supply	23
3.3.2 Chemical Reactors.....	25
3.3.2.1 Microstructured Reactor	25
3.3.2.2 Tubular Fixed Bed Reactor	27
3.3.3 Process Control System.....	28
3.3.3.1 Hardware	28
3.3.3.2 Software	29
3.3.4 Gaschromatography	32

4	VO_x/γ-Al₂O₃ Catalysts in the Oxidative Dehydrogenation of Propane	33
4.1	Influence of Preparation Method on Catalytic Behavior	33
4.1.1	Catalyst Preparation and Characterization	33
4.1.2	Nature of VO _x Species	35
4.1.3	Role of VO _x Species in Catalysis	40
4.2	Tailor-made Catalysts for Microstructured Reactors	44
4.2.1	Catalyst Preparation and Characterization	44
4.2.2	Functional Catalyst Characterization	46
5	Reactor Manufacturing and Catalytic Coatings	49
5.1	Fabrication of Reactor Modules	49
5.2	Preparation of Coatings	52
5.3	Catalytic Performance Tests	53
5.3.1	Activity of Reactor Material	54
5.3.2	Coatings from VO _x /γ-Al ₂ O ₃ Particles	55
5.3.3	Coatings from γ-Al ₂ O ₃ Particles plus Impregnation	59
5.3.4	Coatings from Vanadium Precursor and γ-Al ₂ O ₃ Particles	61
5.3.5	Influence of Reactor Design	63
5.3.6	Catalytic Long-term Performance	65
6	Reactor Characterization and Kinetic Investigations	66
6.1	Reactor Designs	66
6.2	Residence Time Distributions	67
6.3	Comparison of Kinetic Model and Experimental Results	70
7	Conclusions and Outlook	78
8	Literature	82
Appendix A: Flow chart		89
Appendix B: List of Publications		90
Appendix C: Curriculum Vitae		92

List of Figures

Figure 2-1: Characteristic length scales in chemical engineering (depicted from [5]).....	3
Figure 2-2: Dependency between radius and surface-to-volume ratio of a tubular reactor. .	4
Figure 3-1: Flow chart of experimental set-up for performing catalytic measurements.	22
Figure 3-2: Photograph of experimental set-up for catalytic measurements.	23
Figure 3-3: Photographs of (a) mass flow controller equipped with a pre-filter unit, (b) flow rotameter for nitrogen flush of hotbox, and (c) static gas mixer.	24
Figure 3-4: Photographs of (a) microstructured reactor, (b) equipped with thermocouples, (c) with tubing, and (d) cooling coil at reactor outlet.	25
Figure 3-5: Photographs of (a) open hotbox, (b) holder for positing microstructured reactors, and (c) microstructured reactor equipped with heating blocks.	26
Figure 3-6: Photographs of (a) separated parts of tubular reactor, (b) magnification of catalyst bed between two layers of quartz, (c) reactor with tubing situated in insulation, and (d) scale for determining the position of the thermocouple.....	27
Figure 3-7: Schematic overview of electrical signals of experimental set-up.	28
Figure 3-8: Screenshot of process flow for operating the experimental set-up.	30
Figure 3-9: Magnified screenshots of (a) temperature control and (b) temperature trend window for microstructured reactor.	31
Figure 3-10: Photograph of (a) oven unit with separation columns and (b) screenshot of gas chromatography analysis software.	32
Figure 4-1: SEM images of (a) V-I-1.5 and (b) V-I-8.8, scale bar 1 μm and 200 nm.	35
Figure 4-2: Raman spectra recorded at 514 nm laser excitation at room temperature after dehydration of (a) impregnated and (b) ball-milled catalysts.	36
Figure 4-3: UV-vis spectra of V-II-1.5 before and after calcination at 500 $^{\circ}\text{C}$ in a 20/80 O_2/Ne flow (40 $\text{ml}_\text{n} \text{ min}^{-1}$).	37
Figure 4-4: Tauc's plots of (a) impregnated and (b) ball-milled catalysts oxidized in a 20/80 O_2/Ne flow at 500 $^{\circ}\text{C}$	38
Figure 4-5: E_g values of all investigated materials as a function of VO_x surface density.	38
Figure 4-6: TPR profiles of (a) impregnated and (b) ball-milled catalysts in a 5/95 H_2/Ar flow (25 $\text{ml}_\text{n} \text{ min}^{-1}$, catalyst masses 35 to 180 mg, heating rate 10 $^{\circ}\text{C min}^{-1}$).	39
Figure 4-7: Activity for (a) propane conversion and (b) selectivity towards propene of catalysts from wet saturation impregnation (■, ◆) and ball-milling (□, ◇).	41
Figure 4-8: Reaction rate (a) and propene selectivity at 5 % propane conversion (b) as a function of E_g for catalysts derived from wet saturation impregnation (■) and ball-milling (□).	42

Figure 4-9: Schematic illustration of electron transfer from O^{2-} to V^{5+} upon breaking the C-H bond in C_3H_8 adsorbed over VO_x and under photon irradiation.	43
Figure 4-10: (a) BET surface area at 77 K, (b) UV-vis spectra in O_2 flow at 773 K, (c) XRD patterns measured at room temperature, and (d) Raman spectra (recorded at room temperature after dehydration) of investigated $VO_x/\gamma-Al_2O_3$ catalyst samples with varying vanadium content; (a) and (c) also contain data of pure $\gamma-Al_2O_3$, (c) and (d) also of crystalline V_2O_5	45
Figure 4-11: Catalytic activity for (a) varying modified residence times at 723 K, (b) increasing vanadium content (volume flow $120\text{ ml}_n\text{ min}^{-1}$), and selectivity conversion trajectories for (c) differently loaded catalysts at 723 K, and (d) different temperatures for a 5.3 wt.-% V catalyst, all measured at a constant molar ratio of $C_3H_8/O_2/N_2 = 2/1/4$	47
Figure 5-1: Simplified manufacturing concept for microstructured reactors.	49
Figure 5-2: Schematic drawing of microstructured reactor (a) and photographs of the single channel platelet (b), the thermocouple platelet (c), and the top and bottom platelets (d,e).	50
Figure 5-3: SEM micrographs of a solder joint with corresponding EDX line scan.	51
Figure 5-4: Activity of reactor material for (a) C_3H_x conversion and (b) O_2 conversion (single channel design, $C_3H_x/O_2/N_2 = 2/1/4$, flow rate $60\text{ ml}_n\text{ min}^{-1}$).	54
Figure 5-5: SEM images of a coating made from $\gamma-Al_2O_3$ particles containing Al-tri-sec-butylate as binder material, scale bar (a) $200\text{ }\mu\text{m}$ and (b) $20\text{ }\mu\text{m}$	56
Figure 5-6: SEM images of a coating made from $\gamma-Al_2O_3$ particles containing polyvinyl pyrrolidone as binder material, scale bar (a) $200\text{ }\mu\text{m}$ and (b) $20\text{ }\mu\text{m}$	56
Figure 5-7: Activity (a) and selectivity (b) of coating formulations - \square reference 4.6 wt.-% V, \bullet Al-tri-sec-butylate, \blacktriangle tetraethoxysilane, \blacklozenge hydroxypropyl cellulose, \blacklozenge polyvinyl pyrrolidone ($450\text{ }^\circ\text{C}$, $C_3H_8/O_2/N_2 = 2/1/4$, flow rate $30\text{ to }240\text{ ml}_n\text{ min}^{-1}$, catalyst mass 20 mg).	57
Figure 5-8: Activity (a) and selectivity (b) of catalytic coatings - \square reference 4.6 wt.-% V, \bullet Al-tri-sec-butylate, \blacktriangle tetraethoxysilane, \blacklozenge hydroxypropyl cellulose, \blacklozenge polyvinyl pyrrolidone ($450\text{ }^\circ\text{C}$, $C_3H_8/O_2/N_2 = 2/1/4$, flow rate $30\text{ to }240\text{ ml}_n\text{ min}^{-1}$, catalyst mass $48\text{ to }82\text{ mg}$).	58
Figure 5-9: Comparison of activity (a) and selectivity (b) of impregnated coating (\bullet) and reference (\square) ($450\text{ }^\circ\text{C}$, $C_3H_8/O_2/N_2 = 2/1/4$, flow rate $30\text{ to }240\text{ ml}_n\text{ min}^{-1}$).	60
Figure 5-10: SEM images of coatings made from $\gamma-Al_2O_3$ particles containing (a) Al-tri-sec-butylate and (b) polyvinyl pyrrolidone as binder materials, scale bar $200\text{ }\mu\text{m}$	62

Figure 5-11: Comparison of activity (a) and selectivity (b) of coatings made from $\text{VO}_x/\gamma\text{-Al}_2\text{O}_3$ particles (■, □) and $\text{VO}(\text{acac})_2/\gamma\text{-alumina}$ particles (●, ○), closed symbols Al-tri-sec-butylate, open symbols polyvinyl pyrrolidone as binder material (450 °C, $\text{C}_3\text{H}_8/\text{O}_2/\text{N}_2 = 2/1/4$, flow rate 30 to 240 $\text{ml}_n \text{ min}^{-1}$).	63
Figure 5-12: Comparison of “face-to-back” (■) and “face-to-face” (○) assembly mode (single channel design, tetraethoxysilane as binder material, $\text{C}_3\text{H}_8/\text{O}_2/\text{N}_2 = 2/1/4$, flow rate 60 $\text{ml}_n \text{ min}^{-1}$, catalyst mass 50 mg).	63
Figure 5-13: Comparison of single (■) and multi (○) channel design (hydroxypropyl cellulose as binder material, 450 °C, $\text{C}_3\text{H}_8/\text{O}_2/\text{N}_2 = 2/1/4$, flow rate 30 to 240 $\text{ml}_n \text{ min}^{-1}$, catalyst mass 100 mg).	64
Figure 5-14: Long-term performance over 150 h (single channel design, hydroxypropyl cellulose as binder material, 500 °C, $\text{C}_3\text{H}_8/\text{O}_2/\text{N}_2 = 2/1/4$, flow rate 100 $\text{ml}_n \text{ min}^{-1}$, catalyst mass 68 mg).	65
Figure 6-1: Schematic drawing of alternative reactor design for distributing O_2 over the catalyst bed (a) and photographs of both multi channel platelets (b,c).	66
Figure 6-2: Response functions of mass spectrometer (◇), single channel designs (■ face-to-back, ● face-to-face) and multi channel design (▲) to O_2/N_2 step injection experiments (flow rate 60 $\text{ml}_n \text{ min}^{-1}$).	68
Figure 6-3: Fit of adjusted model (dashed lines) to experimental data (■ response function of microstructured reactor including mass spectrometer, ◇ response function of mass spectrometer individually) in order to estimate $\tau_{\text{MR},2}$ and Bo_2 for microstructured reactor (solid line, flow rate 60 $\text{ml}_n \text{ min}^{-1}$).	69
Figure 6-4: Comparison of predicted model data with experimental data for (a) propane conversion and (b) propene selectivity ($\text{C}_3\text{H}_8/\text{O}_2/\text{N}_2 = 2/1/4$, flow rate 30 to 240 $\text{ml}_n \text{ min}^{-1}$).	72
Figure 6-5: Simulated temperature gradient and conversion degrees of propane and oxygen along the catalytic bed in a microstructured reactor ($\text{C}_3\text{H}_8/\text{O}_2/\text{N}_2 = 2/1/4$, flow rate 30 to 240 $\text{ml}_n \text{ min}^{-1}$).	73
Figure 6-6: Comparison of predicted model data with experimental data for co-feed mode of reactants and distributed oxygen feed (450 °C, $\text{C}_3\text{H}_8/\text{O}_2/\text{N}_2 = 2/1/4$, total flow rate 30 to 240 $\text{ml}_n \text{ min}^{-1}$).	75
Figure 6-7: Theoretical propane conversion (a) and propene selectivity (b) for adjusted oxygen reaction orders compared to experimental data (450 °C, $\text{C}_3\text{H}_8/\text{O}_2/\text{N}_2 = 2/1/4$, flow rate 30 to 240 $\text{ml}_n \text{ min}^{-1}$).	76

List of Tables

Table 4-1:	Summary of samples used for characterization and catalytic testing.....	34
Table 5-1:	Formulations for preparing coatings from $\text{VO}_x/\gamma\text{-Al}_2\text{O}_3$ particles.....	55
Table 5-2:	Formulations for preparing coatings from $\text{VO}(\text{acac})_2$ and $\gamma\text{-Al}_2\text{O}_3$ particles.....	61
Table 6-1:	Residence times (τ_{hyd} , τ_{MR}) and Bodenstein numbers (Bo) of reactor designs determined from parameter estimation. Index 1 corresponds to adapted model with PFTR, index 2 to adapted model with PFTR/ CSTRs.....	70
Table 6-2:	Kinetic parameters applied for modeling isothermal microstructured reactor....	71

Symbols and Abbreviations

Latin Characters

a	m^{-1}	Specific surface area
c_i	mol l^{-1}	Concentration of component i
c_0	mol l^{-1}	Initial concentration
c_p	$\text{J kg}^{-1} \text{K}^{-1}$	Specific heat capacity
d	m	Diameter
d_h	m	Hydraulic diameter
h	J s	Planck constant (6.626×10^{-34})
k	$\text{s}^{-1} (\text{m}^3 \text{mol}^{-1})^{m-1}$	Rate constant (with reaction order m)
k_∞	$\text{s}^{-1} (\text{m}^3 \text{mol}^{-1})^{m-1}$	Pre-exponential factor (with reaction order m)
k_w	$\text{J s}^{-1} \text{m}^{-2} \text{K}^{-1}$	Overall heat transfer coefficient
l	m	Reactor length
m	-	Reaction order
m_{Cat}	mg	Catalyst mass
n	-	Reaction order
p	Pa, bar	Pressure
Δp	Pa, bar	Pressure drop
\dot{q}	$\text{J s}^{-1} \text{m}^{-3}$	Specific heat removal rate
$\dot{q}_{r,0}$	$\text{J s}^{-1} \text{m}^{-3}$	Specific heat production rate
r	m	Local radius
r_m	$\text{mol kg}^{-1} \text{s}^{-1}$	Reaction rate normalized to catalyst mass
$(r_{\text{eff}})_s$	$\text{mol m}^{-2} \text{s}^{-1}$	Reaction rate normalized to catalyst surface
$(r_{\text{eff}})_v$	$\text{mol m}^{-3} \text{s}^{-1}$	Reaction rate normalized to reactor volume
t	s	Effective residence time
u	m s^{-1}	Linear flow velocity
u_{max}	m s^{-1}	Maximum linear flow velocity
A_w	m^2	Heat transfer area
D_e	$\text{m}^2 \text{s}^{-1}$	Effective diffusion coefficient
D_i	$\text{m}^2 \text{s}^{-1}$	Molecular diffusion coefficient
D_{ax}	$\text{m}^2 \text{s}^{-1}$	Axial dispersion coefficient
$E(\theta)$	-	Residence time distribution function
E_A	J mol^{-1}	Activation energy
E_g	eV	Edge energy
$F(R_\infty)$	-	Kubelka-Munk function
$F(\theta)$	-	Cumulative residence time distribution function

$\Delta_r H$	J mol^{-1}	Reaction enthalpy
N	-	Number of CSTRs in cascade
R	m	Radius
R_m	$\text{J mol}^{-1} \text{K}^{-1}$	Universal gas constant (8.314)
R_∞	-	Reflectance of an infinitely thick layer
S	%	Selectivity
S_{BET}	$\text{m}^2 \text{g}^{-1}$	Specific surface area
T	$^{\circ}\text{C}, \text{K}$	Temperature
T_0	$^{\circ}\text{C}, \text{K}$	Initial temperature
T_{max}	$^{\circ}\text{C}, \text{K}$	Temperature of maximum reduction rate
T_w	$^{\circ}\text{C}, \text{K}$	Temperature of reactor wall
ΔT_m	K	Mean logarithmic temperature difference
ΔT_{large}	K	Large temperature difference between hot/ cold stream
ΔT_{small}	K	Small temperature difference between hot/ cold stream
V_m	m^3	Molar volume at 0 $^{\circ}\text{C}$ and 101325 Pa
V_r	m^3	Reactor volume
\dot{V}	$\text{ml}_n \text{min}^{-1}$	Volume flow
X	%	Conversion

Greek Characters

α	$\text{J s}^{-1} \text{m}^{-2} \text{K}$	Heat transfer coefficient
δ_{Cat}	μm	Thickness of catalytic coating
δ_w	m	Thickness of reactor wall
η	$\text{kg m}^{-1} \text{s}^{-1}$	Dynamic viscosity
λ	nm	Wavelength
λ_w	$\text{J s}^{-1} \text{m}^{-1} \text{K}^{-1}$	Heat conductivity coefficient of reactor wall
ν	s^{-1}	Frequency
π	-	Circular constant (3.142)
θ	-	Reduced residence time
θ_{diff}	$^{\circ}$	Diffraction angle
ρ	kg m^{-3}	Specific density
τ	s	Mean residence time
τ_{Cascade}	s	Mean residence time of cascade of CSTRs
τ_{diff}	s	Time constant of diffusion
τ_{hyd}	s	Hydrodynamic residence time

τ_{mod}	kg s m^{-3}	Modified residence time
τ_{MR}	s	Mean residence time of micro reactor
τ_{PFTR}	s	Mean residence time of PFTR

Characteristic Numbers

Bo	-	Bodenstein number
Re	-	Reynolds number
Fo	-	Fourier number

Abbreviations

BET	Brunauer, Emmett, Teller
CCD	Charge Coupled Device
CVD	Chemical Vapor Deposition
CSTR	Continuous Stirred Tank Reactor
DRS	Diffuse Reflectance Spectroscopy
EDX	Energy-Dispersive X-ray Spectroscopy
FID	Flame Ionization Detector
GC	Gas Chromatography
ICP-OES	Inductively Coupled Plasma-Optical Emission Spectroscopy
LRS	Laser Raman Spectroscopy
MFC	Mass Flow Controller
MRT	Micro Reaction Technology
ODP	Oxidative Dehydrogenation of Propane
PCS	Process Control System
PFTR	Plug Flow Tubular Reactor
PVD	Physical Vapor Deposition
RTD	Residence Time Distribution
SEM	Scanning Electron Microscopy
TCD	Thermal Conductivity Detector
TPR	Temperature Programmed Reduction
UV-vis	Ultra Violet-Visible
XRD	X-ray Diffractometry
XRF	X-ray Fluorescence

1 Introduction and Objectives

Micro reaction technology (MRT) and chemical micro processing originated in the 1990s from a trend in academic research towards miniaturization of unit operations in chemical process development. After decades of working on scale-up problems, engineers and scientist from various disciplines began to extensively investigate the characteristics of performing chemical unit operations on a micro scale. Competencies from the fields of chemistry, chemical engineering, micro mechanics, micro electronics, and micro analytics had to be combined in order to successfully master the complexity of this new technology. Despite many doubts since the very beginning, today it is evident that MRT is on its way to maturity leading the path to more efficient and environmentally benign chemical development and production processes. The successful organization of ten International Conferences on Microreaction Technology (IMRET) since 1997 impressively shows the constant and even growing interest in this highly innovative field of research.

Besides saving space and material for operating and producing microstructured components, MRT offers some outstanding advantages in comparison to conventional reactor systems such as extremely efficient heat and mass transfer properties, narrow residence time distributions, and enhanced process safety. Especially in the field of kinetic investigations, these advantages have commonly led to the generation of more reliable information that allowed for the subsequent improvement of industrial processes, resulting in higher product selectivities and yields. Due to their small physical size, micro reactors have been predominantly applied in lab-scale applications. However, many joint projects between academia and industry have shown that it is possible to successfully transfer micro reaction technology even to large-scale production processes.

The characteristics of microstructured devices appear to be very useful for performing fast and strongly exothermic heterogeneously catalyzed gas phase reactions. This type of reaction often suffers from heat and mass transfer limitations in conventional reactor geometries. In particular, partial oxidations of hydrocarbons might benefit from the advantages offered by micro reaction technology. In many cases, the catalytic deep oxidation of reactants is strongly exothermic, resulting in pronounced temperature profiles along the catalyst bed in conventional fixed bed reactors, which commonly decrease selectivity towards the desired reaction products. As a sensitive test reaction, the oxidative dehydrogenation of propane (ODP) to propene was chosen to evaluate the applicability of microstructured reactors for fast and strongly exothermic heterogeneously catalyzed gas phase reactions. The ODP has been extensively investigated during the past decades but the major challenge being the formulation of a catalyst with sufficient propene selectivity has not yet been overcome. How-

ever, the simultaneous development of innovative reaction technologies and new catalyst formulations might finally lead to an economically feasible process for the oxidative dehydrogenation of propane.

Apart from the advantages of micro reaction technology for chemical development and production processes, there are two fundamental drawbacks to this promising technology. The wide-spread application of microstructured devices has been prevented due to the relatively high costs for their fabrication. Although more sophisticated manufacturing methods for microstructured devices from a wide variety of materials have been developed, mass production still constitutes a major problem. In addition, the absence of a coherent concept to fundamentally increase the limited through-put of microstructured devices has not been presented yet, though a lot of research is focused on this challenge.

Therefore, the main objective of the present study was the development of a scalable, flexible, low-cost manufacturing concept for microstructured reactor modules applicable for a wide variety of heterogeneously catalyzed gas phase reactions. The aim was to ensure consistency in the development process for this type of reaction, allowing for prospective applications from lab- to industrial-scale. The reactor modules were exclusively fabricated at the Department of Micro Reactor Technology at the Atotech Deutschland GmbH, whereas all performance tests were carried out at the Institute of Chemistry at the Technical University of Berlin. Major goals of the co-operation were the development of a reliable bonding-method for fabricating microstructured devices and the optimization of techniques for depositing stable and selective catalyst coatings on the micro channel surfaces. The obtained modules were tested with respect to reaction engineering aspects in the oxidative dehydrogenation of propane in order to evaluate the potential of all developed methods in comparison to a conventional fixed bed reactor. The joint approach between academia and industry was chosen to efficiently combine competencies from the fields of manufacturing microstructured reactors and applying them for catalytic reactions in chemical process development and production.

2 Fundamentals and State of the Art

2.1 Micro Reaction Technology

The potential of micro reaction technology and chemical micro processing for substantially improving the efficiency of process development and chemical production processes has long been promoted in the literature [1-5]. Over the past two decades, many studies have been carried out on various sample reactions using a wide range of reactor designs [3,4,6-10]. However, most research activities aimed at lab-scale applications with only few attempts to enter industrial-scale production regimes. The following sub-chapters will provide an overview of the field.

2.1.1 Definitions and Components

Any type of *micro technology* is based on the principal of miniaturization. Typical length scales of micro technologies fall into the range of 0.1 to 1,000 μm . Examples for micro technologies are micro electronics, micro mechanics, micro fluidics, micro analytics, and *micro reaction technology*, which deals with performing chemical reactions and unit operations on a micro scale. In order to simplify orientation, Figure 2-1 shows various aspects of chemical engineering on a length scale from 1 Å to 10 m.

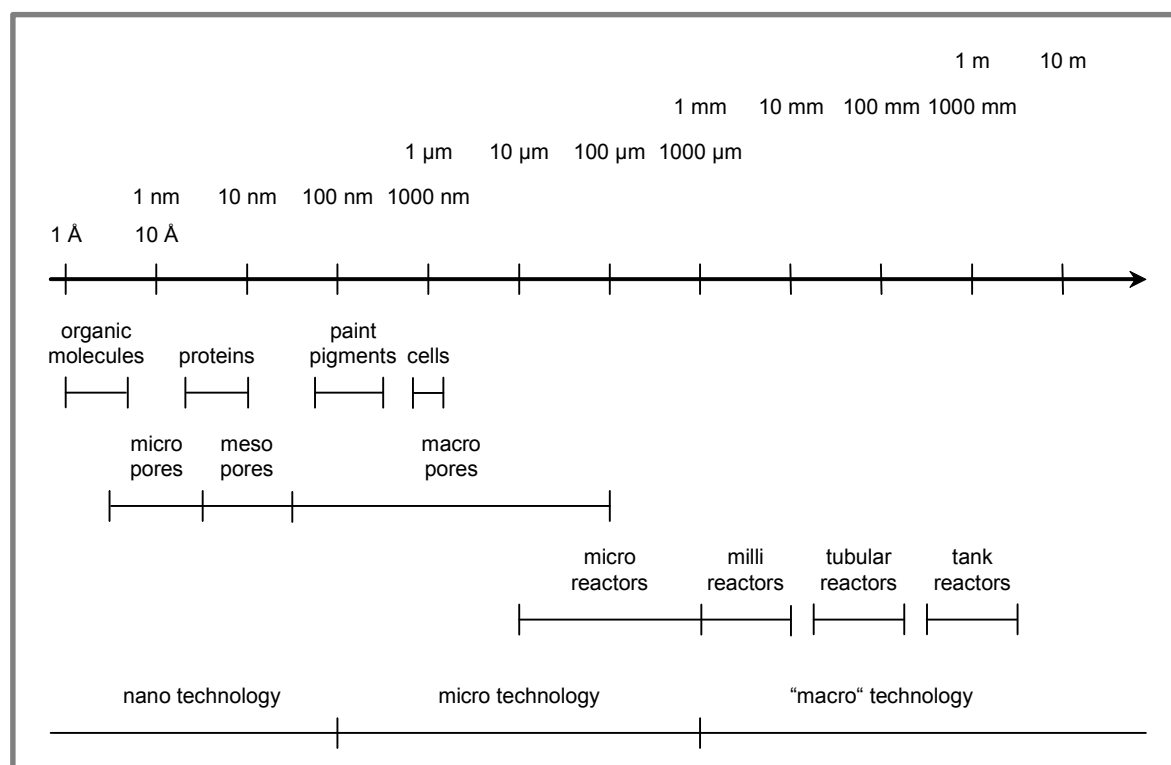


Figure 2-1: Characteristic length scales in chemical engineering (depicted from [5]).

By decreasing linear dimensions of devices for performing chemical unit operations, the surface-to-volume ratio of these devices dramatically increases. For an idealized tubular reactor, the surface-to-volume ratio can be calculated according to $2/R$, where R is the radius of a cylindrical geometric form. Figure 2-2 shows this dependency on a double logarithmic scale. If the radius of a chemical reactor is decreased from 2 m to 50 μm (i.e., from a large tank reactor to a small micro reactor), the surface-to-volume ratio increases by a factor of 40,000 (i.e., from 1 to 40,000 m^{-1}).

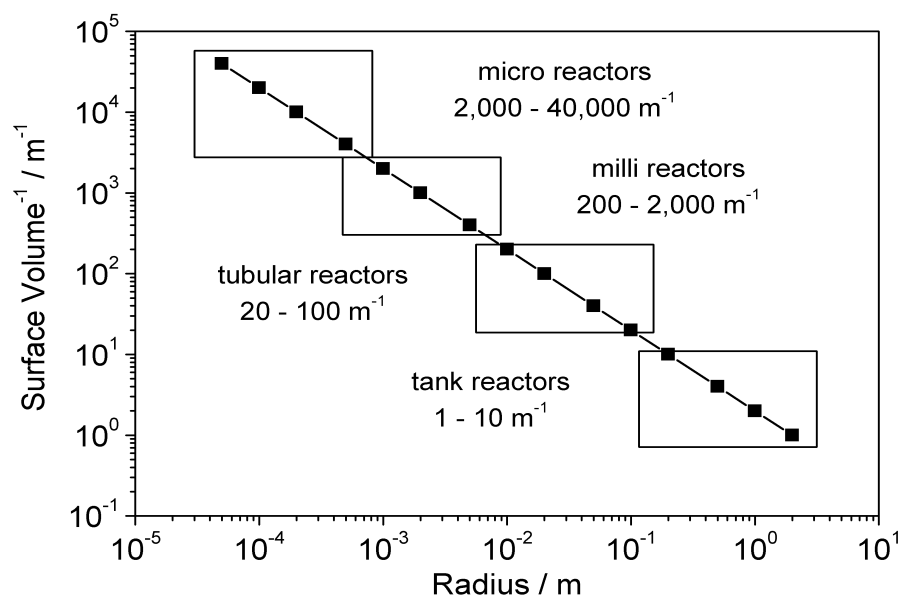


Figure 2-2: Dependency between radius and surface-to-volume ratio of a tubular reactor.

This dramatic decrease of linear dimensions leads to the increasing relevance of so called *micro effects* [5]. These effects (i.e., intensified mass transfer by molecular diffusion, intensified heat transfer, and intensified surface phenomena) are well known in theory but do not play a major role on the macro scale, since they are generally superimposed by other effects such as convective heat or mass transfer. However, micro effects provide the governing principles for all phenomena on the micro scale that are responsible for the fundamental advantages of microstructured devices in comparison to conventional devices.

All micro technologies owe their existence to the development of increasingly sophisticated *micro structuring techniques*. These techniques allow for the fabrication of defined 3D micro structures on various substrates. Important micro structuring techniques for manufacturing chemical micro components are described in Chapter 2.1.3.

By combining the functionalities of several micro technologies, more complex *micro systems* can be obtained, which are often highly integrated, automated, and seemingly “intelligent” [9,11]. Also *chemical micro processing* can be regarded as a micro system, since it unites micro electronics, micro fluidics, micro reaction technology, micro separations, and micro analytics. Examples for industrial chemical micro systems will be given in Chapter 2.1.4., especially addressing strategies to increase the limited through-put of micro components.

Microstructured components for performing chemical unit operations are commonly grouped into four major fields: Micro mixers, micro heat exchangers, micro separators, and micro reactors. A good overview of the variety of microstructured devices is provided by Ehrfeld et al. [3,4], Klemm et al. [5], and Hessel et al. [7-9]. However, it has to be noted that these four groups of micro components cannot be examined independently, since micro mixers, micro heat exchangers and sometimes combinations thereof are commonly used for carrying out chemical reactions instead of strictly serving their original purpose.

There are two main categories of *micro mixers*: Laminar diffusion mixers and split-recombine mixers [3-5,7,12]. As was explained before, molecular diffusion becomes relevant on the micro scale. This phenomenon is utilized in all laminar diffusion mixers by physically contacting both streams that are due to be mixed. Mixing is then achieved by diffusion of both components in each other. T- and Y-type mixers can be regarded as rather simple but in many cases sufficient designs, whereas multi lamination mixers with different degrees of sophistication are also available. The second category comprises all sorts of split-recombine mixers. These devices achieve mixing through consecutive steps of splitting the flow that is due to be mixed and afterwards recombining it. There are also alternative mixer designs that are still under development and will probably be restricted to special applications. Among these designs micro jet mixers [13] and ultrasound micro mixers [14] can be found.

Micro heat exchangers exist in various designs that are also known from conventional technology such as cross or counter flow heat exchangers [3-5,8,15]. The main advantages from miniaturization stems from the increased specific surface area of up to $40,000\text{ m}^{-1}$ and the elevated overall heat transfer coefficients. Compared to conventional plate heat exchangers, microstructured devices allow heat transfer rates that are higher by a factor of 1,000 [16]. Since micro heat exchangers are among the most comprehensive examples in chemical micro processing, they are already used for industrial applications such as chemical production (process heat integration) or crude oil treatment on oil platforms.

The range of available *micro separators* is limited, though essentially needed for combining microstructured components to fully functional micro systems. However, some separation

principles such as extraction and rectification have been realized so far. Liquid-liquid extraction can be carried out in simple micro mixers as described above [17]. In order to achieve a sufficient degree of separation, high exchange interfaces are required between the mixture and the extracting agent. Devices for performing rectifications are still under development. However, a prototype of a micro rectification column has been presented already [18].

Micro reactors are generally a combination of the functionalities described for micro mixers and micro heat exchangers. However, there are also specialized components such as micro falling film reactors [19] or micro photo reactors [20-22]. Homogeneous gas and liquid phase reactions can be carried out in specially adapted micro mixers. Multi phase reactions such as heterogeneously catalyzed gas phase reactions or gas/ liquid reactions require more sophisticated reactor designs [5,7,8,10]. Especially the insertion of a solid catalyst into the micro channels is connected to many challenges. Therefore, this aspect will be separately discussed in Chapter 2.1.3.3.

2.1.2 Advantages and Disadvantages

Micro reaction technology and chemical micro processing has several advantages compared to conventional equipment for performing unit operations. These advantages are commonly quoted in the relevant literature. However, for a well-grounded understanding of the potential of this innovative technology, also disadvantages have to be taken into account. Both, advantages and disadvantages can be grouped into two areas: Engineering aspects and organizational aspects, which will be discussed in the following sub-chapters.

2.1.2.1 Engineering Aspects

All advantages and disadvantages of micro reaction technology with respect to engineering aspects are related to the miniaturization of linear reactor dimensions. As explained above, the significant phenomena on the micro scale are mainly due to the increased importance of micro effects. Emig and Klemm provide a comprehensive introduction to the field in their textbook “Technische Chemie” [16].

The dimensionless Reynolds number Re is commonly used to describe hydrodynamic flow regimes and is calculated according to Equation 2-1. Reynolds numbers below 2,300 are characteristic for laminar flows, whereas Reynolds numbers above 2,300 are characteristic for turbulent flows.

$$Re = \frac{u \cdot \rho \cdot d_h}{\eta} \quad (2-1)$$

where u is the linear flow velocity of the fluid, ρ the density of the fluid, d_h the hydraulic diameter, and η the dynamic viscosity. The hydrodynamic flow regime in microstructured devices is predominantly laminar. This is due to the small hydraulic diameter d_h of the micro channels, which becomes the dominating parameter for calculating Re . Typical Reynolds numbers in microstructured components fall into the range from 10 to 500, being far below the critical Re value for turbulent flows [16].

Since laminar flow regimes are characteristic for micro devices, the Hagen-Poiseuille equation has to be applied for calculating the pressure drop Δp in a micro channel as given through Equation 2-2:

$$\Delta p = \dot{V} \cdot \frac{l}{R^4} \cdot \eta \cdot \frac{8}{\pi} \quad (2-2)$$

where \dot{V} is the volume flow, l the reactor length, and R the radius of the micro channel. By The maximum linear flow velocity u_{\max} of a fluid can be calculated according to Equation 2-3:

$$u_{\max} = \frac{R^2}{4\eta} \cdot \frac{\Delta p}{l} \quad (2-3)$$

In addition, the local flow velocity $u(r)$ can be calculated according to Equation 2-4, resulting in the parabolic flow profile of laminar flows in tubular reactors.

$$u(r) = u_{\max} \left[1 - \left(\frac{r}{R} \right)^2 \right] \quad (2-4)$$

Laminar flow regimes are known to produce fairly wide residence time distribution (RTD) functions. However, microstructured devices do not show this behavior. In contrast, they are valued for their narrow RTD functions. This can be explained as follows: Mass transfer through molecular diffusion cannot be neglected on the micro scale in comparison to the macro scale. Since the mean free path of gas molecules is in the length scale of typical dimension of internal microstructures, intensive radial mixing neutralizes the parabolic flow profile predicted for laminar flow regimes [16,23,24]. The same phenomenon is responsible

for the high efficiency of micro mixers. The time constant of diffusion τ_{diff} can be calculated according to Equation 2-5:

$$\tau_{\text{diff}} = \frac{R^2}{D_i} \quad (2-5)$$

where D_i is the molecular diffusion coefficient. Typical values of D_i for gases are $1 \times 10^{-5} \text{ m}^2 \text{ s}^{-1}$ and $1 \times 10^{-9} \text{ m}^2 \text{ s}^{-1}$ for liquids. Consequently, the time constant of diffusion in microstructured devices fall into the range of 0.01 to 100 ms for gases and 0.1 to 1,000 s for liquids [16]. The dimensionless Fourier number Fo is defined as the ratio of the residence time τ and the time constant of diffusion τ_{diff} according to Equation 2-6:

$$Fo = \frac{\tau}{\tau_{\text{diff}}} \quad (2-6)$$

On the micro scale, values of the Fourier number are usually ≥ 1 , due to the extremely small denominator of Equation 2-6. Therefore, efficient (radial) mixing through molecular diffusion is achievable. On the macro scale, values of the Fourier number are commonly $\ll 1$, confirming the above statement that molecular diffusion can be neglected in comparison to convective mass transport.

Heat transfer phenomena on the micro scale can be described with the same set of basic equations as has been developed for the macro scale. The specific heat removal rate \dot{q} is given through Equation 2-7:

$$\dot{q} = k_w \cdot a \cdot \Delta T_m \quad (2-7)$$

where k_w is the overall heat transfer coefficient, a the specific surface area of the micro device, and ΔT_m the logarithmic mean temperature difference. The value of k_w is calculated according to Equation 2-8:

$$\frac{1}{k_w} = \frac{1}{\alpha_1} + \frac{\delta_w}{\lambda_w} + \frac{1}{\alpha_2} \quad (2-8)$$

where α_1 is the heat transfer coefficient from the cooling agent to the heat exchanger wall, δ_w the thickness of the wall, λ_w the heat conductivity coefficient of the heat exchanger material, and α_2 the heat transfer coefficient from the process fluid to the heat exchanger wall. The logarithmic mean temperature difference, universally applicable for counter current and parallel flow heat exchangers, is given through Equation 2-9:

$$\Delta T_m = \frac{\Delta T_{\text{large}} - \Delta T_{\text{small}}}{\ln\left(\frac{\Delta T_{\text{large}}}{\Delta T_{\text{small}}}\right)} \quad (2-9)$$

where ΔT_{large} is the large temperature difference between the hot and the cold stream and ΔT_{small} the small temperature difference between the hot and the cold stream. The main differences between macro and micro scale heat exchangers are the values of k_w and a . The overall heat transfer coefficients in micro channels fall into the range of $1,000 \text{ W m}^{-2} \text{ K}^{-1}$ for gases and $10,000$ to $40,000 \text{ W m}^{-2} \text{ K}^{-1}$ for liquids, which is about 10 to 30 times higher than in plate heat exchangers [16]. The surface-to-volume ratio in microstructured devices lies between $2,000$ and $40,000 \text{ m}^{-1}$, being about 100 times higher than in conventional technology. Therefore, the overall efficiency of micro heat exchangers can be increased by the factor of 1,000 compared to plate heat exchangers. This aspect is widely regarded as the most valuable advantage of micro reaction technology, which has some consequences for the thermal behavior of microstructured devices. The specific heat production rate $\dot{q}_{r,0}$ of an exothermic reaction can be calculated according to Equation 2-10:

$$\dot{q}_{r,0} = k(T_0) \cdot c_0^n \cdot \Delta_r H \quad (2-10)$$

where $k(T_0)$ is the kinetic rate constant, T_0 the initial temperature of the reaction mixture, c_0 the initial concentration of the relevant reactant, n the reaction order, and $\Delta_r H$ the reaction enthalpy. Since realizable heat removal rates in microstructured heat exchangers are extremely high in comparison to conventional technology, near isothermal process conditions can be achieved even if strongly exothermic reactions are investigated. The ability to efficiently remove heat from the reaction mixture is also beneficial for preventing thermal run-aways, both leading to a strong enhancement of process safety with respect to thermal aspects. Furthermore, the perspective of process intensification by using microstructured reactors is commonly cited in the relevant literature [11,25-28]. Since conventional technology is not capable to remove heat as efficient as micro reactors, the specific heat production rate

has to be artificially decreased in order to stay in control of the chemical process. In many cases, the kinetic rate constant k is manipulated by a decrease of the initial temperature T_0 or a dilution of the catalyst. Alternatively, c_0 might be decreased by a dilution of the reaction mixture or by a slow or stage-wise dosage of the reactants. All of these measures can be avoided, if microstructured devices are applied, utilizing the full kinetic potential of the reaction instead of artificially slowing it down.

In addition to the thermal safety issues discussed above, microstructured devices are often said to be inherently safe. In case of an explosion of the reaction mixture, the small geometric dimensions of the microstructure might be able to quench the uncontrollable chain reaction by frequently contacting free radicals with the reactor walls [29-33]. However, lately doubts about this theory have been raised, followed by experimental evidence [34]. Another aspect to be considered is the fact that most chemical plants also consist of non-microstructured devices, which are not “inherently” protected from thermal explosions. The same holds true for the argument that microstructured devices contain only small hold-ups of hazardous substances, minimizing negative consequences in case of an accident.

However, there are also downsides to micro reaction technology with respect to engineering aspects. The predominantly complex fabrication processes (see Chapter 2.1.3) lead to high manufacturing costs, which might have a major impact on the economic feasibility of a newly developed process. In addition, missing microstructured unit operations (e.g., separations, handling of solid materials), actuators, and sensors prevent the full integration of micro devices in fully functional and reliable micro systems. Most importantly, the limited throughput of microstructured devices due to their small physical size is a key problem that must not be underestimated. As will be shown in Chapter 2.1.4, the scale-up of production capacity is by no means a trivial problem. There are competing approaches to this challenge that will be discussed later.

2.1.2.2 Organizational Aspects

In terms of organizational aspects, the faster generation of reliable kinetic data is one the main advantages [35,36]. As described above, mass and heat transfer limitations can be avoided, revealing the intrinsic kinetics of the investigated reaction. The obtained information is highly valuable for theoretical process simulations. In addition, the continuous operation mode allows for an easier variation of process conditions during an experimental series.

One of the most cited organizational advantages of micro reaction technology is the faster transfer of production processes from research and development to production [3,4]. Since

many processes in chemical industry are carried out in continuous flow, the complex and time-consuming transfer from batch to continuous operation can be avoided. The developed process might directly be transferred from lab-scale to (small) production-scale by simply multiplying the number of microstructured units [3,37]. Therefore, a faster overall development process can be implemented, resulting in a decreased time-to-market, which is a key driver in modern competition between chemical companies. However, this concept works only to a certain extent and cannot be generalized for all efforts to transfer lab-scale to industrial-scale.

As mentioned before, micro reaction technology is based on continuous flow processes. However, many small-scale production campaigns in the pharmaceutical and fine chemistry industry are carried out in discontinuous (semi-)batch processes. There are fundamental advantages and disadvantages connected to both production regimes that have to be balanced against each other, since applying micro reaction technology is generally equivalent with replacing a discontinuous batch process through a continuous flow process. The main advantage of a discontinuous production regime is its high flexibility, since a variety of unit operations is commonly combined in so called multi-purpose plants. However, product quality is subject to slight changes, because exact reproducibility of batch processes is difficult to achieve. In comparison, continuous processes are less flexible in terms of variability for different reactions due to the commonly high degree of integration and specialization. On the other side, product quality is highly reproducible and once the process is implemented, it requires less labor input than discontinuous batch processes. Therefore, it has to be carefully examined whether a process can benefit from a continuous production regime that is characteristic for micro reaction technology.

2.1.3 Fabrication Methods

2.1.3.1 Micro Structuring Techniques

The increasing success of all micro technologies has been assisted by improved 3D micro structuring techniques applicable for a wide range of materials. Especially for performing chemical unit operations in microstructured devices, key criteria such as geometric precision (important for controlling fluid dynamics) and stability (i.e., thermal, mechanical, and chemical) have to be guaranteed.

Fine or precision engineering methods typically comprise conventional structuring techniques such as milling, drilling, and turning adapted to the micro scale. The size of the applied tools falls into the range of 50 to 100 μm , which are very sensitive to abrasion and destruction. Smallest achievable dimensions lie between 10 and 100 μm with a precision of about

$\pm 10 \mu\text{m}$. These methods are suitable for machining materials such as metals, polymers, glasses, and ceramics [3-5,38].

Electrical discharge machining is also frequently used for micro structuring. However, the choice of material is limited, since electrical conductivity of the substrate is a prerequisite. Smallest achievable dimensions lie in the range between 20 and 30 μm , with a precision of about $\pm 2 \mu\text{m}$ [3-5,38].

Micro sand blasting has rarely been reported in the literature and seems to be a more exotic application. However, it can be used for structuring brittle materials such as glasses [38].

Laser micro machining is utilized for drilling, cutting, and 2D ablating. Typically, Nd:YAG, carbon dioxide, and excimer laser are applied. Smallest achievable dimensions fall into the range of 5 to 10 μm , whereas precision is fairly high ($\pm 1 \mu\text{m}$). However, their power density and subsequently their efficiency are still relatively low [3-5,38].

Molding techniques use suitable tools for molding microstructures into preferentially soft substrates (i.e., polymers or thin metal foils). In addition, a wide range of methods has been developed that utilize pre-structured micro molds for injection molding techniques [3-5,38].

Lithography is not defined as a micro structuring method in its actual sense, but is an important technique to be combined with other micro structuring methods. It utilizes laser, high-energy electron, and ion beams as well as UV- and X-ray (i.e., synchrotron) radiation to create microstructures on a resist layer that is normally deposited on a substrate. Depending on the type of the resist layer, the exposed areas either stay on the substrate (i.e., positive resist) or can be removed from the substrate (i.e., negative resist). This pre-formed microstructure is then used as a mask for following structuring techniques. Smallest achievable dimensions fall into the range of 2 to 5 μm with extremely high precision ($< 0.5 \mu\text{m}$) [3-5,38].

Etching procedures are commonly divided into dry and wet variants. In both cases, a lithographic mask has to be applied before material can be removed from the substrate. Dry etching procedures utilize gaseous ion beams, whereas wet etching procedures depend on the application of a liquid etchant (i.e., typically strong inorganic acids such as hydrochloric, nitric, and hydrofluoric acid). It can be distinguished between isotropic and anisotropic etching methods, meaning directionally independent/ directionally dependent. In other words, isotropic etching works towards all spatial directions, whereas anisotropic etching works towards a preferential direction [3-5,38].

The *LIGA method* (German acronym for **L**itographie, **G**alvanoumformung, **A**bformung) is a combination of deep lithography, electroforming, and molding. It aims at the production of molding tools that can be subsequently used for the production of micro structures [3-5,38].

2.1.3.2 Assembly Techniques

After creating the microstructure on foils, sheets, or platelets made from various materials by using methods as described above, the individual components have to be assembled to fully functional devices. It can be distinguished between permanent and non-permanent bonding-methods. In case of the permanent methods, mechanical force has to be applied to separate the single parts, whereas in case of the non-permanent methods, assembly/ disassembly can be frequently repeated.

The most straightforward way to bond individual components to a microstructured device is the application of any type of fasteners with sealings to ensure gas/ liquid tightness. The advantage of this method is the simple handling, which provides the possibility to easily check the internal structure after performing a reaction. However, gas/ liquid tightness cannot be assured under all conditions and an industrial-scale production of this reactor design appears rather complex. Therefore, these reactors are only suited for lab-scale research activities.

In order to adapt manufacturing methods for microstructured devices to mass production, various diffusion soldering [39,40], diffusion brazing, and diffusion/ laser welding techniques have been developed [38]. The main advantage of these techniques is based on the solid material connection between the individual components, guaranteeing gas/ liquid tightness and a high thermal conductivity within the microstructured devices. However, since all of these methods lead to permanent bonds between the separate reactor parts, they cannot be opened easily for inspection. This is a fundamental disadvantage for lab-scale research activities and might lead to economic problems, if frequent catalyst replacement becomes necessary due to rapid deactivation processes.

2.1.3.3 Internal Surface Functionalization

In order to apply microstructured reactors for performing heterogeneously catalyzed gas phase reactions, it is essential to insert a solid catalytic material into the channels. This can either be achieved by filling the channels with a powder catalyst (i.e., micro fixed beds) or by functionalizing the internal surface of the micro reactor (i.e., wall catalysts) [5,28,41]. Since micro fixed beds generally suffer from substantial pressure drops, they do not play a major role in micro reaction technology. Therefore, they will not be discussed in further detail. In comparison, wall catalysts are widely spread for functionalizing the internal surface of micro-

structured reactors and a variety of techniques has been developed to deposit catalytic material on the channel surfaces.

The first major route utilizes the internal surface material of the reactor. The *anodic oxidation of aluminum* creates slightly porous oxide layers on top of the metallic base material. These oxide layers are about 100 times thicker than the natural oxide layer and might be functionalized by impregnation [42-44]. Another way of utilizing the internal reactor surface is the application of *catalytically active materials for fabricating the reactors*. This method has been reported for devices made of copper [45], rhodium [46], and silver [47].

The second major route depends on methods for depositing catalytic materials on the micro channel surfaces. Therefore, they are commonly referred to as “coating methods”. *Chemical Vapor Deposition (CVD)* [29] and *Physical Vapor Deposition (PVD)* [48] are used to deposit gaseous catalyst precursors on the micro channel surfaces. Various *Sol-Gel routes* appear to be the most common methods to deposit support material layers on the micro channel surfaces [23,41,44,49-53]. In the first step, a sol is prepared by suspending metal oxide colloids in a solvent. The hydroxyl groups on the colloid particles induce an increasing number of cross-links between the particles, resulting in the formation of a gel. Typical precursors are alkoxides or silicates. Additionally, organic compounds can be used for preparing stable catalytic coatings. In the second step, the sol is deposited on the micro channel surfaces either by variations of dip- or spray-coating [41]. In the literature, sol-gel methods are frequently cited as “washcoating” methods, since a porous washcoat is prepared that can be impregnated with an active component. However, the expression “*washcoating*” is partly misleading, since in its original sense it used for depositing a porous support layer on ceramic monoliths. A suspension of an inorganic oxide is filled into the channels of the monolith and subsequently blown out. The solid oxide is deposited on the surface of the ceramic material, which leads to a specific surface area about 7,000 times higher than that of the original monolith [5]. Afterwards, the porous top layer can be impregnated with an active component.

2.1.4 Micro Systems for Chemical Production Processes

With increasing success of microstructured devices for performing chemical unit operations in research and development activities, commercial suppliers began to offer fully functional chemical micro processing systems mainly for lab-scale applications. They are commonly designed as “toolbox” systems with a high level of flexibility in order to fulfill the manifold requirements of chemical research and development. A short overview of commercially available lab-scale chemical micro processing systems is provided by Kirschneck [11].

In addition to more research and development oriented applications, some attempts have been undertaken to transfer this promising technology to industrial-scale production processes. As mentioned earlier, one of the major disadvantages of microstructured components is the limited through-put due their small physical size. Conventional *scale-up* has rarely been reported, since increasing the geometric dimensions of a microstructured device neutralizes the micro effects that are responsible for the superior performance of this technology. Especially in the early development phase of chemical micro processing, *numbering-up* (also called *scale-out*) has been commonly praised as a straightforward solution to this problem [3,37]. Supporters reasoned that limited production capacity of one single micro channel or one single microstructured device can be dramatically increased by operating many identical channels or devices in parallel. Increasing the number of single channels in one device is called *internal numbering-up*, whereas increasing the number of microstructured devices is known as *external numbering-up* [54]. However, there are some difficulties related to this approach. In particular, precise process control is difficult to achieve. It has often been reported that even flow distribution over all channels or devices cannot be assured [54-56]. This leads to problems, if high product quality (i.e., pureness) is a major process parameter. Especially with respect to the production of pharmaceuticals, it has to be guaranteed that all reactants pass through identical process conditions, requiring an even flow distribution as a major precondition. However, many research activities focus on this field and first successes have been reported in the literature [54,57,58]. Another problem connected to the numbering-up approach is the high degree of integration that is achieved by operating many channels or devices in parallel. Generally, integration allows for the fabrication of more compact components or systems, which is favorable. However, in order to stay in proper control of a highly integrated chemical micro processing system, an equally sophisticated (i.e., complex and expensive) process control system has to be applied.

Lately, a more pragmatic approach towards increasing production capacity of micro devices seems to take hold in the community, repeatedly referred to as *equal-up* [11,25]. It can be regarded as an intelligent combination of the scale-up approach and the internal numbering-up approach. The first step in the procedure is to investigate the possibilities for scaling-up the dimensions of a microstructured component as much as possible without losing the beneficial micro effects by applying dimensionless parameters. A principal that is commonly quoted in this context is: "As small as necessary, but not as small as possible" [9]. In the second step, a reasonable internal numbering-up is conducted. Finally, it has to be decided, whether the new process should be implemented by exclusively using micro components (so called *monolithic concept*) or whether it should be intelligently combined with conventional "macro" technology (so called *hybrid concept*) [9,25]. As mentioned earlier, pragmatism

seems to be the governing principle for applying microstructured devices in chemical production processes. Therefore, the hybrid concept appears to be the more promising approach for industrial applications of this new technology, which is also documented by projects such as IMPULSE (i.e., Integrated **M**ultiscale **P**rocess **U**nits with **L**ocally **S**tructured **E**lements) [25,59].

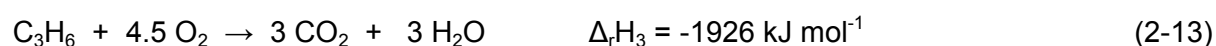
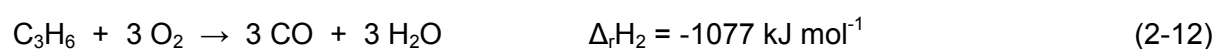
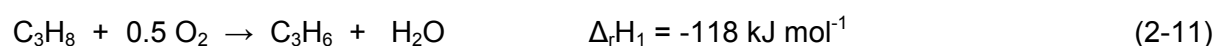
Examples for industrial-scale applications of microstructured devices are still relatively rare. However, researchers at Lonza/ Switzerland performed an analysis to quantify the number of reactions in their portfolio that might benefit from a continuous process using micro reaction technology [60,61], identifying a share of about 50%. Merck/ Germany transferred a strongly exothermic organo-metallic reaction from their research lab to production-scale by using microstructured reactors [62]. Clariant/ Germany published results on the successful industrial synthesis of paint pigments in a three-stage micro reactor pilot plant [63], whereas DSM/ Austria applied a microstructured reactor for the production of 300 t of a high grade polymer product [64]. The most noted industrial-scale application of micro reaction technology is the DEMiS project (German acronym for **D**emonstrationsprojekt zur **E**valuierung der **M**ikroreaktionstechnik in industriellen **S**ystemen) [65]. Krupp-Uhde/ Germany and Degussa/ Germany successfully build a macro-scale reactor with an internal microstructure for the synthesis of propylene oxide from propylene and evaporated hydrogen peroxide. In addition to the published examples from industry, further chemical companies are known to start using micro reaction technology in their production processes but are still reluctant to openly announce their growing commitment for reasons of competition.

2.2 Oxidative Dehydrogenation of Propane

Lower olefins such as propene are important base chemicals for many industrial applications. They are conventionally produced from non-oxidative, high-temperature cracking processes (i.e., steam cracking, fluid catalytic cracking, and deep catalytic cracking) [66]. However, all of these processes are thermodynamically limited, energy-intensive, and commonly suffer from catalyst deactivation by heavy coking. Additionally, the ratio of desired products to undesired by-products is difficult to influence through a variation of process parameters [67].

Therefore, a route that avoids most of these problems appears to be attractive. One of the proposed alternatives is the oxidative dehydrogenation of short alkanes at relatively low temperatures (i.e., 300 to 600 °C). Particularly for the production of propene, the oxidative dehydrogenation of propane (ODP) over supported VO_x catalysts has long been suggested as an alternative reaction pathway [68-72]. The interest in an exclusive production process for propene is mainly due to the steadily growing demand for this product. Propene is mainly pro-

duced from steam cracking of naphtha where ethene is inevitably formed as a by-product. However, the demand for propene grows at a faster rate than the demand for ethene, which makes the on-demand production of propene economically attractive. The ODP reaction offers further advantages, since catalyst coking can be avoided and propane is a cheaper feedstock than naphtha. In addition, this reaction is energetically favored due to a lower energy input and does not suffer from thermodynamic limitations in comparison to the industrially applied processes. A simplified reaction model of the ODP is given through Equations 2-11 to 2-13:



To this day, low selectivity towards propene has been the major drawback to an industrial application of the ODP, although it has been extensively investigated over the last decades [73-75]. Propene yields of more than 30% under anticipated operation conditions have not been exceeded yet. The major challenge is to minimize the formation of carbon oxides (CO_x) via consecutive total oxidation of propene that is favored at high degrees of propane conversion due to a higher reactivity of propene as compared to propane.

Apart from the growing economic interest in the ODP, it has long been subject to academic research, too. Innumerable catalysts have been evaluated for this reaction, focusing on vanadium containing materials, since they belong to the most promising catalytic systems [69,72,76-81]. In general, three major fields of interest can be identified in the relevant literature: (1) Detailed characterization of supported VO_x catalytic materials on molecular level to establish structure-reactivity-relationships, (2) kinetic investigations to elucidate mechanistic aspects of the reaction network, and (3) the application of innovative reactor concepts to overcome the selectivity problem by means of reaction engineering.

Researchers from the first field are mainly concerned about specifying the exact structure of the VO_x species on the surface of the catalyst. Therefore, they investigate several physico-chemical properties such as the influence of support material, the degree of polymerization of VO_x surface species, their reducibility, and electronic structure [82-90]. The obtained information is then related to catalytic behavior. It seems that highly dispersed VO_x species (i.e., monovanadates) over non-acidic supports are more selective than polymerized ones. In con-

trast, polymerized VO_x species (no bulk like crystalline V_2O_5) are considered to be more active than highly dispersed ones [87,88,90-93].

The second field of interest is focused on deriving kinetic parameters from detailed catalytic measurements for a variety of materials. The aim is to build up a mechanistic understanding of the oxidative dehydrogenation of propane by comparing test results with different kinetic models [76,92,94-96]. One of the most proposed reaction mechanisms is the Mars-van Krevelen mechanism, which postulates that oxygen does not react with propane from the gas phase but from the lattice of the catalyst [97,98]. In addition, transient methods and isotopic tracer experiments are commonly used to elucidate relationships that govern selective and non-selective reaction pathways in the ODP [99-103].

Researchers from the third field of interest try to solve the selectivity problem by applying innovative reactor concepts and novel process conditions. Microstructured reactors, membrane reactors, and fluidized bed reactors are among those concepts that raise expectations to achieve economically feasible propene yields [104-110]. Especially by either dosing molecular oxygen over the catalyst bed or by applying alternative oxidizing agents such N_2O , propene selectivity might be enhanced [91,93,111].

In the future, propene selectivity has to increase substantially mainly through improved catalyst performance. Once catalyst development has reached a point where propene yield appears economically feasible (i.e., at about 50% propene yield for a single pass process), particularly microstructured reactors might serve as an advantageous reaction technology to utilize the full kinetic potential of these novel catalysts.

3 Experimental Methods

3.1 Catalyst Preparation

Three different preparation methods were applied in the present study to produce $\text{VO}_x/\gamma\text{-Al}_2\text{O}_3$ catalysts with varying vanadium contents. Materials obtained from the first two methods were exclusively used as powders for experiments in conventional tubular reactors in order to elucidate the impact of the preparation method on the catalytic performance, whereas materials from the third method were used for preparing catalytic coatings for microstructured reactors.

For the first preparation method, vanadyl acetylacetonate (Fluka, item no. 94735) was used to precipitate vanadium on the alumina surface through a wet saturation impregnation technique. This particular technique was chosen because it allows for the stabilization of highly dispersed VO_x species on the catalyst surface [112]. The $\gamma\text{-Al}_2\text{O}_3$ pellets (Alfa Aesar, item no. 43857, diameter 0.3 mm, length 5 mm) were crushed and sieved to obtain particles with a size distribution between 100 and 300 μm . For the first impregnation, 21 g of the support material were added slowly to a saturated mixture of vanadyl acetylacetonate in toluene (Roth, item no. 95583) with a concentration of 66 mmol l^{-1} . The mixture was then heated and treated under reflux for 30 min. Afterwards, the impregnated particles were washed with fresh toluene, dried at 80 $^\circ\text{C}$ in a drying cabinet and finally calcined in air at 500 $^\circ\text{C}$ for 5 h. After the first impregnation cycle was completed, 3 g of the obtained material were kept for characterization and catalytic testing. The remaining grains produced from the first impregnation were treated again as described above. After each step, 3 g were kept for further investigations. This procedure was repeated seven times.

For the second preparation method, crystalline V_2O_5 in the Shcherbinaite modification (GfE Environmental Technology, item no. 2008620) and the same $\gamma\text{-Al}_2\text{O}_3$ pellets as described above were taken for preparing the catalytic materials. Both oxides were used as fine powders. They were homogenized by ball-milling (Retsch PM4) in dried cyclohexane for 60 min at a milling-speed of 110 rpm. The volume of one grinding beaker (inner surface coated with silica carbide) was 350 ml. The balls (also made from silica carbide) were about 10 mm in diameter. After milling, the samples were dried at 100 $^\circ\text{C}$ and subsequently calcined in air at 500 $^\circ\text{C}$ for 4 h.

For the third preparation method, $\text{VO}_x/\gamma\text{-Al}_2\text{O}_3$ catalyst samples were prepared by a specially adapted incipient wetness impregnation method. With regard to the suitability for coating microstructures with thin catalytically active layers, a $\gamma\text{-Al}_2\text{O}_3$ powder (Alfa Aesar, item no.

39812) with a mean particle diameter of 3 μm was chosen as support material. The small particle size requires a specific preparation method. Therefore, the $\gamma\text{-Al}_2\text{O}_3$ powder (approx. 1.5 g) was physically mixed with vanadyl acetylacetonate (Fluka, item no. 94735) in a 1,000 ml round bottom flask. The ratio of the two components was varied to obtain catalytic material with different vanadium content. This mixture was then suspended in methanol (approx. 5 ml) aided by ultrasound (methanol being the only solvent readily supporting full dispersion of $\gamma\text{-Al}_2\text{O}_3$ agglomerates formed from primary particles). Since simple drying methods did not yield a uniform dispersion of the precursor substance on the support material, methanol was removed by rotary evaporation (temperature of the water bath 70 $^\circ\text{C}$, 100 rpm, 600 mbar). Afterwards, the obtained catalysts were calcined at 500 $^\circ\text{C}$ for 5 h. Drying and calcination resulted in the formation of relatively large agglomerates. For catalytic testing these were crushed and sieved into defined fractions.

3.2 Catalyst Characterization

In order to determine the chemical composition of the obtained catalytic materials (i.e., vanadium, aluminum and silicon concentrations of catalyst powders and catalytic coating formulations), Inductively Coupled Plasma-Optical Emission Spectroscopy (ICP-OES) was applied. Before the analysis, all samples were dried at 350 $^\circ\text{C}$ for 2 h in air. Afterwards, the solid catalytic materials were dissolved in concentrated acids aided by microwave-pressure pulping. Measurements were performed either at the Materials Science Department at the Atotech Deutschland GmbH (Varian 720-ES) or at the Institute of Materials Science and Technologies at the Technical University of Berlin (JY Ultima).

Specific surface areas of the catalytic materials were determined by nitrogen adsorption at 77 K using a Micromeritics Gemini III 2375 Surface Area Analyzer equipped with a Vacprep 061 degasser. Before measurements, the powders were heated for 90 min at 250 $^\circ\text{C}$ under vacuum (0.15 bar) to remove water and other adsorbed molecules from the samples' surfaces. Experimental data was analyzed according to the method developed by Brunauer, Emmett, and Teller [113].

Scanning Electron Microscopy (SEM) was applied for structural characterization of the catalytic materials. Specimens were glued onto alumina stubs, gold-coated and examined at the Materials Science Department at the Atotech Deutschland GmbH (Cambridge S360) or at the Institute of Materials Science and Technologies at the Technical University of Berlin (Philips XL20). Typical magnifications of the images were in the range of 100 to 20,000.

The crystalline phase composition of the catalytic materials was determined by X-ray Powder Diffractometry (XRD) at the Institute of Materials Science and Technologies at the Technical University of Berlin. A $2\theta_{\text{diff}}$ -diffractometer (Bruker AXS D5005) with variable divergence slits, position sensitive detector, and a Cu $K\alpha$ radiation source ($\lambda = 0.1542 \text{ nm}$) was used for measurements in the range of $2\theta_{\text{diff}}$ from 10 to 90° . The phase analysis was carried out using the Diffrac-Plus/ Search program.

In-situ Laser Raman Spectroscopy (LRS) was performed using a fiber probe, which was inserted into a Raman cell. The powder samples were placed in a stainless steel sample holder with a 0.6 mm deep rectangular well covering an area of $(12 \times 8) \text{ mm}^2$. Before running the analysis, the samples were dehydrated for 60 min by treatment in a 20/80 O_2/N_2 flow ($50 \text{ ml}_n \text{ min}^{-1}$) at 350°C and subsequently cooled to room temperature. Raman spectra were recorded using 514 nm laser excitation (5 mW) at 5 cm^{-1} spectral resolution (Kaiser Optical). Sampling times were typically 30 min. All experiments were carried out at the Department of Inorganic Chemistry at the Fritz-Haber-Institute of the Max Planck Society.

In order to analyze the degree of polymerization of VO_x species in the differently prepared and loaded $\text{VO}_x/\gamma\text{-Al}_2\text{O}_3$ materials, in-situ UV-vis Diffuse Reflectance Spectroscopy (UV-vis DRS) was applied at the Leibniz-Institut für Katalyse e.V. an der Universität Rostock, Außenstelle Berlin. Experiments were performed using an Avaspec fiber optical spectrometer (Avantes) equipped with a DH-2000 deuterium-halogen light source and a CCD array detector. Pure $\gamma\text{-Al}_2\text{O}_3$ was used as a white reference and the shut aperture as a black reference. A high-temperature reflection probe, consisting of six radiating and one reading optical fibers, was located inside the furnace at a 90° angle to the reactor. The sensor was connected to the spectrometer and the light source by fiber optical cables (length 2 m) consisting of a core of pure silica (diameter 0.4 mm) coated with polyimide. UV-vis spectra were recorded at 500°C in a 20/80 O_2/Ne ($40 \text{ ml}_n \text{ min}^{-1}$) and converted into the Kubelka-Munk function.

Temperature Programmed Reduction (TPR) experiments were performed to get insights into the reducibility of the VO_x species on the surface of the catalytic materials. Prior to TPR measurements, the samples were heated under a 50/50 O_2/He flow ($50 \text{ ml}_n \text{ min}^{-1}$) up to 500°C and kept at this temperature for 30 min. The pre-treatment is necessary in order to fully oxidize the VO_x species before H_2 -reduction. After oxidation, the samples were cooled to 50°C and then heated with 10 K min^{-1} up to 860°C in a gas mixture of 5/95 H_2/Ar with a total gas flow of $25 \text{ ml}_n \text{ min}^{-1}$. Hydrogen consumption was monitored by a mass spectrometer (In-Process Instruments GAM 200).

3.3 Catalytic Performance Tests

As a sensitive test reaction, the oxidative dehydrogenation of propane (ODP) was chosen for evaluating the performance of the obtained $\text{VO}_x/\gamma\text{-Al}_2\text{O}_3$ powder catalysts and microstructured reactors. The experimental set-up used for the catalytic measurements will be illustrated in the following sub-chapters, whereas specific operation conditions will be given individually for all experimental series below. Due to the multitude of details related to the set-up, a ring binder with all relevant documents was prepared and stored in the laboratory.

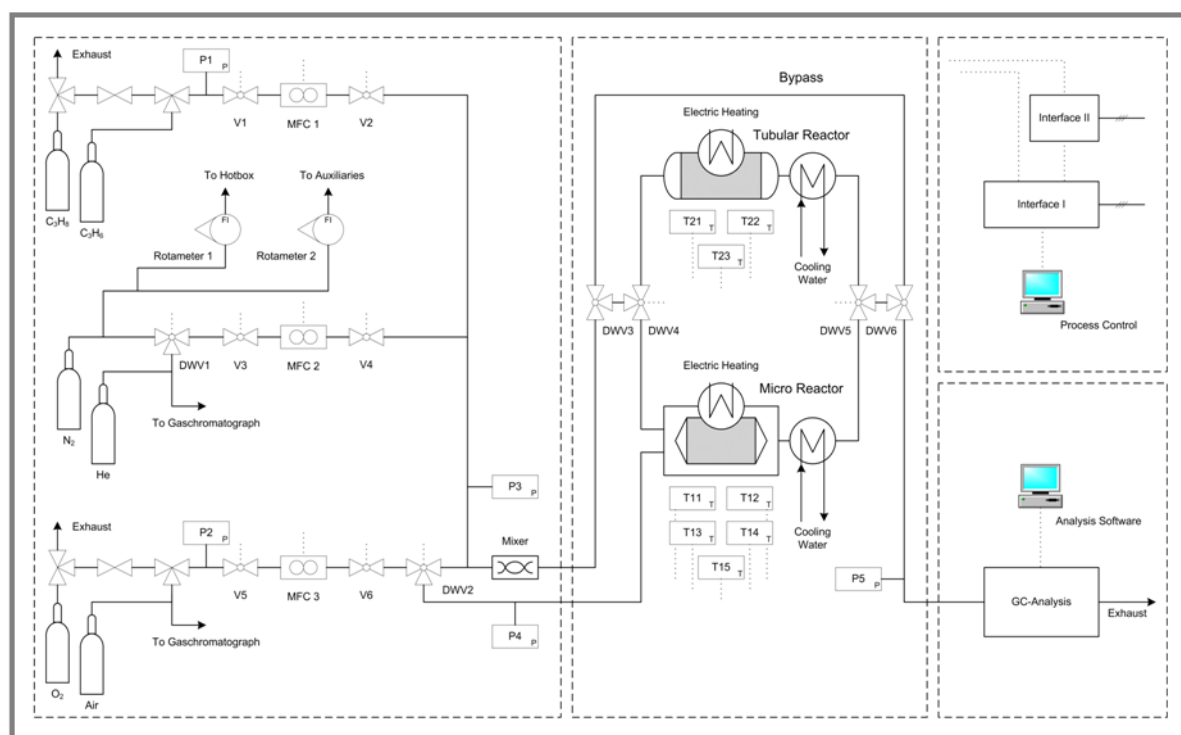


Figure 3-1: Flow chart of experimental set-up for performing catalytic measurements.

Figure 3-1 shows the flow scheme of the experimental set-up, including the gas supply and dosage, the chemical reactors, the process control system, and the gas chromatography (GC) analysis system (for a full-page version of the flow chart see Appendix A). Reactants are supplied from gas cylinders, which are located in a cabinet close to the experimental set-up. The composition of the feed gas can be adjusted by three mass flow controllers (MFC). Before the reactants enter the bypass or one of the reactors (i.e., tubular fixed bed reactor or microstructured reactor), they pass a static mixer in order to ensure proper homogenization of all feed gas components. After the chemical reaction, the gas mixture is cooled down in a condenser to remove water from the flow. The dry gas is then analyzed by an online gas chromatograph. In order to reduce residence time of the reactants in the set-up, all tubing

was chosen to be 1/8" stainless steel. Thereby, response time of the set-up to changes of process parameters is minimized.



Figure 3-2: Photograph of experimental set-up for catalytic measurements.

Figure 3-2 shows a photograph of the experimental set-up. Parts of the gas supply and the MFCs for gas dosage can be seen in the right part of the photograph. The metallic box in the lower centre contains the microstructured reactor, whereas the black tube left of the box contains the tubular fixed bed reactor. The gas chromatograph and parts of the process control system (computer screen) can be seen in the left part of the photograph.

3.3.1 Gas Dosage and Supply

For performing catalytic measurements, the following gases were used: Propane 3.5 (Air Liquide), Propene (DSM), Nitrogen (in-house supply, Linde), Helium 4.6 (Air Liquide), Synthetic Air 5.0 (Air Liquide), and Oxygen (Messer). All gas cylinders are connected via a valve system to the experimental set-up, which allows for the selection of the desired reactants. The valves for choosing propane/ propene and oxygen/ synthetic air have to be operated

manually, whereas the three-way valve DWV1 (German acronym for **Drei-Wege-Ventil**) for choosing nitrogen/ helium has to be switched from the PCS. Pressure gauges P1 and P2 were added for security reasons.

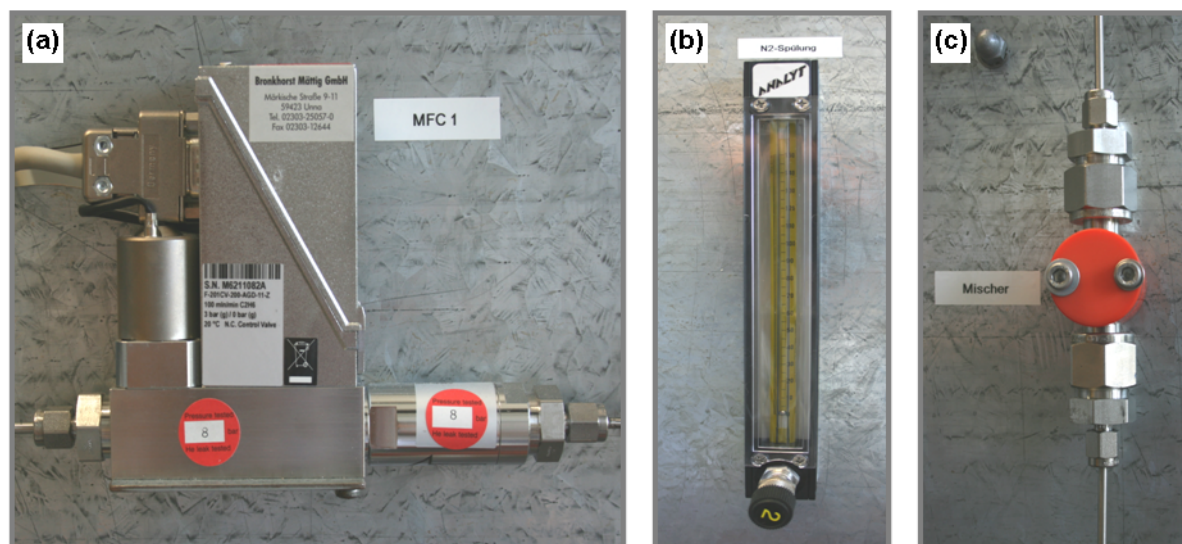


Figure 3-3: Photographs of (a) mass flow controller equipped with a pre-filter unit, (b) flow rotameter for nitrogen flush of hotbox, and (c) static gas mixer.

In order to adjust corresponding volume flows, three mass flow controllers were installed. Figure 3-3 (a) shows a detailed photograph of a MFC. All mass flow controllers have to be operated from the PCS and are calibrated as follows: MFC1 (Propane) $0 \dots 100 \text{ ml}_n \text{ min}^{-1}$, MFC2 (Nitrogen) $0 \dots 200 \text{ ml}_n \text{ min}^{-1}$, and MFC3 (Synthetic Air) $0 \dots 200 \text{ ml}_n \text{ min}^{-1}$. In order to protect the sensitive internal structure of the MFCs from particles and other impurities, they were equipped with a pre-filter. Additionally to the MFCs, two rotameters were installed for gas dosage as can be seen in Figure 3-3 (b).

Valves V1 to V6 can be individually controlled from the process control system. They protect the MFCs from pressure surges upon opening the gas cylinders and are used to connect/disconnect the gas supply from the rest of the set-up. In order to ensure proper mixing of the reactants before entering one of the reactors, they have to pass a static mixer, which is shown in Figure 3-3 (c). It is made of a 1/2" stainless steel tube containing glass pearls with a diameter of 2 to 3 mm. For dosing either oxygen or synthetic air individually to the micro-structured reactor, DWV2 was installed, which allows for the separation of this flow from the hydrocarbons and inerts. Pressure gauges P3 and P4 were included to detect any blockages in the downstream part of the experimental set-up.

3.3.2 Chemical Reactors

As mentioned above, two different types of reactors (i.e., microstructured reactor and tubular fixed bed reactor) were used for performing the catalytic measurements. Since both reactors and their thermal insulations were individually designed, they will be described in more detail. The combination of three-way valves DWV3 to DWV6 allows for the selection of three different operation modes: “Bypass”, “Mikroreaktor”, and “Rohrreaktor”. The bypass is needed for carrying out GC calibration measurements and simultaneously heating up the reactor units.

3.3.2.1 Microstructured Reactor

The microstructured reactors as shown in Figure 3-4 (a) were supplied by the Department of Micro Reactor Technology at the Atotech Deutschland GmbH. Details on their specific design, fabrication, and characterization will be given in Chapters 5 and 6.

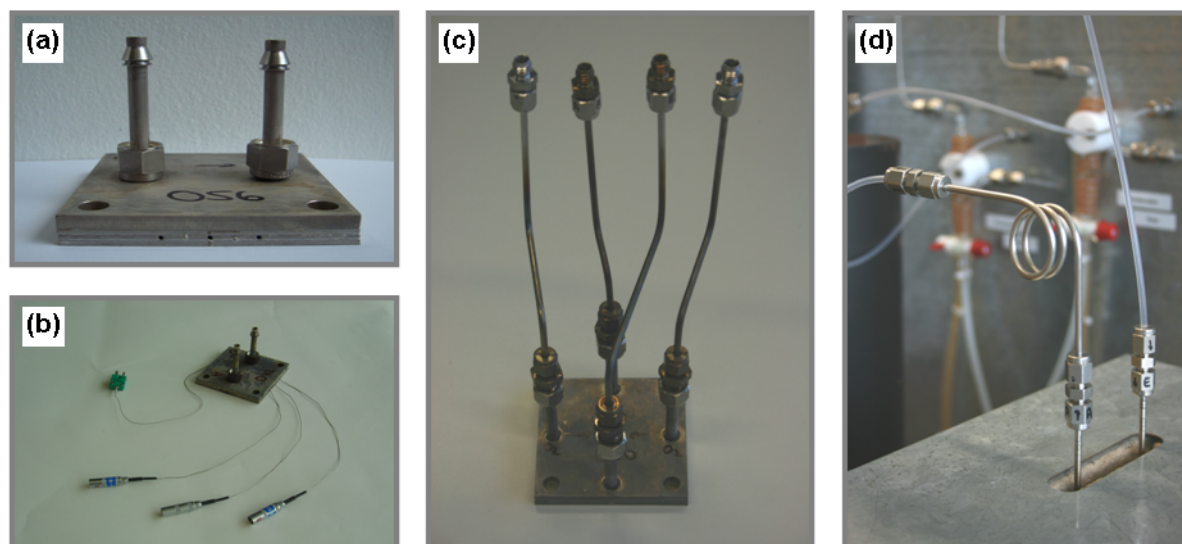


Figure 3-4: Photographs of (a) microstructured reactor, (b) equipped with thermocouples, (c) with tubing, and (d) cooling coil at reactor outlet.

The reactors can be equipped with four thermocouples (diameter 0.5 mm, T11 to T14), which serve for temperature measurement and control (see Figure 3-4 (b)). Depending on the type of microstructured reactor that is used for catalytic measurements, two to four 1/8" stainless steel tubes have to be mounted on top of the reactor tubes for gas in- and outlet as shown in Figure 3-4 (c). Since the reactors are operated at temperatures between 400 to 600 °C, special precautions have to be taken in order to avoid the formation of a permanent connection between the reactor tubes and the 1/8" stainless steel tubes. Therefore, the sealing surfaces between the reactor tubes and the connector have to be lubricated with a thermo stable

paste (e.g., Silver Goop). Finally, the reactors have to be connected to the set-up. Figure 3-4 (d) shows the gas in- and outlet, both made of Teflon hose. Since the hot exhaust gas passing through the outlet would slowly depreciate the Teflon hose, a cooling coil made of 1/8" stainless steel tube was installed.

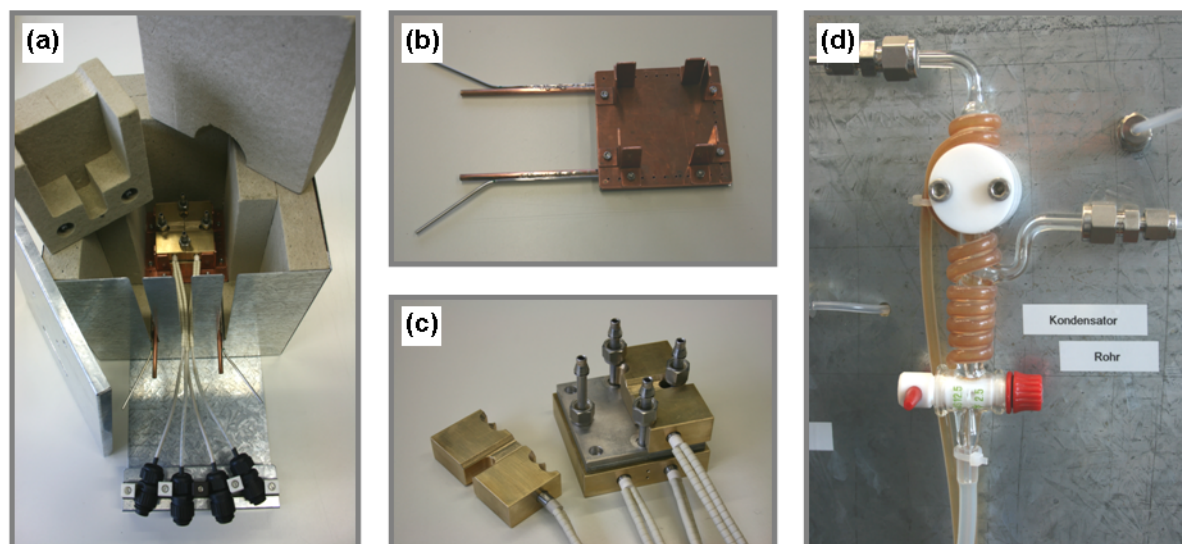


Figure 3-5: Photographs of (a) open hotbox, (b) holder for positing microstructured reactors, and (c) microstructured reactor equipped with heating blocks.

As mentioned before, the reactors can be heated to 400 to 600 °C, which requires an adequate thermal insulation. Therefore, a multi-functional hotbox was designed, which is shown in Figure 3-5 (a). It contains a custom-made copper cooling plate (see Figure 3-5 (b)) and the microstructured reactor with corresponding brass heating blocks (see Figure 3-5 (c)). The cooling plate serves several purposes: It is used for positioning the reactor at the center of the plate, distributing nitrogen within the hotbox to create an inert atmosphere, and removing heat through an air cooling. Nitrogen is fed to the plate through 1/8" stainless steel tubes via one of the rotameters mentioned above and enters the hotbox through a perforation on the fringe of the plate. The air cooling is generally not applied during experiments but rather used to help cooling down the reactor after an experimental series has been completed. Pressurized air is fed from the in-house air supply to the 1/4" copper tube, which meanders under the cooling plate. Thereby, heat is transferred from the hotbox to the passing air. The microstructured reactor is heated by four heating cartridges (160 W each) that are embedded in the brass heating blocks as shown in Figure 3-5 (c). The brass blocks were designed to be used with all reactor designs applied in the present study. The lower block also contains two holes (diameter 1 mm) for inserting thermocouples for temperature control and safeguarding

(T15). Since the partial oxidation of hydrocarbons generally leads to the production of water, the exhaust gas contains considerable amounts of water vapor. In order to protect downstream peripherals and especially the GC system, a water cooled condenser was installed after the microstructured reactor (see Figure 3-5 (d)). In addition, it is also designed to remove solids such as catalyst particles from the gas flow before it enters the three-way valves. The water cooling is connected to a tap behind the experimental set-up and has to be regulated manually.

3.3.2.2 Tubular Fixed Bed Reactor

A conventional tubular fixed bed reactor made from quartz glass was used to compare its thermal and catalytic performance to the performance of the microstructured reactors described above. Figure 3-6 (a) shows two out of three parts of the tubular reactor, being separated from each other for sake of clarity. Both parts have to be reassembled before catalytic material can be inserted.

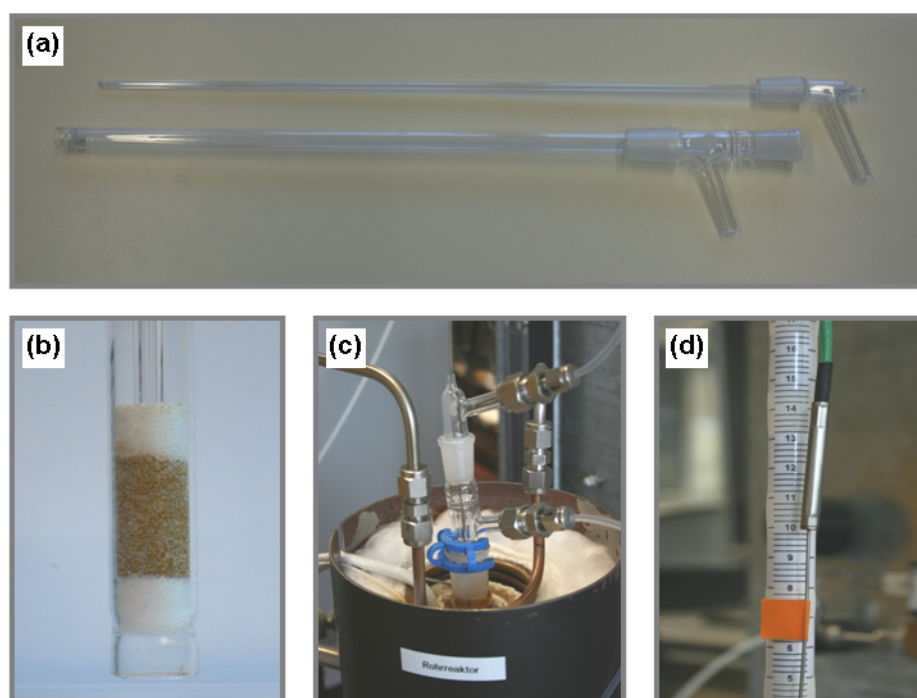


Figure 3-6: Photographs of (a) separated parts of tubular reactor, (b) magnification of catalyst bed between two layers of quartz, (c) reactor with tubing situated in insulation, and (d) scale for determining the position of the thermocouple.

The appearance of a typical fixed bed can be seen in Figure 3-6 (b), containing orange $\text{VO}_x/\gamma\text{-Al}_2\text{O}_3$ particles. The catalyst/ quartz mixture is positioned between two layers of quartz. In order to guide a thermocouple (T23) for temperature measurements through the fixed bed,

a centered glass capillary (i.e., the reactor element in the top part of Figure 3-6 (a)) was used. The two assembled reactor parts were then inserted into the third reactor part that is positioned in the black tube as can be seen in Figure 3-6 (c). It also contains the electrical heating wire (500 W) and a copper coil for air cooling. Similar to the descriptions above, the reactor has to be connected to the experimental set-up by using Teflon hoses with corresponding connectors. However, lubrication of sealing areas is not necessary due to the low thermal conductivity of quartz glass. Thermocouples for temperature control and safeguarding (T21 and T22) were positioned between the heating wire and the external jacket of the reactor (i.e., the third part of the reactor). In order to adjust the position of the moveable thermocouple that is guided through the glass capillary, a millimeter scale was installed over the tubular reactor (see Figure 3-6 (d)).

3.3.3 Process Control System

In order to operate vital parts of the experimental set-up centrally, a process control system (PCS) was installed. It comprises a hardware part, which enables the communication between the peripherals and the PCS and a software part, which provides a visualization of the process and allows interactions between the process control system and the operator.

3.3.3.1 Hardware

The electrical concept of the set-up is schematically shown in Figure 3-7, including all peripherals that are connected to the PCS. The link between the peripherals and the software part of the process control system is provided by two interfaces.

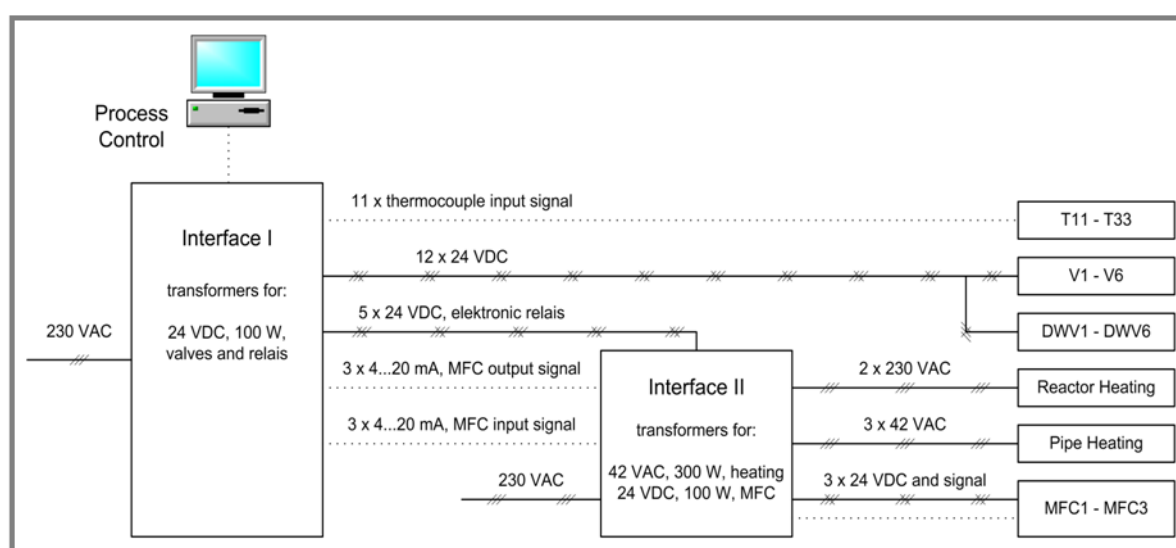


Figure 3-7: Schematic overview of electrical signals of experimental set-up.

Interface I was purchased from a commercial supplier (Ingenieurbüro Schoop), whereas Interface II was manufactured internally at the Institute of Chemistry at the Technical University of Berlin. Both interfaces are powered by 230 VAC. Interface I directly connects the thermocouple input signals with the PCS and includes a converter for generating 24 VDC. This voltage is necessary for operating valves V1 to V6 and DWV1 to DWV6 via twelve digital output signals. In addition, five 24 VDC digital output signals were used to operate electronic relays that are located in the second interface. These relays served as switches for opening and closing the electric circuits installed for heating the reactors (230 VAC, 640 W for the microstructured reactor and 500 W for the tubular reactor) and the tubing before and after the reactors (42 VAC, 3 x 30 W), respectively. However, it has to be noted that heating the tubing was originally planned for the experimental set-up but turned out to be unnecessary and was therefore not installed. Interface II also contains a converter for generating 24 VDC in order to provide power supply for the mass flow controllers. In- and output signals of the MFCs (4...20 mA) were looped through Interface II and linked to the PCS via Interface I. This relatively complex structure was designed mainly for cost reasons, since the inclusion of all electrical transformers and converters into one single interface would have been considerably more expansive.

3.3.3.2 Software

The software enables interactions between the operator and the process control system. Figure 3-8 shows a screenshot of the main window of the PCS. The flow scheme that is displayed is analogous to the flow scheme that was presented in Figure 3-1. All relevant information such as the choice of gas, corresponding volume flows, and temperatures is shown in this process overview. The software package WinErs was also provided by Ingenieurbüro Schoop and used for programming the PCS. The desired operation mode of the set-up can be chosen by clicking one of the bullet points (i.e., “Bypass”, “Mikroreaktor”, “Rohrreaktor”) in the top left part of the main window. Thereby, DVW3 to DWV6 are automatically switched in order permit the gas flow either through the bypass or through one of the two reactors. As mentioned above, gas flows are adjusted by three mass flow controllers, which are calibrated for propane, nitrogen, and synthetic air, respectively. By clicking one of the bullet points on the left side of the main window, different gases with corresponding conversion/ calibration factors for the MFCs can be selected. Except for nitrogen/ helium it has to be verified that the chosen gas is also physically connected to the set-up. The conversion factors are saved in a table that can be accessed as follows: “Alt+Tab” to select WinErs main program, “Bearbeiten” → “Spezielle Blöcke” → “Funktionsgeber”. For each gas a “Funktionsgeber” was defined to supply conversion factors for every gas in comparison to the calibrated gas of each

MFC. However, it has to be noted that some difficulties arose with the correct calibration of the MFCs. As stated above, the output signals for operating the mass flow controllers were chosen to be 4...20 mA. Unfortunately, Interface II does not provide the correct currents (i.e., slight deviations of the minimum/ maximum currents) resulting in an inaccurate behavior of the MFCs. Therefore, all MFC were externally calibrated with an additional mass flow tester (Analyt-MTC Serie 358). The obtained conversion factors were then saved in PCS.

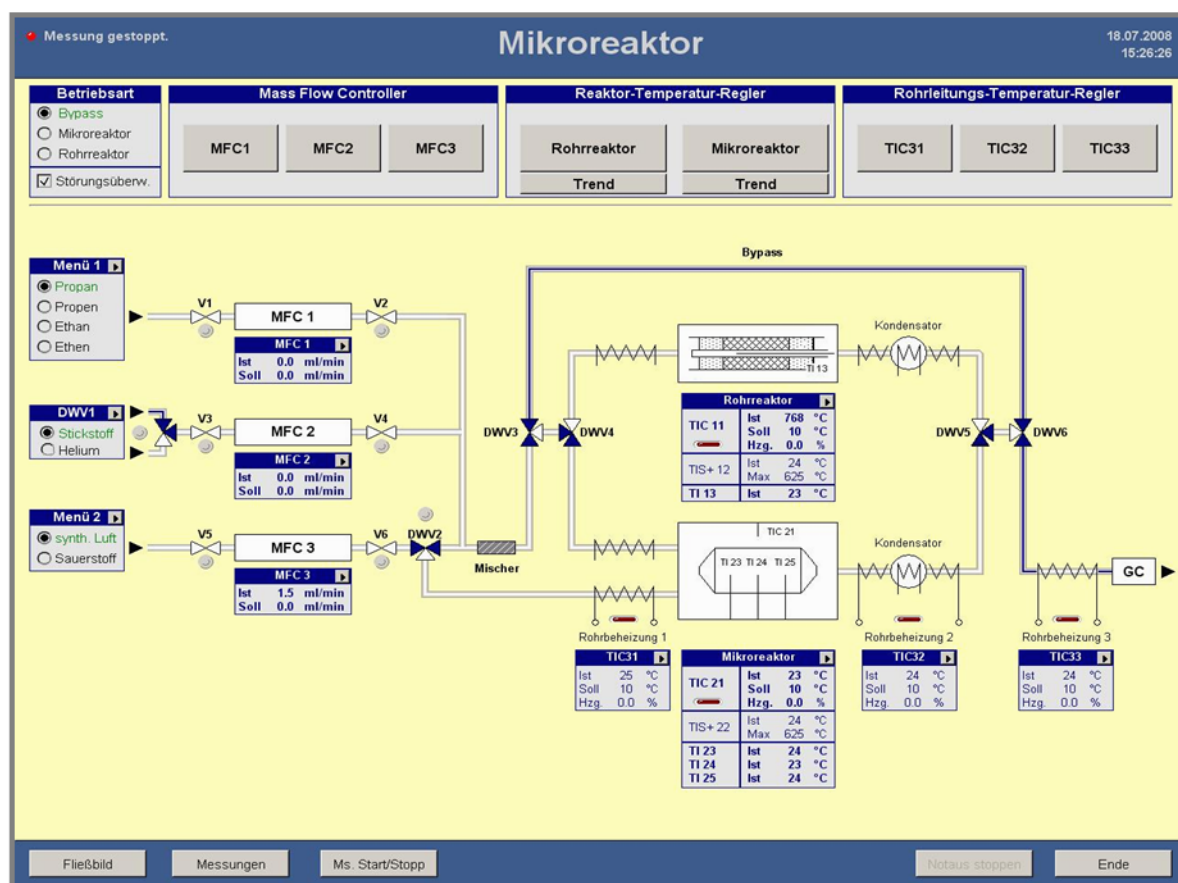


Figure 3-8: Screenshot of process flow for operating the experimental set-up.

In order to design the handling of the experimental set-up as safe as possible even for inexperienced operators, a software based malfunction monitoring system was installed. It can be switched on and off manually in the left top part of the main window by clicking the tick box "Störungsüberwachung". There are two parameters that are constantly surveyed once the system is running. If one of the flows or one of the temperatures deviates from the set-point entered, an alarm message is shown on the screen. The operator is requested to decide, whether the monitoring system should be deactivated or continue to safely shut down the set-up. Unfortunately, the survey of the gas flows does not leave room for small devia-

tions in the range of 0.1 to 0.2 ml_n min⁻¹ between the actual flow and the set-point, making the system in its current configuration rather impracticable.

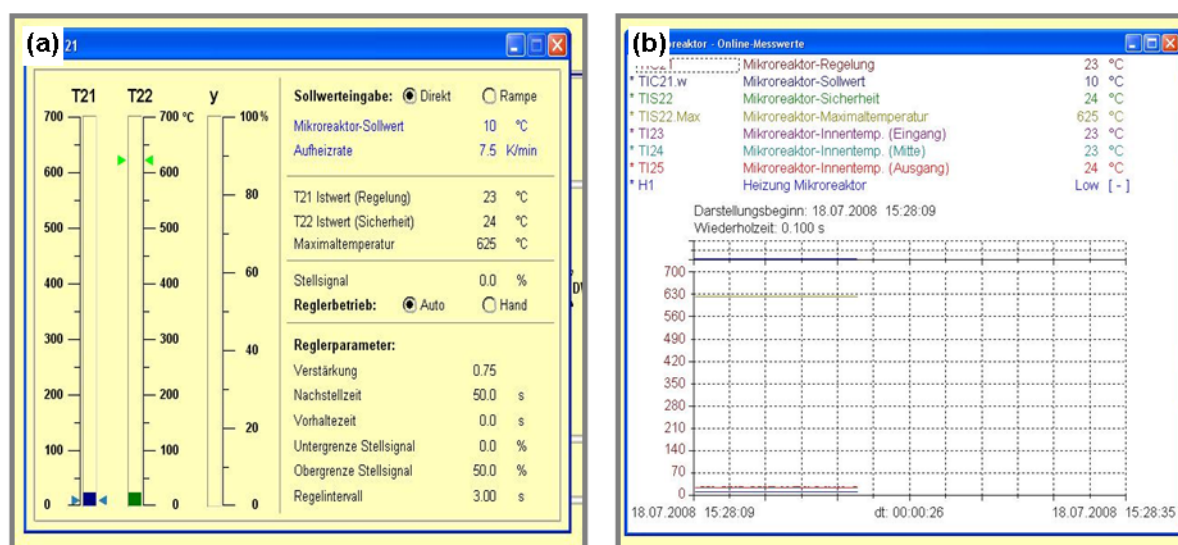


Figure 3-9: Magnified screenshots of (a) temperature control and (b) temperature trend window for microstructured reactor.

Upon a large variety of functionalities that are offered by the PCS, two of them will be described in more detail since they are directly relevant for carrying out catalytic measurements. There are four buttons located in the middle of the top fringe of the main window (i.e., “Rohrreaktor”, “Mikroreaktor”, 2x “Trend”). Clicking one of the reactor buttons opens a dialog window shown in Figure 3-9 (a). This window enables the operator to adjust all parameters that are important for controlling the temperature behavior of the chosen reactor. Most importantly is the set-point for the reactor temperature. By selecting either “Direkt” or “Rampe”, the operator can choose if the temperature should be changed as fast as possible or with a specified rate, which can be entered upon clicking “Aufheizrate”. The operator can also choose, if the temperature control should be carried out by the PCS automatically (“Auto”) or manually (“Hand”). Another important item is the maximum temperature (“Maximaltemperatur”), which sets the limit for the malfunction monitoring system to initiate the shut-off procedure. The temperature control was designed as a PID (German acronym for **P**roportional, **I**ntegral, **D**ifferential) controller. The corresponding parameters can be changed by altering “Verstärkung”, “Nachstellzeit”, and “Vorhaltezeit”. However, it has to be noted that the D part (“Vorhaltezeit”) of the controller does not work properly because of deficiencies in the PCS. Therefore, this parameter was constantly set to zero. In order to optimize the temperature control of the reactors, the script of the PCS has to be adjusted accordingly. The second im-

portant feature is the trend window, which is shown in Figure 3-9 (b). It provides a graphical overview of all temperature curves related to the chosen reactor. The window can be opened by clicking the button “Trend” in the main window of the process control system.

3.3.4 Gaschromatography

Reaction products are analyzed online by a specifically modified gas chromatograph (Shimadzu GC-2014) equipped with two packed columns (i.e., HayeSep Q, 80-100 mesh column and molecular sieve 13X, 60-80 mesh column) for separating O₂, N₂, CO, CO₂, and C₁₊ hydrocarbons. Oxygen and nitrogen are detected by a thermal conductivity detector (TCD), whereas hydrocarbons and methanized carbon oxides are detected by a flame ionization detector (FID). Figure 3-10 (a) shows the oven unit of the gas chromatograph. Helium is used as carrier gas, whereas the FID is operated with hydrogen and synthetic air. The duration of one GC analysis is about 28 min, which is long enough to achieve steady state conditions after reaction parameters are changed. Correlations between peak areas and gas concentrations were established by using test gases and gas mixtures obtained from the MFCs.

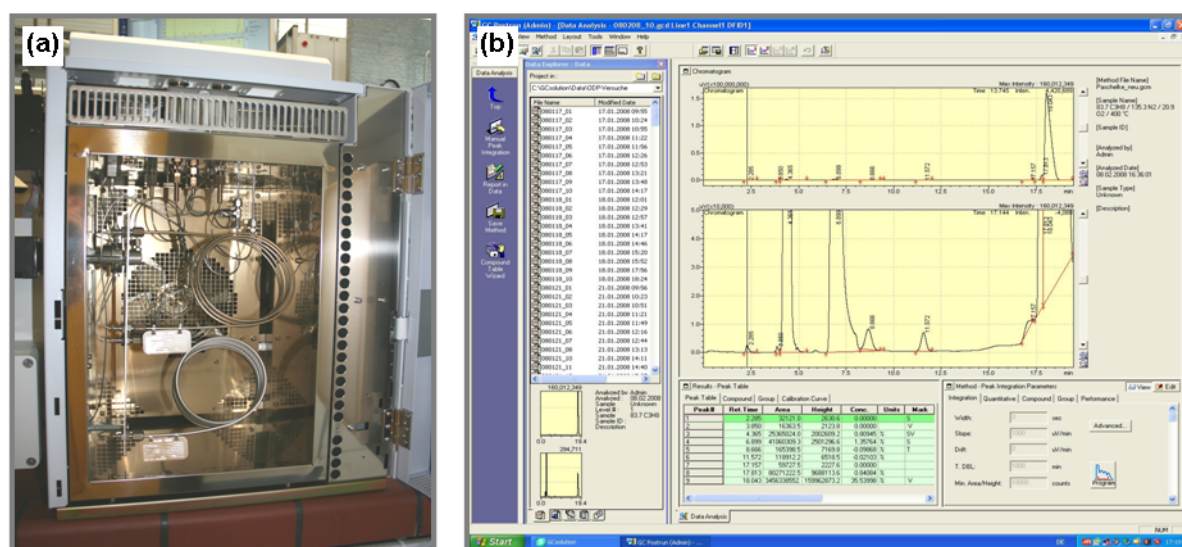


Figure 3-10: Photograph of (a) oven unit with separation columns and (b) screenshot of gas chromatography analysis software.

The gas chromatograph can either be operated by using the interface on the front of the instrument or by using a software system. Figure 3-10 (b) shows a screenshot of a typical chromatogram from ODP experiments. Details on the GC system and the corresponding software can be found in the online manual.

4 VO_x/γ-Al₂O₃ Catalysts in the Oxidative Dehydrogenation of Propane

Vanadium containing catalysts for the oxidative dehydrogenation of propane are commonly obtained from wet impregnation techniques of various supports [72,114-116]. However, no investigations have been performed on materials prepared by ball-milling of support and active component. In the first step, it is important to understand, whether the nature of VO_x species and their catalytic behavior are influenced by the type of vanadium precursor and the preparation method applied. In the second step, a tailor-made catalytic material has to be developed, being suitable for coating the channel surfaces of a microstructured reactor.

4.1 Influence of Preparation Method on Catalytic Behavior

4.1.1 Catalyst Preparation and Characterization

Two sets of VO_x/γ-Al₂O₃ catalysts with increasing vanadium loadings were prepared by wet saturation impregnation of γ-Al₂O₃ and by ball-milling of crystalline V₂O₅ and the same γ-Al₂O₃ (see Chapter 3.1). In order to compare the influence of the preparation method and the resulting nature of VO_x species on the catalytic performance, the vanadium loading was chosen similar for both preparation methods. The samples were thoroughly characterized to get insights into the nature of VO_x species, their distribution, and redox properties. The degree of polymerization of VO_x surface species was investigated and correlated with catalytic activity and selectivity.

The names given to the catalytic samples were organized as follows: “V-X-Y”, where X resembles the preparation method (I = wet saturation impregnation or II = ball-milling of the individual oxides) and Y resembles the apparent surface density of the VO_x species in V atoms per nm². For example, V-I-1.5 refers to a VO_x/γ-Al₂O₃ catalyst prepared by wet saturation impregnation, possessing an apparent VO_x surface density of 1.5 V nm⁻².

The vanadium content and the specific BET surface areas (*S*_{BET}) of the catalytic materials and the pure γ-Al₂O₃ are shown in Table 4-1. For the samples prepared by the wet saturation impregnation method, the vanadium content continuously increases from 1.36 to 6.74 wt.-%. However, it seems that the amount of vanadium that is precipitated on the alumina support during one impregnation cycle is limited. This might be due to the relatively large acetylacetonate complex that occupies a substantial fraction of the alumina surface limiting the space for other VO(acac)₂ molecules to interact with the support surface. Additionally, it was found that the amount of vanadium precipitated per impregnation cycle does not seem to depend on the time the catalyst is treated under reflux. In contrast to the wet impregnation technique,

the amount of vanadium in the catalytic materials that are produced from ball-milling can easily be determined by adding exactly the desired quantity of V_2O_5 to the alumina support.

Table 4-1: Summary of samples used for characterization and catalytic testing.

Impregnation	$\gamma\text{-Al}_2\text{O}_3$	V-I-1.5	V-I-4.3	V-I-5.3	V-I-8.8
V-content [wt.-%]	-	1.36	3.64	4.39	6.74
S_{BET} [$\text{m}^2 \text{g}^{-1}$]	125	109.4	103.4	101.7	97.5
V-density [V nm^{-2}]	-	1.5	4.3	5.3	8.8
Ball-milling	$\gamma\text{-Al}_2\text{O}_3$	V-II-1.5	V-II-4.8	V-II-5.3	V-II-8.8
V-content [wt.-%]	-	1.32	3.96	4.39	6.46
S_{BET} [$\text{m}^2 \text{g}^{-1}$]	125	105.4	101.1	99.4	93.4
V-density [V nm^{-2}]	-	1.5	4.8	5.3	8.8

For the multiply impregnated catalysts, the surface area slightly decreases with increasing vanadium content to a minimum value of $97.5 \text{ m}^2 \text{g}^{-1}$ for V-I-8.8. This is probably due to clogging of pores with VO_x species decreasing the surface area that is accessible for nitrogen adsorption. A similar effect of vanadium loading on the S_{BET} values is also valid for the catalysts prepared by ball-milling of the individual oxides. The lowest S_{BET} of $93.4 \text{ m}^2 \text{g}^{-1}$ was determined for V-II-8.8.

Taking the vanadium content in each catalytic material and the BET surface areas, the apparent VO_x surface densities were calculated as V atoms per nm^2 of the catalytic material. As it is shown in Table 4-1, the densities vary between 1.5 and 8.8 V nm^{-2} . Values of 2.3 and 7.5 V nm^{-2} are suggested to be characteristic for monovanadate and polyvanadate monolayers, respectively [117]. Based on the calculated VO_x surface densities, it is suggested that the obtained materials with 1.5 V nm^{-2} contain predominantly highly dispersed VO_x species. However, an increase in vanadium loading results generally in a transformation of highly dispersed VO_x species to polymerized ones. At the same time, the dispersion of VO_x species decreases simultaneously. Further insights into the distribution of VO_x species on the catalyst surface were derived from in-situ Laser Raman Spectroscopy and UV-vis DRS analysis as well as from X-ray Diffraction and Temperature Programmed Reduction tests.

Both sets of catalytic materials were used for X-ray diffraction (XRD) analysis. All examined samples show broad features of pure $\gamma\text{-Al}_2\text{O}_3$. None of the catalytic samples prepared by wet

saturation impregnation shows any signs of crystalline V_2O_5 . This may be explained either as the presence of only small crystalline particles or as surface VO_x species that cannot be detected by XRD due to the absence of long-range order. On the other hand, V-II-8.8 obtained from ball-milling shows characteristic peaks for V_2O_5 at angles of $2\theta_{diff} = 20^\circ$ (001), 22° (101), 26° (110) and 31° (301, 400). In addition, indications for crystalline V_2O_5 can be found in samples V-II-5.3 and V-II-4.8.

Scanning electron microscopy (SEM) was used to visualize the catalysts' surface. SEM images of V-I-1.5 and V-I-8.8 are shown in Figure 4-1. They were taken with a magnification of 10,000 in case of the lowly loaded sample and 20,000 in case of the highly loaded sample.

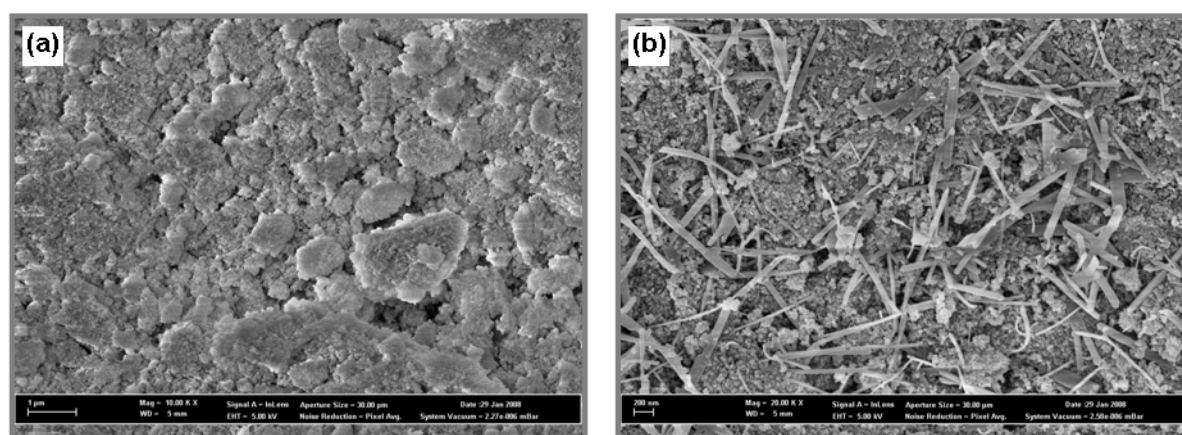


Figure 4-1: SEM images of (a) V-I-1.5 and (b) V-I-8.8, scale bar 1 μm and 200 nm.

V-I-1.5 in Figure 4-1 (a) shows only typical features of the γ - Al_2O_3 support material. There is no indication of crystalline V_2O_5 , whereas the surface of V-I-8.8 in Figure 4-1 (b) is slightly covered with orthorhombic V_2O_5 needles. In comparison, V-II-8.8 obtained from ball-milling shows fractured vanadia particles with a size much larger than the needles mentioned above (images not shown for sake of brevity). In case of the catalysts from ball-milling, these particles were also detected by XRD experiments.

4.1.2 Nature of VO_x Species

Since sensitivity of X-ray diffraction is limited to detect crystalline V_2O_5 and blind to dispersed VO_x species, Laser Raman Spectroscopy (LRS) and UV-vis DRS characterization studies were also undertaken in order to obtain more definitive information about the possible presence of crystalline V_2O_5 nanoparticles and surface VO_x species. Figure 4-2 (a) and (b) show Raman spectra within the spectral range from 750 to 1150 cm^{-1} since characteristic bands

due to the V=O stretching vibration of crystalline V_2O_5 as well as dispersed VO_x species can be detected in this interval [118].

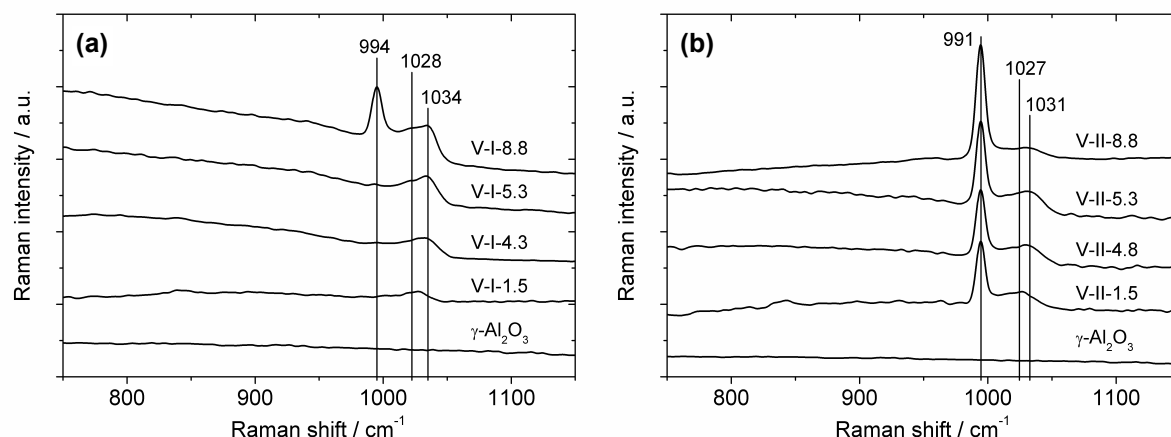


Figure 4-2: Raman spectra recorded at 514 nm laser excitation at room temperature after dehydration of (a) impregnated and (b) ball-milled catalysts.

The band at about 990 cm^{-1} is a sensitive indicator for crystalline V_2O_5 . For samples prepared by wet saturation impregnation, only V-I-8.8 shows a band at this Raman shift, confirming SEM results and indicating that the VO_x species in the other samples in this set must be well dispersed on the surface of the catalysts. However, it should be noted that the Raman cross section of V=O bonds in crystalline V_2O_5 is about ten times higher than that in dispersed VO_x [119]. Although this estimate was done on the basis of silica supported materials, it serves as a good approximation for alumina supported materials as well. Therefore, the band at 994 cm^{-1} in the spectrum of the sample with the highest loading points to the presence of only moderate amounts of crystalline V_2O_5 compared to the amount of dispersed VO_x (band above 1000 cm^{-1}). This band shifts from 1028 to 1034 cm^{-1} for V-I-1.5 and V-I-8.8, respectively and can be assigned to the symmetric vibration of the terminal V=O bond [120,121]. The shift is due to the evolution of dispersed VO_x surface species from monovanadates to polyvanadates to crystalline V_2O_5 on the alumina support. In comparison, the Raman spectra of the samples prepared by ball-milling are dominated by a distinct band at 991 cm^{-1} indicating the presence of crystalline V_2O_5 . However, the band above 1000 cm^{-1} shows that a significant proportion of the originally crystalline V_2O_5 has spread on the alumina surface during the calcination step [89], forming dispersed VO_x species, if cross sections are taken into account. This band also undergoes a slight change from 1027 to 1031 cm^{-1} , which can be explained as above.

Raman experiments clearly showed that in addition to crystalline V_2O_5 all samples contain dispersed VO_x species, too. In order to get further insights into the type and degree of polymerization of the VO_x species, UV-vis DRS was performed for both sets of catalytic materials. The spectra were recorded at 500 °C in a 20/80 O_2/Ne flow. For the set of catalysts prepared by wet saturation impregnation the characteristic absorbance shifts to higher wavelengths with an increase in vanadium loading (spectra not shown for sake of brevity). This shift indicates an increasing degree of polymerization and/ or co-ordination of the VO_x species. The same trend can be observed for the samples prepared by ball-milling.

Results from Raman spectroscopy gave already rise to the assumption that some of the crystalline V_2O_5 that was used for preparing the second set of catalytic samples must have spread on the catalysts' surface to form amorphous VO_x species. In order to verify this hypothesis, UV-vis spectra of the low loaded sample obtained from ball-milling (V-II-1.5) was recorded before and after calcination at 500 °C. As it is shown in Figure 4-3, the spectrum before calcination is relatively broad which can be attributed to pure crystalline V_2O_5 . Similarly shaped spectra were also recorded for the samples with a higher VO_x surface density indicating only little differences between all uncalcined catalytic materials. However, after calcination the characteristic absorbance shifts to smaller wavelengths. Therefore, it can be concluded that a significant proportion of the crystalline V_2O_5 spreads on the catalysts' surface and forms dispersed VO_x species.

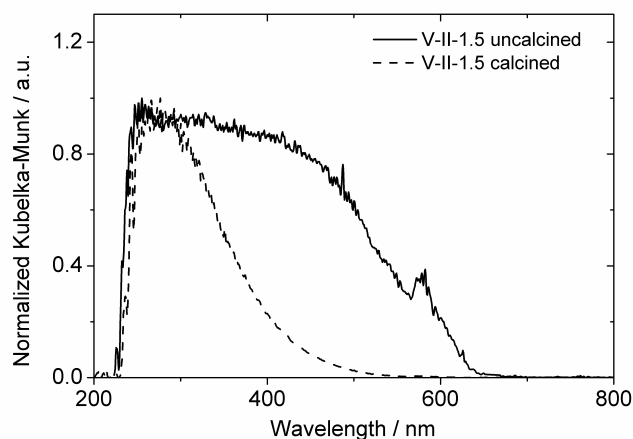


Figure 4-3: UV-vis spectra of V-II-1.5 before and after calcination at 500 °C in a 20/80 O_2/Ne flow ($40\text{ ml}_n\text{ min}^{-1}$).

Since UV-vis spectra reflect the structure of valence and conduction bands in bulk solids, absorption edge energies were used in order to quantify the electronic properties of the studied materials. To this end, we applied Tauc's law [122]. The edge energy is determined from

the intersect of a linear function of $[F(R_{\infty}) \times h\nu]^{1/2}$ vs. $h\nu$ with the $h\nu$ axis as it is shown in Figure 4-4.

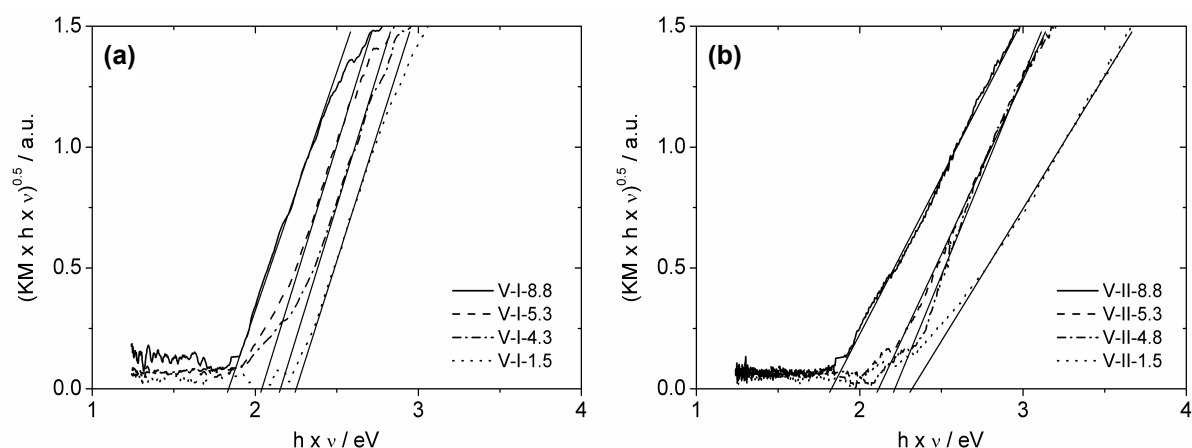


Figure 4-4: Tauc's plots of (a) impregnated and (b) ball-milled catalysts oxidized in a 20/80 O_2/Ne flow at 500 °C.

The estimated edge energies E_g for both sets of catalytic materials are summarized in Figure 4-5 as a function of apparent VO_x surface density. It can be seen that E_g generally decreases with an increase in VO_x surface density for both sets of catalytic materials. However, edge energies for the V-II series at similar VO_x surface densities are higher than for the V-I series. The reason for this finding could not be fully resolved. Also the decrease of edge energies for the V-II series is somewhat more pronounced than for the V-I series. Similar results have previously been reported by Chen et al. for Al_2O_3 supported VO_x species [77].

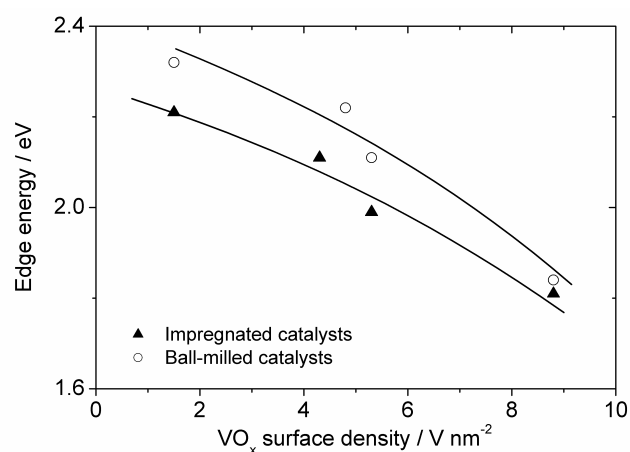


Figure 4-5: E_g values of all investigated materials as a function of VO_x surface density.

In order to get insights into the reducibility of the different VO_x species, Temperature Programmed Reduction (TPR) experiments with hydrogen were performed over both sets of catalytic materials. Figure 4-6 shows the outlet H_2 concentration as a function of temperature. For comparison, the H_2 concentration profile of V_2O_5 is also presented. It is characterized by two distinct peaks at temperatures of 673 and 705 °C, which is in good accordance with the literature [118,123]. For catalysts prepared by wet saturation impregnation, the temperature of maximum reduction rate (T_{max}) varies with VO_x surface coverage. A single peak with a minimum at 535 °C can be found for V-I-1.5, which first shifts to lower temperatures for V-I-4.3 (518 °C) and V-I-5.3 (505 °C) before it shifts back to 521 °C for V-I-8.8. It is generally accepted that polymeric VO_x species are reduced at somewhat lower temperatures than monomeric VO_x species and V_2O_5 crystallites. These findings are in good agreement with studies by Martínez-Huerta et al. who found a resembling behavior for their $\text{VO}_x/\gamma\text{-Al}_2\text{O}_3$ samples [124]. The same trends can be found for the catalytic materials produced from ball-milling (i.e., a shift to lower and consequently back to higher T_{max} values for increasing VO_x surface coverage). However, the observed T_{max} values are generally higher than for the impregnated samples, which can be attributed to the larger fraction of V_2O_5 crystallites that exist in the V-II series. In addition, starting from V-II-5.3 a slight shoulder to the left of the main peak can be found in the profiles. This shoulder is assigned to well-dispersed polymeric VO_x species that co-exist with crystalline V_2O_5 in this set of samples.

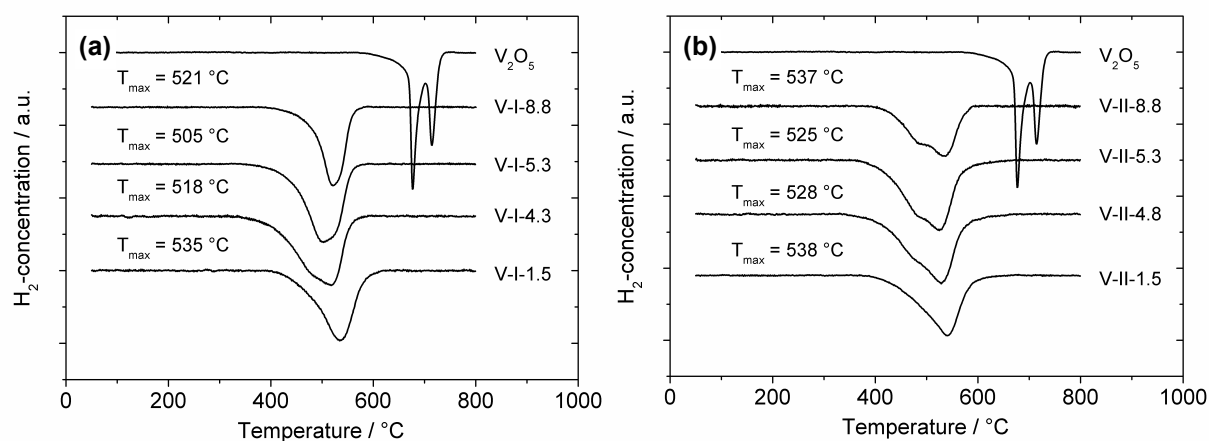


Figure 4-6: TPR profiles of (a) impregnated and (b) ball-milled catalysts in a 5/95 H_2/Ar flow (25 mln min^{-1} , catalyst masses 35 to 180 mg, heating rate 10 °C min^{-1}).

The peaks related to the maximum of H_2 consumption at 673 and 705 °C over pure crystalline V_2O_5 cannot be found in any of the catalytic samples that are known to contain vanadia crystallites. This phenomenon is due of the domain size of vanadia crystals, which is much

larger in bulk V_2O_5 than in the crystallites that can be found on the catalysts' surface [114]. The two high temperatures peaks at 673 and 705 °C (and a third peak at about 860 °C) were assigned by Bosch et al. to a reduction sequence of bulk V_2O_5 as follows: $V_2O_5 \rightarrow V_6O_{13} \rightarrow V_2O_4 \rightarrow V_2O_3$ [125]. In comparison, smaller vanadia surface crystallites are reduced at significantly lower temperatures and do not undergo this specific sequence, which explains the absence of these peaks in all examined samples.

4.1.3 Role of VO_x Species in Catalysis

ODP experiments were carried out using a six-channel screening apparatus with fixed bed tubular continuous flow reactors made of quartz glass (inner diameter 6 mm) with plug flow hydrodynamics at ambient pressure. For catalytic measurements both sets of materials were taken as fine powders with a particle diameter $< 100 \mu m$ (the grains from wet saturation impregnation were ground again) to positively avoid mass transport phenomena. For better heat transfer, all catalysts were diluted with 1.5 g quartz sand, resulting in similar lengths of the fixed bed. The reactors containing the diluted catalyst between two layers of quartz were immersed into a fluidized bed of sand serving as a thermostat to provide near isothermal operation conditions. Blind tests of empty reactors, reactors filled with quartz sand and pure $\gamma-Al_2O_3$ did not lead to detectable conversions up to 500 °C. The composition of the inlet flow was $C_3H_8/O_2/N_2 = 2/1/4$, using synthetic air as oxygen source. Catalytic tests were carried out at 500 °C. In order to achieve different degrees of C_3H_8 conversion, catalyst amounts and total volume flows were varied from 5 to 100 mg and 30 to 200 $ml_n \text{ min}^{-1}$, respectively. As reaction products, C_3H_6 , CO, CO_2 , and H_2O were detected. Propane conversion ($X_{C_3H_8}$) and propene selectivity ($S_{C_3H_6}$) were calculated from inlet and outlet concentrations according to Equations 4-1 and 4-2, whereas reaction rates [$mol_{C_3H_8} \text{ g}^{-1} \text{ s}^{-1}$] were determined according to Equation 4-3:

$$X = \frac{c_{C_3H_{8,0}} - c_{C_3H_8}}{c_{C_3H_{8,0}}} \quad (4-1)$$

$$S = \frac{c_{C_3H_6}}{c_{C_3H_{8,0}} - c_{C_3H_8}} \quad (4-2)$$

where $c_{C_3H_{8,0}}$ is the concentration of propane at the reactor inlet and $c_{C_3H_8}$ and $c_{C_3H_6}$ are the concentrations of propane and propene at the reactor outlet.

$$r_m = \frac{X_{C_3H_8} \cdot p_{C_3H_8} \cdot \dot{V}}{m_{Cat} \cdot V_m} \quad (4-3)$$

where $p_{C_3H_8}$ is the partial pressures of propane at the reactor inlet, \dot{V} the total volumetric flow of reactants, m_{Cat} the catalyst mass used for experiments, and V_m the molar gas volume at 0 °C and 101325 Pa.

Figure 4-7 shows a comparison between samples with a low and a high VO_x surface density, respectively. In general, propane conversion increases with increasing modified residence time as can be seen in Figure 4-7 (a). This is true for all samples although the increase is slightly stronger for catalysts with a higher VO_x surface density. This figure also demonstrates that the overall activity increases with an increase in VO_x surface density. However, propene selectivity decreases with increasing propane conversion as shown in Figure 4-7 (b). The decrease is due to the consecutive combustion of primarily formed propene to CO_x . Additionally, it can be observed that catalysts with higher VO_x surface densities are not as selective as catalysts with a lower VO_x surface density. This is in good accordance with the literature and experiments that were conducted previously [112]. Interestingly, activity and selectivity behavior is almost identical for both catalytic materials that were obtained from very different preparation methods and vanadium precursors.

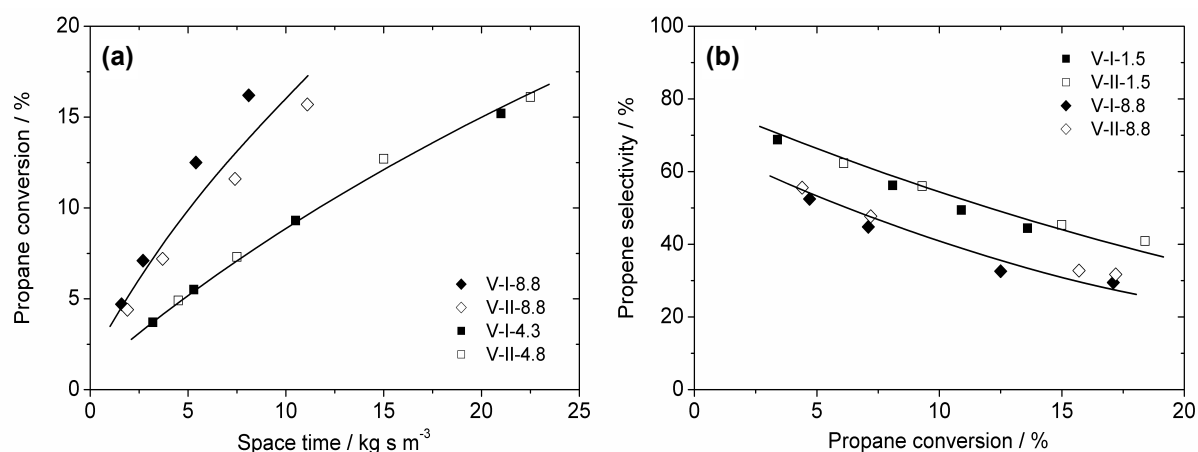


Figure 4-7: Activity for (a) propane conversion and (b) selectivity towards propene of catalysts from wet saturation impregnation (■,◆) and ball-milling (□,◇).

The results of our characterization analysis gave evidence that the degree of polymerization of the VO_x species increases with increasing VO_x surface density for both sets of catalytic materials. In the same way, catalytic activity increases with increasing VO_x surface density,

whereas selectivity towards propene decreases at similar degrees of propane conversion. Figure 4-8 (a) shows propane consumption rates calculated corresponding to Equation 4-1 versus edge energies estimated from the transformed UV-vis spectra for both sets of $\text{VO}_x/\gamma\text{-Al}_2\text{O}_3$ materials, whereas Figure 4-8 (b) shows selectivity towards propene at about 5 % C_3H_8 conversion also versus edge energies.

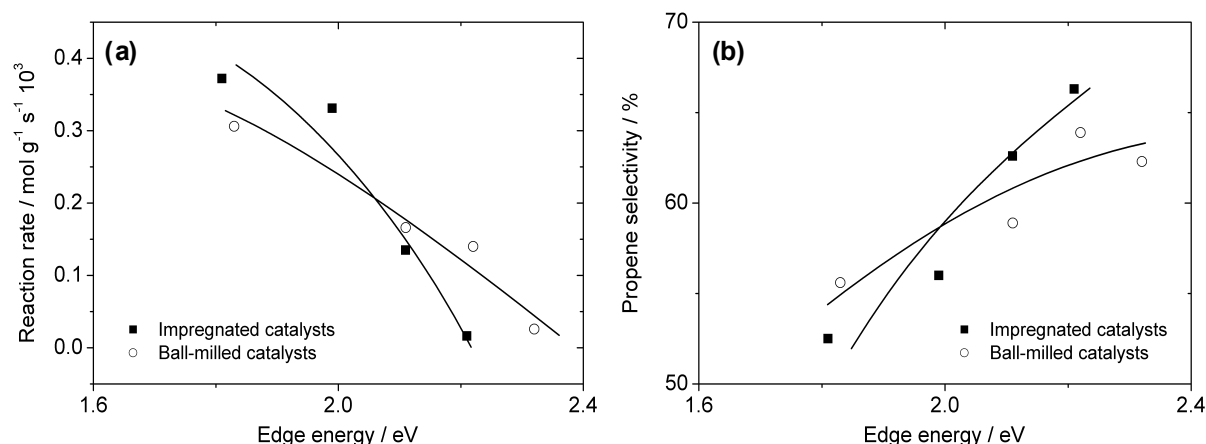


Figure 4-8: Reaction rate (a) and propene selectivity at 5 % propane conversion (b) as a function of E_g for catalysts derived from wet saturation impregnation (■) and ball-milling (○).

It can be seen that with decreasing edge energy, overall catalytic activity generally increases. Since the edge energy is related to the band gap in the electronic structure of VO_x species, it is expected that the total electrical conductivity of $\text{VO}_x/\gamma\text{-Al}_2\text{O}_3$ materials increases with a decrease in edge energy (i.e., an increase in the apparent vanadium surface density). Kondratenko and Baerns have previously proven that $\text{VO}_x/\gamma\text{-Al}_2\text{O}_3$ materials are typical n-type conductors and their conductivity increases with an increase in vanadium loading [91]. The increase in conductivity is due to an increased concentration of charge carriers (i.e., electrons). Generally, the electron concentration is determined by the energy gap between the valence (lattice oxygen) and conducting (metal cations) bands; the lower the gap, the higher the electron concentration. According to [77], the activation energy for breaking the C-H bond in C_3H_8 adsorbed over VO_x species depends on the energy for electron transfer from the oxygen to the metal center. Based on the discussion above, it is suggested that the increase in catalytic activity with a decrease in edge energy (as shown in Figure 4-8 (a)) is due to an improved ability of metal cations for accepting electrons. Figure 4-9 schematically illustrates the electron transfer from O^{2-} to V^{5+} upon breaking of the C-H bond in propane over VO_x species and under photon excitation of this species. It has to be stressed that this illustration is

not only valid for vanadyl oxygen species but also for bridged oxygen species between two vanadium species or between one vanadium atom and one metal species of the support.

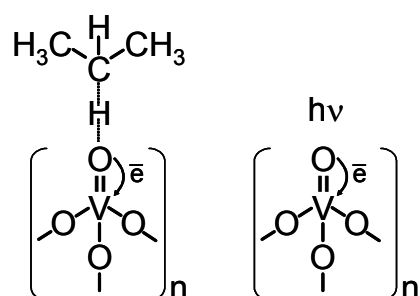


Figure 4-9: Schematic illustration of electron transfer from O^{2-} to V^{5+} upon breaking the C-H bond in C_3H_8 adsorbed over VO_x and under photon irradiation.

However, the dependencies for the V-I and V-II series slightly differ (i.e., the increase in activity is more pronounced for the impregnated samples than for the samples from ball-milling). For both series with increasing vanadium content the distribution of VO_x surface species shifts from monovanadates to polyvanadates to crystalline V_2O_5 . The same behavior was previously reported and also quantified through UV-vis DRS experiments by co-workers of Wachs' group [126,127]. However, our Raman characterization showed that all samples of the V-II series contain crystalline V_2O_5 , which is known to be less active for propane conversion and less selective towards propene. Therefore, the dependency of the reaction rate on edge energy for the samples from ball-milling is not as pronounced as for the samples from wet saturation impregnation.

Selectivity towards propene at similar degrees of propane conversion generally increases with increasing edge energies as shown in Figure 4-8 (b). It implies that VO_x species with a higher degree of polymerization tend to be less selective towards propene production than VO_x species with a lower degree of polymerization. As described above, total electrical conductivity of the $VO_x/\gamma-Al_2O_3$ materials increases with decreasing edge energies, which results in a higher activity for propane conversion. However, catalytic activity does not only increase for propane conversion as described by the rate constant $k(C_3H_8)$, but also for propene conversion as described by the rate constant $k(C_3H_6)$. If activity increases with increasing vanadium content (i.e., increasing degree of polymerization), selectivity towards propene depends on the ratio of $k(C_3H_6)/k(C_3H_8)$. The stronger the increase of $k(C_3H_6)$ with increasing vanadium content in comparison to the increase of $k(C_3H_8)$, the lower the selectivity towards propene. This relationship was previously shown by Argyle et al. [88].

However, it has to be noted that the dependencies for the V-I and V-II series experience a slightly different slope. The increase in selectivity with increasing E_g is more pronounced for the impregnated samples than for samples from ball-milling. Since all samples from ball-milling contain crystalline vanadia, which is known to be less active and less selective, the transformation of the fraction of dispersed VO_x surface species from monovanadates to polyanadates to V_2O_5 crystallites is not as significant as in the samples from wet saturation impregnation. Therefore, the dependency in Figure 4-8 (b) for the V-II series is less intense as for the V-I series.

4.2 Tailor-made Catalysts for Microstructured Reactors

4.2.1 Catalyst Preparation and Characterization

$\text{VO}_x/\gamma\text{-Al}_2\text{O}_3$ powder catalyst samples with varying vanadium content were prepared according to the descriptions in Chapter 3.1 and thoroughly characterized. Four different catalytic materials with vanadium contents of 1.4, 3.4, 5.3, and 7.8 wt.-% V were obtained. The corresponding VO_x surface densities were determined to be 2.1, 5.2, 8.3, and 12.5 V nm^{-2} , respectively. The BET surface area of the investigated catalysts as a function of their vanadium content is shown in Figure 4-10 (a). The pure $\gamma\text{-Al}_2\text{O}_3$ support material provides a surface area of $80 \text{ m}^2 \text{ g}^{-1}$. With increasing vanadium content the catalyst suffers a loss of surface area, probably due to clogging of micropores with vanadia.

To get insight into the dispersion of the vanadia species on the catalyst surface, UV-vis DRS, XRD and LRS experiments were performed. UV-vis spectra of the investigated catalysts are shown in Figure 4-10 (b). It can be seen that with increasing vanadium content the characteristic absorbance becomes wider and shifts to higher wavelengths indicating an increasing degree of polymerization and/ or co-ordination of the VO_x species. By analogy with literature [91,118], it can be concluded that the 1.4 wt.-% V sample contains well dispersed VO_x species, whereas the 3.4 wt.-% V sample additionally contains oligomerized, but still dispersed aggregates. The 5.3 and 7.8 wt.-% V samples are dominated by bands of V-O-V bonds indicating the presence of polymerized and crystalline vanadia bulk phase. However, it is difficult to identify separate vanadia species from this data.

The results of the UV-vis DRS analysis are confirmed by the XRD patterns of the catalysts that can be seen in Figure 4-10 (c). Independent of the loading, the diffractograms are dominated by broad features of $\gamma\text{-Al}_2\text{O}_3$, which correspond to the diffractogram of the pure $\gamma\text{-Al}_2\text{O}_3$ support shown at the top of the diagram. The diffractogram of crystalline V_2O_5 is given at the bottom of the diagram, serving as a reference for crystalline V_2O_5 bulk phase on the cata-

lyst's surface. It has characteristic peaks at $2\theta_{\text{diff}} = 20, 22, 26,$ and 31° . The pattern of crystalline V_2O_5 can be observed only in the 7.8 wt.-% V sample's diffractogram but are not detectable for the catalysts with ≤ 5.3 wt.-% V.

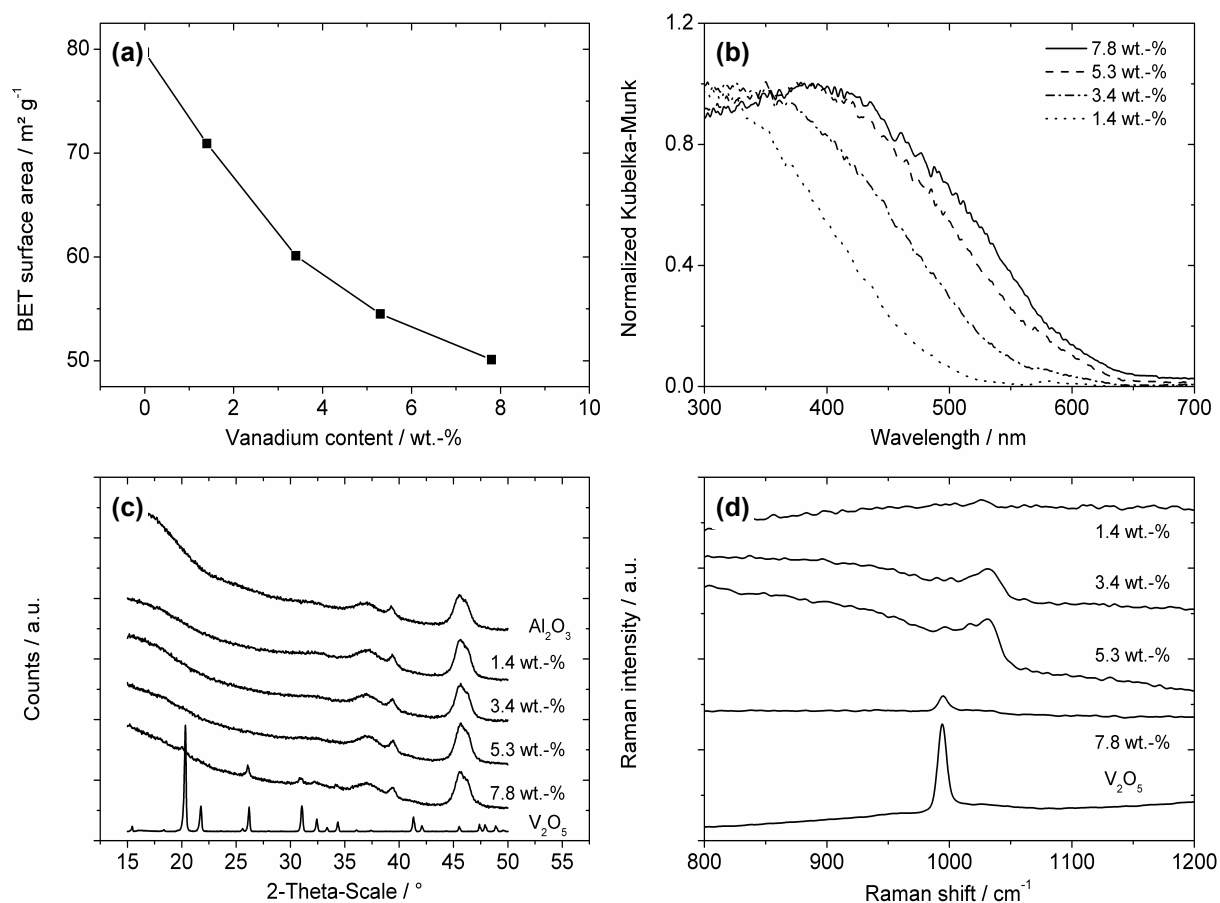


Figure 4-10: (a) BET surface area at 77 K, (b) UV-vis spectra in O_2 flow at 773 K, (c) XRD patterns measured at room temperature, and (d) Raman spectra (recorded at room temperature after dehydration) of investigated $\text{VO}_x/\gamma\text{-Al}_2\text{O}_3$ catalyst samples with varying vanadium content; (a) and (c) also contain data of pure $\gamma\text{-Al}_2\text{O}_3$, (c) and (d) also of crystalline V_2O_5 .

Since sensitivity of X-ray diffraction for crystalline V_2O_5 is limited, the investigated catalysts were further characterized by Laser Raman Spectroscopy. The spectral range from 800 to 1200 cm^{-1} is shown in Figure 4-10 (d), since characteristic peaks due to the $\text{V}=\text{O}$ stretching vibration of crystalline V_2O_5 as well as dispersed VO_x species can be detected in this range [118]. At the bottom of Figure 4-10 (d), the spectrum of crystalline V_2O_5 is shown as reference. The band at 994 cm^{-1} is a sensitive indicator for crystalline V_2O_5 . The catalyst with 7.8 wt.-% V shows a strong band at 994 cm^{-1} indicating a significant fraction of V_2O_5 . However, it should be noted that the Raman cross section of $\text{V}=\text{O}$ in crystalline V_2O_5 is about 10

times higher than that in dispersed vanadia [119]. Therefore, the shoulder at 994 cm^{-1} in the spectrum of the catalyst with 5.3 wt.-% V points to the presence of only little crystalline V_2O_5 as compared to the amount of dispersed vanadia (band around 1026 cm^{-1}). The shoulder of the band at 1017 cm^{-1} may indicate a second type of dispersed VO_x species. At a vanadium content of $\leq 3.4\text{ wt.-% V}$ the band of crystalline V_2O_5 is no more detectable, which strongly suggests that only negligible amounts of crystalline V_2O_5 are present. For the catalyst with 1.4 wt.-% V almost no VO_x can be detected due to the low vanadium content.

4.2.2 Functional Catalyst Characterization

ODP experiments were carried out using a six-channel screening apparatus in fixed bed tubular continuous flow reactors made of quartz glass (inner diameter 6 mm) with plug flow hydrodynamics at ambient pressure. The catalyst particle diameter was chosen to be 100 to 300 μm . For better heat transfer, all catalyst samples were diluted with 1.9 g quartz sand, resulting in similar lengths of the fixed bed. The reactors containing the diluted catalyst between two layers of quartz were immersed into a fluidized bed of sand serving as a thermostat to provide near isothermal operation conditions. Blind tests of empty reactors, quartz sand, and pure $\gamma\text{-Al}_2\text{O}_3$ did not lead to detectable conversions up to $500\text{ }^\circ\text{C}$. The composition of the inlet flow was $\text{C}_3\text{H}_8/\text{O}_2/\text{N}_2 = 2/1/4$, using synthetic air as oxygen source. Experiments were carried out in a temperature range from 400 to $525\text{ }^\circ\text{C}$ with catalyst masses from 7.6 to 199.7 mg and total volume flows from 30 to $240\text{ ml}_n\text{ min}^{-1}$. As reaction products C_3H_6 , CO, CO_2 , and H_2O were detected. Propane conversion ($X_{\text{C}_3\text{H}_8}$) and propene selectivity ($S_{\text{C}_3\text{H}_6}$) were calculated from inlet and outlet concentrations according to Equations 4-1 and 4-2.

All catalytic samples were tested for their activity and selectivity in the ODP. As can be seen from Figure 4-11 (a), propane conversion increases almost linearly with an increase in modified residence time under isothermal conditions. The catalyst with 7.8 wt.-% V shows the highest activity followed by the less loaded catalysts. However, the increase of activity with increasing vanadium content does not seem to be linear.

Therefore, the catalysts' activities on the basis of propane conversion per catalyst mass with increasing vanadium content are shown in Figure 4-11 (b). The activity of the investigated $\text{VO}_x/\gamma\text{-Al}_2\text{O}_3$ catalysts in the ODP increases with increasing vanadium content. The increase is not linear since in case of the presence of crystalline V_2O_5 , a certain amount of vanadia cannot interact catalytically because it is not accessible for gas phase reactants. The same effect results from clogging of micropores at higher loadings.

Due to limited capacities for loading microstructured reactors with catalytic material, the catalyst with 5.3 wt.-% V possessing a rather high activity was chosen for further coating experiments. The use of highly active catalysts is favorable in micro reactors, since reaction heat can be dissipated easily due to the high surface-to-volume ratio of the microstructure.

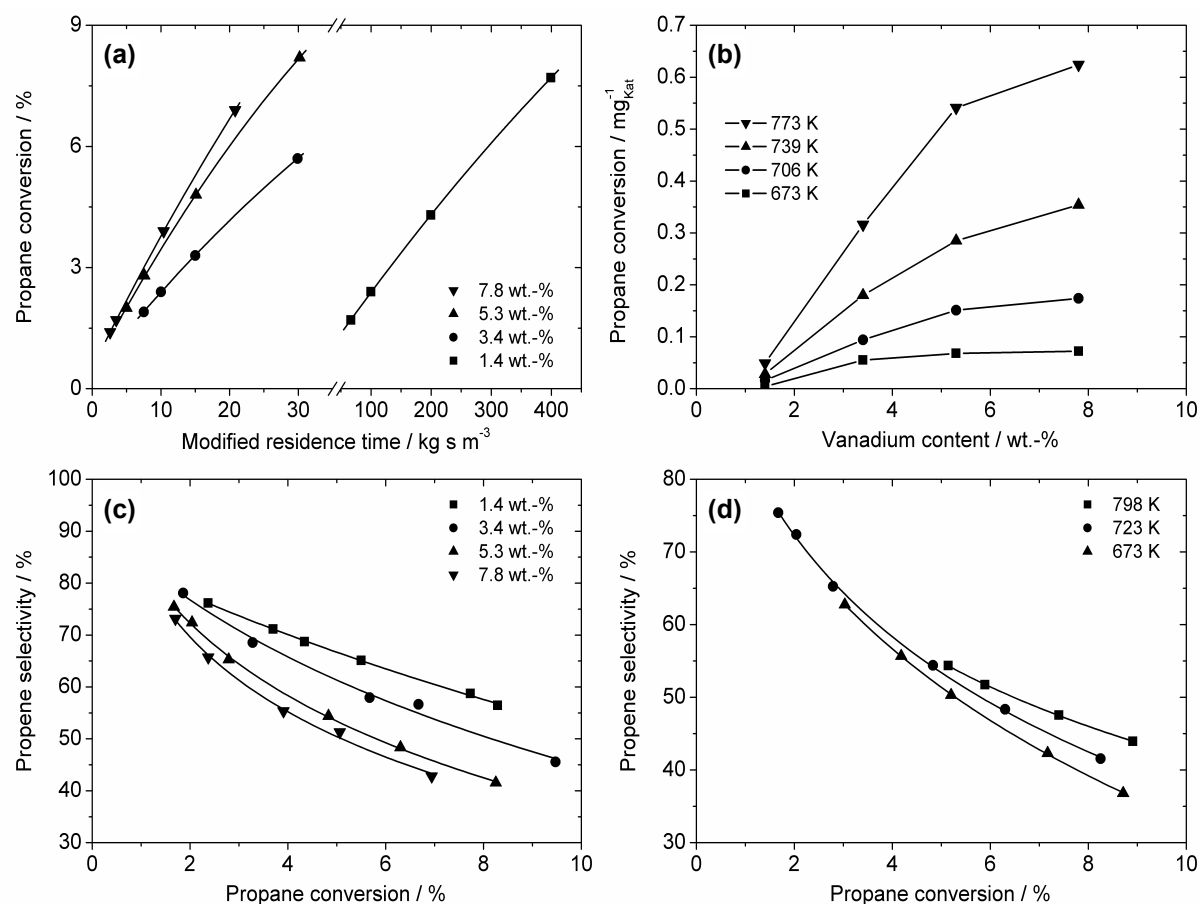


Figure 4-11: Catalytic activity for (a) varying modified residence times at 723 K, (b) increasing vanadium content (volume flow 120 ml_n min⁻¹), and selectivity conversion trajectories for (c) differently loaded catalysts at 723 K, and (d) different temperatures for a 5.3 wt.-% V catalyst, all measured at a constant molar ratio of C₃H₈/O₂/N₂ = 2/1/4.

Additionally to activity aspects, the catalytic materials were tested for selectivity. Selectivity conversion trajectories were measured under isothermal conditions at 450 °C only by a variation of residence time. As shown in Figure 4-11 (c), selectivity towards propene is strongly dependent on propane conversion and surface coverage of the support material.

In general, selectivity decreases with increasing conversion because propene is rapidly oxidized to CO and CO₂ [112]. Total oxidation of propane to CO_x can be neglected since the S-axis intercept for all trajectories seems to be near 100%, indicating the absence of parallel

reactions to the oxidative dehydrogenation. The loss of selectivity goes parallel with increasing surface coverage with vanadia on the support material, being in good accordance with a study by Argyle et al. [88]. Consequently, the lower selectivity may be attributed to the presence of higher polymerized VO_x species and crystalline V₂O₅. It appears that isolated VO_x species and/ or smaller VO_x aggregates provide the highest selectivity in the ODP. This may be explained by the absence of directly neighbored active sites, minimizing consecutive combustion of propene at low vanadia loadings. From physico-chemical characterization it is difficult to determine the exact structure of the VO_x species. However, with regard to an optimum propene yield, the use of a highly dispersed VO_x/γ-Al₂O₃ catalyst seems to be reasonable although activity aspects have to be considered (as explained above).

The dependence of selectivity on temperature for a 5.3 wt.-% V catalyst was investigated, too. As can be seen from Figure 4-11 (d), propene selectivity increases with increasing temperature, which is in good agreement with the literature [112]. This positive effect seems to be stronger at higher propane conversions. However, the impact of temperature is only weak in comparison to a variation of the vanadium content.

5 Reactor Manufacturing and Catalytic Coatings

The development and optimization of the microstructured reactors was focused on the preparation of the catalytic coatings and the soldering process of the modules. The stability of both, coatings and reactors is crucial for the maintenance of a high catalytic long-term performance, safe operation conditions, and economic feasibility. However, our research activities were not exclusively focused on the ODP reaction. Therefore, all methods and processes were developed with respect to the general applicability of microstructured reactors for heterogeneously catalyzed gas phase reactions.

5.1 Fabrication of Reactor Modules

The concept that was followed for fabricating the microstructured reactors is schematically shown in Figure 5-1. In the first step, micro channels were created by wet chemical etching on stainless steel platelets (length 75 mm, width 75 mm, thickness 0.5 mm).

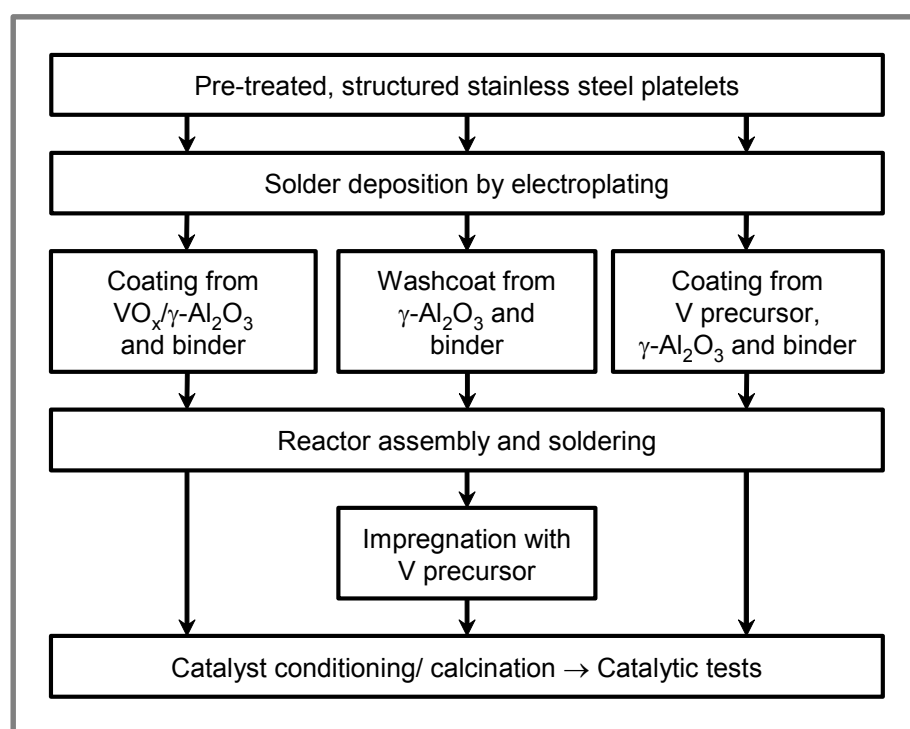


Figure 5-1: Simplified manufacturing concept for microstructured reactors.

In the second step, a tailor-made solder system from individual layers of Ni (barrier layer between the base and solder material), Ag, and Sn was deposited on the platelets by standard galvanic techniques developed by Atotech Deutschland GmbH [39,40]. Coating thickness and thickness distribution thereof were detected by XRF (Fischerscope XDVM-T5). Areas on

the platelets subsequently used for bonding were protected with a peelable mask leaving only the micro channels exposed. The specialized procedures for coating the micro channel surfaces with catalyst are described below.

Figure 5-2 (a) shows a schematic drawing of the microstructured reactors that were used for the following part of the present study. They consist of four single channel platelets (channel geometry: length 31 mm, width 25 mm, depth 0.23 mm, volume per channel 0.169 cm^3 , internal surface area per channel 7.35 cm^2 , without considering roughness of the etched base material) as shown in Figure 5-2 (b). In addition, a modified platelet design for inserting four thermocouples in between the catalyst coated platelets was applied (see Figure 5-2 (c)). Three thermocouples for temperature measurement were placed at equal distances along the catalyst bed, whereas the fourth thermocouple for temperature control was placed in some distance from the catalyst bed. The catalyst coated platelets were assembled with two thermocouple platelets, a top platelet (thickness 5 mm, stainless steel, see Figure 5-2 (d)), and a bottom platelet (thickness 1 mm, stainless steel, see Figure 5-2 (e)), pressed together, and soldered at $400 \text{ }^\circ\text{C}$ under vacuum conditions [40]. Tubes used as gas in- and outlet were attached to the top platelets by welding, before final assembly of the reactors.

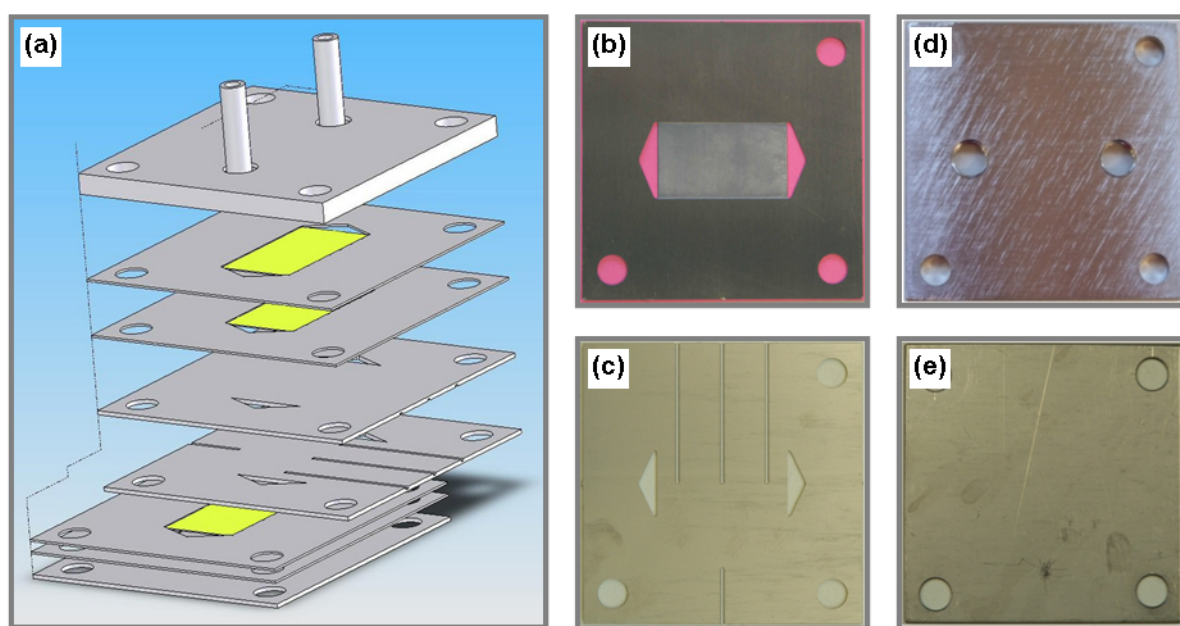


Figure 5-2: Schematic drawing of microstructured reactor (a) and photographs of the single channel platelet (b), the thermocouple platelet (c), and the top and bottom platelets (d,e).

The applied manufacturing method for the reactor modules with a catalytic coating deposited on the micro channel surfaces prior to soldering (catalyst “pre-coat”) led to low-cost micro-

structured components. For a variation of reactor volume or catalyst mass, additional channel platelets can be used for manufacturing the reactors. The soldering technique enables a full area metallic contact between individual reactor platelets leading to an enhanced heat conductivity compared to competitive assembly technologies like laser welding or the use of fasteners and sealings without a full metallic contact in the structured part of the reactor. Undesired gas bypasses are also suppressed through this manufacturing concept. However, due to the fabrication process, the modules cannot be opened after a performance test without destroying them. Compared to the potential of a low-cost mass production process and the enhanced heat transfer properties, this aspect seems to be only a minor drawback. SEM micrographs in two different magnifications and the corresponding EDX line scan of a solder joint are shown in Figure 5-3. It can be seen that the individual solder material layers:

Reactor material – Ni_{barrier} – Ag – Sn | | Sn – Ag – Ni_{barrier} – Reactor material

were transformed to a solid solution of Sn in Ag:

Reactor material – Ni_{barrier} – Ag_xSn_y – Ni_{barrier} – Reactor material

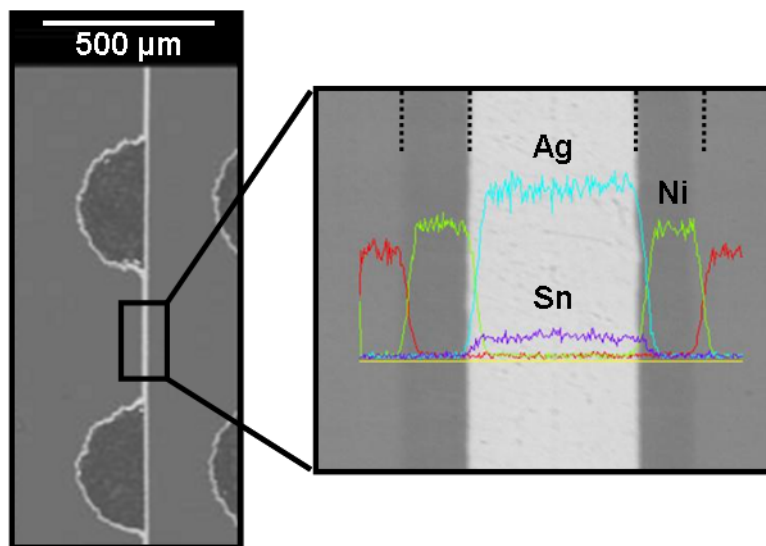


Figure 5-3: SEM micrographs of a solder joint with corresponding EDX line scan.

All microstructured reactors were tested for gas leaks before any further applications. The gas outlet was closed with a gas tight fitting and the gas inlet was connected to a pressure hose. The reactors were then submerged in water and set under pressure (2 to 3 bar) for ten

minutes. Leaks were detected by rising air bubbles. Some reactors were also tested for their thermal stability. They were heated under a pressure of 1.5 bar for three to nine days. After cooling they were tested for gas leaks again. Various tests resulted in sufficient temperature and pressure stability of the modules up to 600 °C at ambient internal pressure, making them safe tools for performing strongly exothermic reactions at high temperatures in a large range of feed compositions. Typical burst pressures of such stacks range between 20 and 30 bar at room temperature. Higher pressure stability can be reached with either a thicker bottom platelet (e.g., thickness 5 mm) or a housing for the reactors.

5.2 Preparation of Coatings

For a fast and efficient development and optimization of the catalytic coatings, unstructured test platelets made of the same stainless steel as the microstructured platelets were used for initial coating experiments. The coatings on these test platelets were taken for evaluating adhesion of the ceramic support on the metallic surface, analysis of the surface morphology, and determination of coating thickness. Furthermore, the coatings were scraped from the test platelets in order to obtain powders that can be used for physico-chemical analysis and catalytic tests. In the second step, the most promising coating formulations were selected for manufacturing entire microstructured reactors.

Formulations for coating the micro channel surfaces were prepared by dispersing either γ -alumina (Alfa Aesar, 99%, average particle size 3 μm) or pre-prepared $\text{VO}_x/\gamma\text{-Al}_2\text{O}_3$ particles in 2-propanol. The pre-prepared catalyst was obtained from a preparation technique that was presented in Chapter 3.1. In order to clearly separate catalyst effects from effects due to a change of the reactor geometry, the material was thoroughly characterized and catalytically tested as described in Chapter 4.2. Independent of the preparation method, chemical binder systems were used to stabilize the ceramic catalyst materials on the metallic reactor surface. The application of binder materials turned out to be essential for mechanically and thermally stable catalyst coatings. Several binder compositions were tested in order to produce coatings with a sufficient adhesion on solder coated substrates. Said binders, i.e., tetraethoxysilane (Merck, 99%), Al-tri-sec-butyrate (Aldrich, 97%), hydroxypropyl cellulose (Aldrich, 99%), and polyvinyl pyrrolidone (Merck, 99%) were obtained by dissolving the organic materials or pre-hydrolyzing the metal alkoxides in water or 2-propanol followed by addition of the alcoholic slurry of support or catalyst particles. Typical weight ratios of particle : binder were 5 : 1 and 10 : 1, respectively. The final mixtures ready for deposition were diluted to a solid content in the range of 10 to 25 wt.-% and treated with ultrasound. After spray coating, the platelets were heated to 100 to 120 °C for 1 h. The mask was removed and the platelets were

weighed to calculate the catalyst loading. Most of the experiments were performed with formulations made from a binder and pre-prepared $\text{VO}_x/\gamma\text{-Al}_2\text{O}_3$ particles, which were deposited on the micro channel surfaces prior to reactor assembly.

In an alternative series of experiments, platelets with pure γ -alumina coatings were assembled and soldered to a complete reactor. This reactor was then attached to a peristaltic pump to impregnate the γ -alumina coating with a pre-heated 0.04 g l^{-1} solution of $\text{VO}(\text{acac})_2$ (Fluka, 97%) in toluene. After soldering and before performance tests, the catalytic coating was calcined under a flow of synthetic air by keeping the entire reactor at 500°C for 5 h.

In another series of experiments, a slurry of γ -alumina particles, dissolved $\text{VO}(\text{acac})_2$, and binder material was coated on the micro channel surfaces prior to reactor assembly. After soldering and before performance tests, the catalytic coating was calcined.

The adhesion of all coatings was tested after applying a standard soldering temperature treatment under vacuum conditions to individual micro channel platelets by tape test (ASTM D 3359-02). A strip of defined size and adhesive strength was pressed on the catalytic coating and rapidly removed. Coatings with sufficient adhesion (i.e., 4 or higher on the tape test scale corresponding to only minor amounts of particles on the adhesive strip) were used for manufacturing entire reactors and successive performance tests as described below. Coating thickness and coating uniformity were monitored with an optical microscope (Olympus BX51M) on cross sections of coated micro channels.

5.3 Catalytic Performance Tests

Catalytic tests of powders obtained from coatings and complete reactors were carried out using the same experimental setup. For measuring the powders, a six-channel screening apparatus with fixed bed continuous flow tubular reactors made of quartz glass with an inner diameter of 6 mm were used. The particle diameter of the powders was below $100 \mu\text{m}$ to positively avoid mass transfer limitations. For better heat transfer, all samples were diluted with 1.5 g quartz. The fixed bed tubular reactors were immersed into a fluidized bed of sand serving as a thermostat. The microstructured reactors containing the catalytic coatings were heated between two brass plates (on top and below the reactor) equipped with four heating cartridges. Both, the reactor and the heating plates were placed in a hotbox for thermal insulation. In case of reactor leakage, the interior of the hotbox was constantly flushed with nitrogen to create an inert atmosphere. In addition to experiments with reactors containing catalytic coatings, the plain reactor material was also tested for catalytic activity.

For comparing the performance of the differently prepared powders and the coatings of the microstructured reactors, standard reaction conditions were chosen as follows: The reactor temperature was kept at 450 °C and the ratio of the C₃H₈/O₂/N₂ inlet flow was 2/1/4, using synthetic air as oxygen source. In order to achieve different degrees of propane conversion, total volume flows were varied from 30 to 240 ml_n min⁻¹. The catalyst mass of the powders was always 20 mg. The mass of the catalytic coatings in the microstructured reactors varied between 48 and 228 mg. Propane conversion and propene selectivity were calculated from inlet and outlet concentrations corresponding to Equations 5-1 and 5-2.

$$X = \frac{C_{C_3H_{8,0}} - C_{C_3H_8}}{C_{C_3H_{8,0}}} \quad (5-1)$$

$$S = \frac{C_{C_3H_6}}{C_{C_3H_{8,0}} - C_{C_3H_8}} \quad (5-2)$$

5.3.1 Activity of Reactor Material

Prior to experiments with microstructured reactors containing catalytic coatings, the internal reactor surface was tested for activity in the oxidative dehydrogenation of propane. Figure 5-4 (a) shows conversion of propane and propene as a function of temperature, whereas Figure 5-4 (b) shows corresponding oxygen conversion degrees. The reactor was assembled from four structured single channel platelets and two thermocouple platelets. Feed composition of C₃H_x/O₂/N₂ was 2/1/4 at a constant flow rate of 60 ml_n min⁻¹.

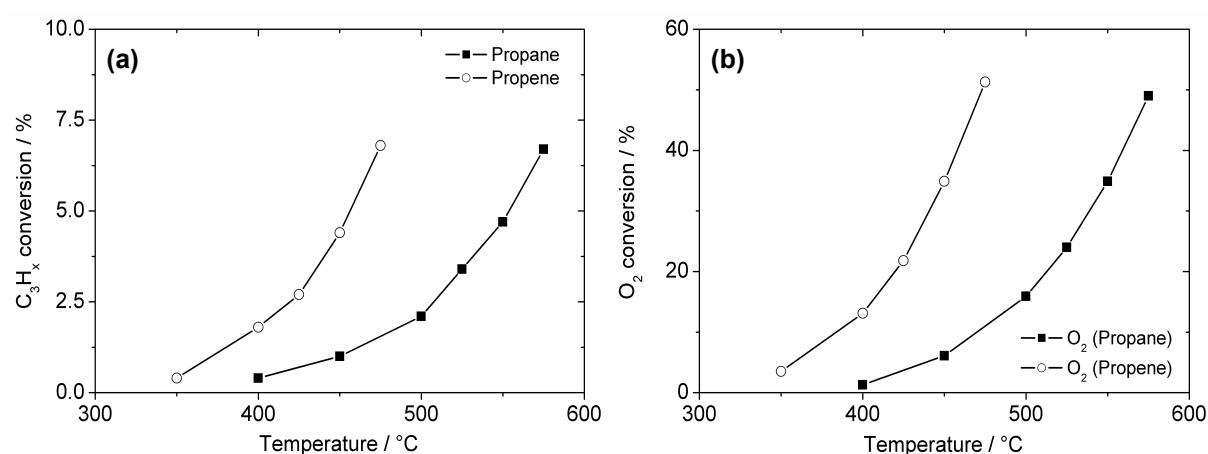


Figure 5-4: Activity of reactor material for (a) C₃H_x conversion and (b) O₂ conversion (single channel design, C₃H_x/O₂/N₂ = 2/1/4, flow rate 60 ml_n min⁻¹).

Conversion of C_3H_x and O_2 exponentially increases with increasing temperature. The main reaction product was analyzed to be CO_2 . Importantly, propene is converted at substantially lower temperatures than propane, which makes the desired product more prone to unselective consecutive reactions. This might be attributed to a small proportion of catalytic activity that originates from the exposed metal surfaces and to a significant proportion of cracking that cannot be neglected in this temperature range [128]. However, compared to catalyst loaded reactors, C_3H_x and O_2 conversion is very small.

5.3.2 Coatings from $VO_x/\gamma-Al_2O_3$ Particles

For all coatings in this series, the same catalytic material was used in order to ensure comparable results. Prior to experiments, the material was analyzed by ICP-OES resulting in a vanadium content of 4.6 wt.-% and an aluminum content of 44.3 wt.-%. BET surface areas were determined for the plain γ -alumina support ($78.7\text{ m}^2\text{ g}^{-1}$), the catalyst used for the coatings ($51.5\text{ m}^2\text{ g}^{-1}$) and the inorganic binder materials after hydrolysis (alumina ex Al-tri-sec-butylate - $345\text{ m}^2\text{ g}^{-1}$ and silica ex tetraethoxysilane - $281\text{ m}^2\text{ g}^{-1}$).

Upon numerous coating formulations, the most promising for each binder system was chosen for further experiments. The decision was mainly based on preliminary adhesion tests. Table 5-1 summarizes the characteristics of these formulations.

Table 5-1: Formulations for preparing coatings from $VO_x/\gamma-Al_2O_3$ particles.

Coating formulation	Cat:Binder	Adhesion	S_{BET} [$\text{m}^2\text{ g}^{-1}$]	Loading [mg]
$VO_x/\gamma-Al_2O_3$ + Al-tri-sec-butylate	5:1	4	104.8	71.0
$VO_x/\gamma-Al_2O_3$ + Tetraethoxysilane	5:1	4	85.9	48.0
$VO_x/\gamma-Al_2O_3$ + Hydroxypropyl cellulose	5:1	4	51.6	65.0
$VO_x/\gamma-Al_2O_3$ + Polyvinyl pyrrolidone	5:1	4	50.5	82.0

All coatings were prepared with a particle : binder weight ratio of 5 : 1 and showed sufficient adhesion on the metallic substrate rated with 4 on the tape test scale (i.e., only minor amounts of particles on the adhesive strip). It is likely that these coatings will also endure more severe ODP process conditions. Specific surface areas of the formulations were influenced by the type of binder material that was used. In case of the inorganic binders, S_{BET} was substantially increased, which can be attributed to the high surface area of the hydro-

lyzed binder materials. Similar findings were frequently reported in the literature when applying alkoxides or silicates as support or binder materials [44,49,129]. In contrast, S_{BET} of the formulations containing organic binders were only slightly influenced compared to the original $\text{VO}_x/\gamma\text{-Al}_2\text{O}_3$ particles. Catalyst loading of the fabricated microstructured reactors varied between 48 and 82 mg. The extra mass of binder materials was taken into account.

In order to examine adhesion and morphology of the coatings on a microscopic level, SEM was applied. Figure 5-5 shows a coating made from $\text{VO}_x/\gamma\text{-Al}_2\text{O}_3$ particles and Al-tri-sec-butylate in two different magnifications (scale bar 200 μm and 20 μm , respectively). It can be seen that the coating is relatively uniform and homogenous, but slightly rough and porous.

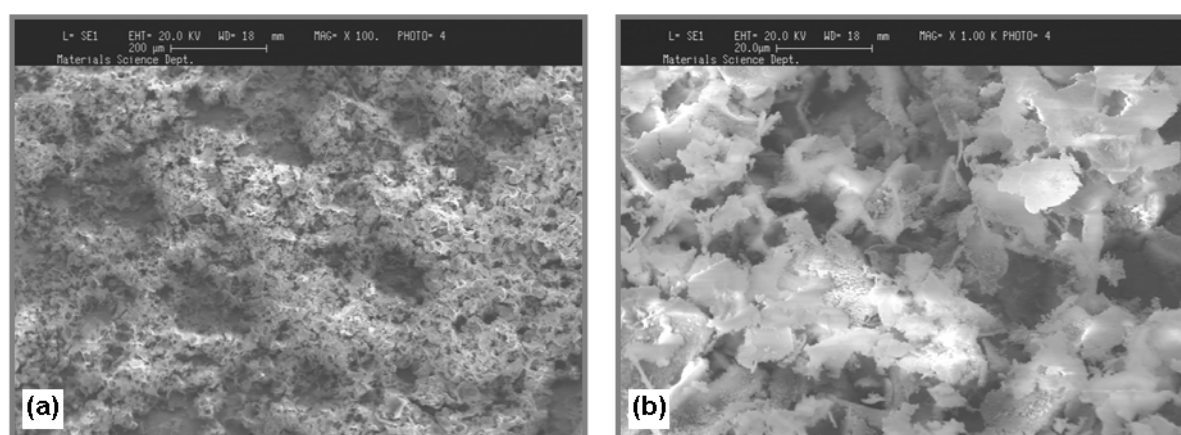


Figure 5-5: SEM images of a coating made from $\gamma\text{-Al}_2\text{O}_3$ particles containing Al-tri-sec-butylate as binder material, scale bar (a) 200 μm and (b) 20 μm .

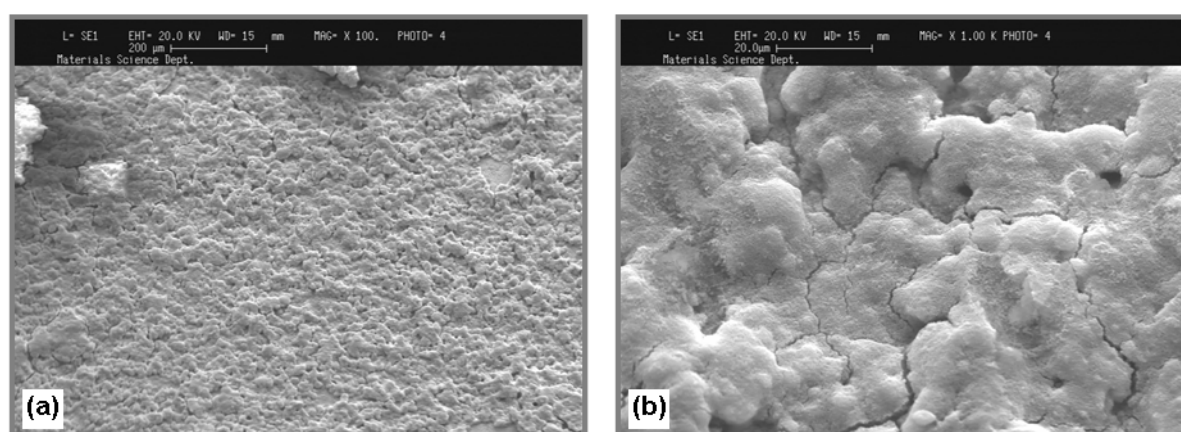


Figure 5-6: SEM images of a coating made from $\gamma\text{-Al}_2\text{O}_3$ particles containing polyvinyl pyrrolidone as binder material, scale bar (a) 200 μm and (b) 20 μm .

In comparison, Figure 5-6 shows a coating containing polyvinyl pyrrolidone as a binder material in two different magnifications (scale bar 200 μm and 20 μm , respectively). This coating also looks uniform and homogenous. However, it appears less rough and shows individual pores and cracks on the surface.

SEM images were also taken from other coatings, but are not shown for sake of brevity. Their optical impression changes with the application of different binder materials. However, all coatings were sufficiently uniform and homogeneous.

The thickness of the coatings made from $\text{VO}_x/\gamma\text{-Al}_2\text{O}_3$ particles and binder materials was determined by analyzing cross sections from different parts of the steel platelets. It was measured to be in the range of 5 to 25 μm after soldering treatment. Similar values were found for all other preparation methods. The cross sections also confirmed uniformity and homogeneity of the coatings.

As mentioned above, coating formulations were first tested as powders in a six-channel screening apparatus in tubular quartz glass reactors for catalytic activity and selectivity. Propane conversion at similar modified residence times seems to be almost identical for powders made from organic binders (hydroxypropyl cellulose and polyvinyl pyrrolidone) and the reference catalyst (see Figure 5-7 (a)). Inorganic binders such as Al-tri-sec-butylate and tetraethoxysilane clearly decrease catalytic activity.

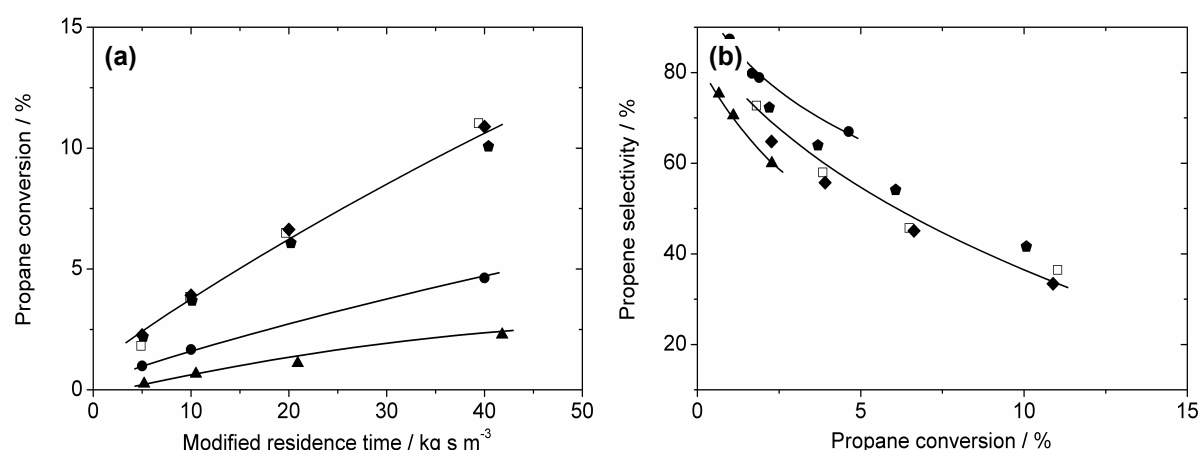


Figure 5-7: Activity (a) and selectivity (b) of coating formulations - □ reference 4.6 wt.-% V, ● Al-tri-sec-butylate, ▲ tetraethoxysilane, ◆ hydroxypropyl cellulose, ♦ polyvinyl pyrrolidone (450 °C, $\text{C}_3\text{H}_8/\text{O}_2/\text{N}_2 = 2/1/4$, flow rate 30 to 240 $\text{ml}_\text{n} \text{ min}^{-1}$, catalyst mass 20 mg).

A similar behavior was observed for propene selectivity. Organic binders do not influence selectivity, whereas inorganic binders show an ambiguous catalytic performance (see Figure 5-7 (b)). The alumina binder seems to increase propene selectivity in comparison to the reference material. However, the silica binder shows a negative influence on the selective formation of propene. All binder systems that were tested as powders were afterwards used for manufacturing fully functional microstructured reactors with catalytic coatings in the channels. Results of the performance tests of these reactors are shown in Figure 5-8.

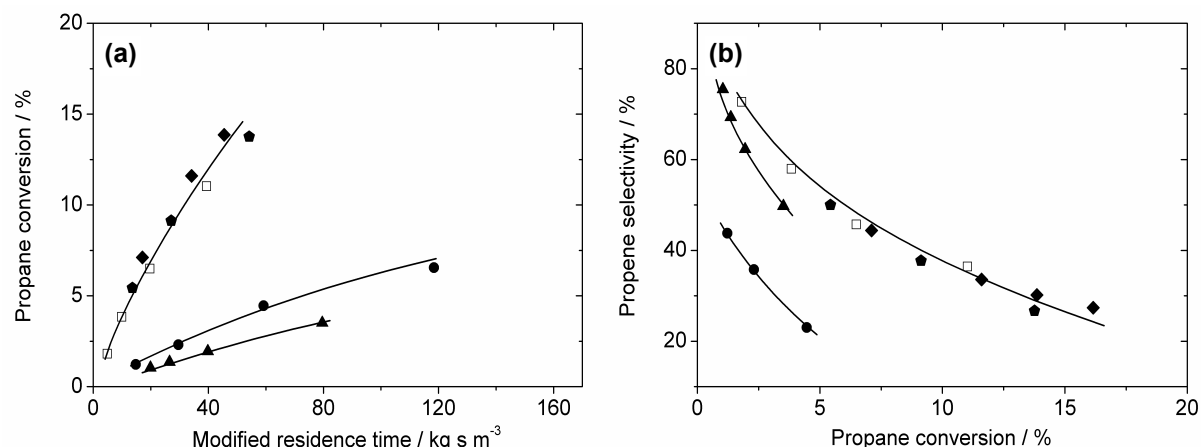


Figure 5-8: Activity (a) and selectivity (b) of catalytic coatings - □ reference 4.6 wt.-% V, ● Al-tri-sec-butylate, ▲ tetraethoxysilane, ◆ hydroxypropyl cellulose, ◆ polyvinyl pyrrolidone (450 °C, C₃H₈/O₂/N₂ = 2/1/4, flow rate 30 to 240 ml_n min⁻¹, catalyst mass 48 to 82 mg).

Catalytic behavior of the microstructured reactors is almost identical with the powder catalysts. It can be concluded that reaction parameters such as temperature and residence time as well as catalyst morphology are similar for the coatings inside the microstructured reactors and the powder catalysts. Therefore, a fast and efficient catalyst screening can be done without manufacturing a reactor module for each coating formulation.

Similar to the results from the tubular quartz glass reactors, catalytic coatings made from organic binders show a comparable activity for propane conversion as the reference catalyst. In addition, these coatings do not influence selectivity behavior, either. However, coatings made from inorganic binders show the same negative influence on catalytic activity as the powders made from these coatings. Activity for propane conversion is substantially decreased as can be seen in Figure 5-8 (a). For propene selectivity, the positive influence of the alumina binder could not be confirmed for the catalytic coating in the microstructured reactor. Both inorganic binder systems restrain the selective formation of propene (see Figure 5-8 (b)). In addition to the results shown for the powders and microstructured reactors, a vast

variety of alternative formulations were also screened in order to find promising catalytic coatings. However, these results are not shown in detail.

As described before, various binder systems were applied in order to stabilize the catalytic coatings on the metallic reactor surface. Organic binders were found to have only minor influence on catalytic activity and selectivity. Since all organic binders are assumed to be removed during preparation of the coatings by temperature treatment, the properties of the catalytic material appear to be unchanged. No carbon residues were found in the catalytic coatings after the soldering procedure. The complete removal of organic binder materials from the coating was also observed by Pfeifer et al. [52]. This is not the case when inorganic binders are applied, since they stay within the coatings. They substantially decrease activity for propane conversion and selectivity towards propene (at least in case of the silica containing binder). Since activity and selectivity are decreased, propene yields for these coatings were among the worst. This might be due to a change of the morphology of the catalysts, in particular the relationship between support material (γ -Al₂O₃) and the active VO_x surface species. It is known that the performance of the ODP reaction is sensitively influenced by the vanadium loading and different support materials [77,83,88,130,131]. If the composition of the catalytic material is changed through the insertion of an inorganic binder material, it might be possible that also the catalytic behavior will be changed. Another explanation for the decreased activity might be the encapsulation of catalyst particles with binder material particles. If catalytically active surface species are buried under a thin layer of alumina or silica, these surface species might not be accessible for gas phase reactants anymore. The same reason for decreased catalytic activity of their coatings was proposed by Nijhuis et al. [132] and Groppi et al. [133], who used sodium silicate (waterglass) and silica sols as binder materials. However, the origin of the influence of inorganic binder materials on catalytic performance has not been finally resolved yet.

5.3.3 Coatings from γ -Al₂O₃ Particles plus Impregnation

The impregnation of porous support materials with precious metals or transition metal precursors is a common pathway for the preparation of catalysts for a wide range of heterogeneously catalyzed gas phase reactions [50,52,134]. Therefore, this preparation route is potentially interesting for many reactions that can benefit from micro reaction technology. Our technique of impregnating γ -alumina with a solution of vanadyl acetylacetonate in toluene was first developed by Frank et al. [112] and further investigated as part of the present study.

Similar to the experiments described above, all tested binder systems were used to deposit stable γ -alumina coatings on the micro channel surfaces. These formulations were also char-

acterized in terms of adhesion, specific surface area, and coating morphology. Results were comparable to the results from the first preparation method.

For impregnating these γ -alumina coatings with a solution of $\text{VO}(\text{acac})_2$ in toluene, only tetraethoxysilane was chosen as a binder system for further experiments since it yields the most stable coatings. After one impregnation cycle, vanadium contents of the coatings were determined to be about 1 to 2 wt.-%. This is in good accordance with results from previous experiments, where γ -alumina particles were similarly impregnated with a vanadium precursor solution [112]. The relative low receptivity of the support material for $\text{VO}(\text{acac})_2$ molecules is probably due to the large acetylacetonate complex that occupies substantial proportions of the support material's surface. Therefore, multiple impregnation cycles with interim calcination procedures have to be applied to achieve higher VO_x concentrations.

The reactor obtained from this manufacturing route was also compared to a powder catalyst that was tested in a tubular quartz glass reactor. Figure 5-9 shows activity and selectivity behavior of the catalytic coating (1.1 wt.-% vanadium) and the powder catalyst (1.4 wt.-% vanadium). The powder catalyst was also prepared by an impregnation technique as described in [112].

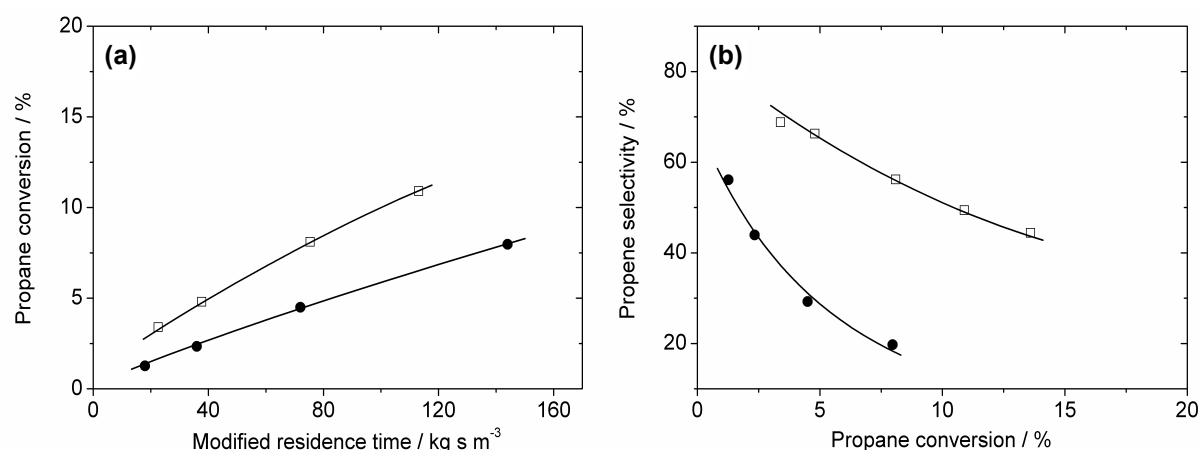


Figure 5-9: Comparison of activity (a) and selectivity (b) of impregnated coating (●) and reference (□) (450°C , $\text{C}_3\text{H}_8/\text{O}_2/\text{N}_2 = 2/1/4$, flow rate 30 to $240 \text{ ml}_n \text{ min}^{-1}$).

It can be seen that activity and selectivity of the catalytic coating measured in the microstructured reactor are somewhat lower than for the powder catalyst. The slight deviations might be due several reasons: The catalytic materials are not identical in terms of vanadium content, chemical composition (in case of the coating, silica is also present due to the inorganic binder that was used to prepare the coating in the first place), and impregnation conditions.

Especially the influence of the inorganic binder might be responsible for both, decreased activity and selectivity in case of the coating. Similar results were reported by Zapf et al. [50], who compared catalytic coatings made from $\gamma\text{-Al}_2\text{O}_3$ / polyvinyl alcohol, $\gamma\text{-Al}_2\text{O}_3$ / boehmite, and $\gamma\text{-Al}_2\text{O}_3$ / $\alpha\text{-Al}_2\text{O}_3$ in the methanol steam reforming reaction. However, it could be shown that this particular manufacturing route for our microstructured reactors is a possible way to insert catalytically active material into the microstructure after assembly and soldering.

5.3.4 Coatings from Vanadium Precursor and $\gamma\text{-Al}_2\text{O}_3$ Particles

In order to simplify preliminary catalyst and subsequent coating preparation, this method combines both steps in one. Since very similar conditions are applied during the two preparation processes, the catalytically active material can be created “in-situ” while the coating formulation is produced. Therefore, the vanadium precursor, γ -alumina particles, and the binder material are mixed into one solution that is afterwards deposited on the micro channel surfaces. Table 5-2 summarizes the properties of the most promising formulations that were tested in the present study.

Table 5-2: Formulations for preparing coatings from $\text{VO}(\text{acac})_2$ and $\gamma\text{-Al}_2\text{O}_3$ particles.

Coating formulation	Cat:Binder	Adhesion	S_{BET} [$\text{m}^2 \text{g}^{-1}$]	Loading [mg]	V [wt.-%]	Al [wt.-%]
$\text{VO}(\text{acac})_2 + \gamma\text{-Al}_2\text{O}_3 +$ Al-tri-sec-butylate	5:1	3	138.9	79.2	4.4	53.4
$\text{VO}(\text{acac})_2 + \gamma\text{-Al}_2\text{O}_3 +$ Tetraethoxysilane	5:1	4	227.6	30.0	3.6	34.2
$\text{VO}(\text{acac})_2 + \gamma\text{-Al}_2\text{O}_3 +$ Hydroxypropyl cellulose	5:1	3	50.9	151.7	4.6	45.0
$\text{VO}(\text{acac})_2 + \gamma\text{-Al}_2\text{O}_3 +$ Polyvinyl pyrrolidone	5:1	4	54.8	87.5	5.0	43.3

In summary, adhesion on the metallic substrate was found to be sufficient for further experiments. However, in case of the Al-tri-sec-butylate and the hydroxypropyl cellulose binder material, the tape test showed only a value of 3 on the tape test scale (i.e., small amounts of particles on the adhesive strip). In terms of specific surface area, the same dependencies as for the first preparation route were found. Inorganic binders increase S_{BET} values substantially, whereas organic binders show only minor influence on the surface area compared to

the $\text{VO}_x/\gamma\text{-Al}_2\text{O}_3$ reference material. Vanadium contents of the coatings varied between 3.6 and 5.0 wt.-%, which is similar to the vanadium content of the pre-prepared $\text{VO}_x/\gamma\text{-Al}_2\text{O}_3$ particles (4.6 wt.-% vanadium).

Since most of the coating properties appear to be comparable to the coating properties that were found for the first preparation route, SEM was applied to analyze any deviations that might prevail in terms of coating morphology. Figure 5-10 (a) shows an image of a coating made from Al-tri-sec-butylate, whereas Figure 5-10 (b) shows an image of a coating made from polyvinyl pyrrolidone (scale bar 200 μm , respectively).

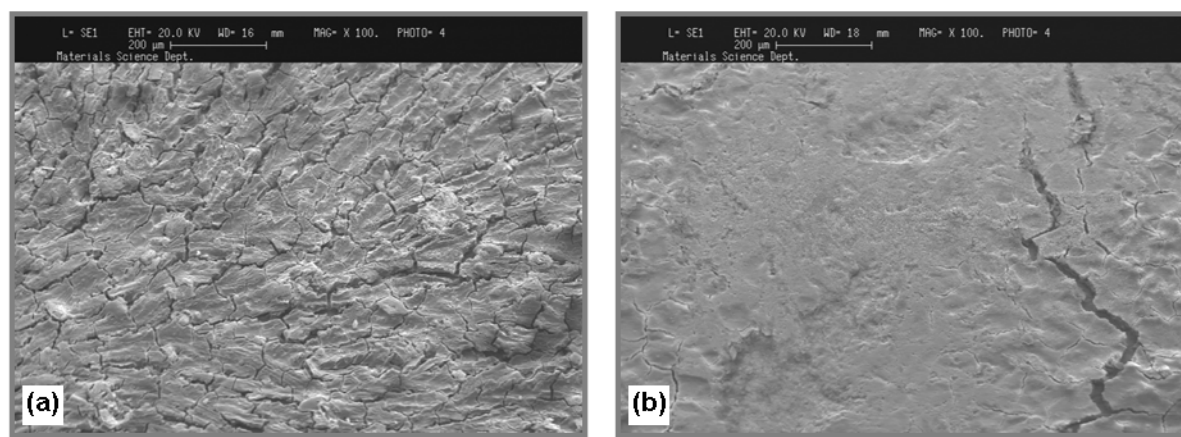


Figure 5-10: SEM images of coatings made from $\gamma\text{-Al}_2\text{O}_3$ particles containing (a) Al-tri-sec-butylate and (b) polyvinyl pyrrolidone as binder materials, scale bar 200 μm .

These coatings appear more compact than the coatings made from pre-prepared $\text{VO}_x/\gamma\text{-Al}_2\text{O}_3$ particles. However, especially the coating made from Al-tri-sec-butylate looks relatively fractured, which might explain its weaker adhesion. In general, it can be observed that the coatings from the first preparation route are more porous, whereas the coatings from this preparation route show a higher density.

As described above, the preparation method for the catalytic coatings following this route is very similar to the route that was applied for the first type of reactors. Therefore, reactors from this manufacturing route were catalytically compared to reactors from the first route. Activity and selectivity behavior for coatings made from polyvinyl pyrrolidone and Al-tri-sec-butylate binders is shown in Figure 5-11. Reactors containing coatings stabilized with organic binders show very similar catalytic behavior. The same is true for coatings stabilized with inorganic binders. Therefore, it can be concluded that both preparation methods lead to essentially the same coating characteristics.

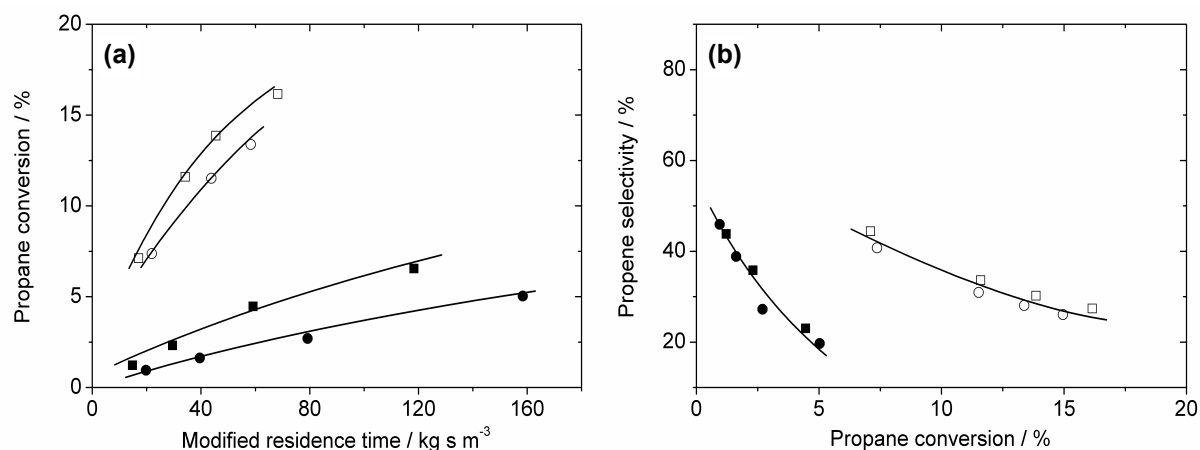


Figure 5-11: Comparison of activity (a) and selectivity (b) of coatings made from VO_x/γ-Al₂O₃ particles (■,□) and VO(acac)₃/γ-alumina particles (●,○), closed symbols Al-tri-sec-butylate, open symbols polyvinyl pyrrolidone as binder material (450 °C, C₃H₈/O₂/N₂ = 2/1/4, flow rate 30 to 240 ml_n min⁻¹).

5.3.5 Influence of Reactor Design

In addition to different preparation methods of the coatings, the influence of the reactor design on catalytic performance was investigated. The assembly mode that was used for all previous experiments (i.e., “face-to-back” of the structured platelets) was changed to “face-to-face” in order to minimize the exposed metallic reactor surface. Since unselective catalytic activity of the reactor material cannot be totally excluded, it might help to increase propene selectivity if most of the inner surface is covered with catalytic material.

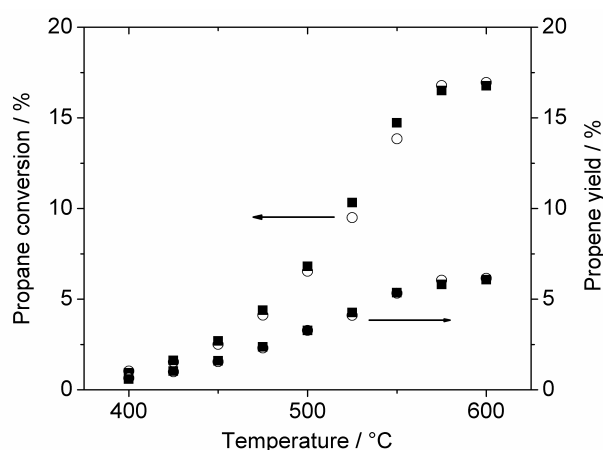


Figure 5-12: Comparison of “face-to-back” (■) and “face-to-face” (○) assembly mode (single channel design, tetraethoxysilane as binder material, C₃H₈/O₂/N₂ = 2/1/4, flow rate 60 ml_n min⁻¹, catalyst mass 50 mg).

Figure 5-12 shows propane conversion and propene yield as a function of temperature for two comparable reactors under equal reaction conditions (tetraethoxysilane as binder material for pre-prepared $\text{VO}_x/\gamma\text{-Al}_2\text{O}_3$ particles, flow rate $60 \text{ ml}_n \text{ min}^{-1}$, catalyst mass approx. 50 mg), which differ only in their assembly mode. Propane conversions and corresponding propene yields are almost identical for both reactors. Therefore, it seems to be unimportant, whether reactor material is exposed to the gas phase, since catalytic performance is not influenced by the assembly mode.

In another experiment, the single channel design was compared to a multi channel design (22 channels per platelet, channel geometry: length 54 mm, width 1 mm, depth 0.3 mm, volume per platelet 0.356 cm^3 , internal surface area per channel 11.9 cm^2). Apart from the channel geometry, the main difference between both designs is the ratio of inner reactor surface to reactor volume. In case of the single channel design, this ratio is about 8700 m^{-1} , whereas for the multi channel design this ratio is about 6700 m^{-1} . Figure 5-13 shows the selectivity-conversion trajectories at 450°C for two comparable reactors (hydroxypropyl cellulose as binder material for pre-prepared $\text{VO}_x/\gamma\text{-Al}_2\text{O}_3$ particles, flow rate $60 \text{ ml}_n \text{ min}^{-1}$, catalyst mass approx. 100 mg), which differ only in their channel geometry.

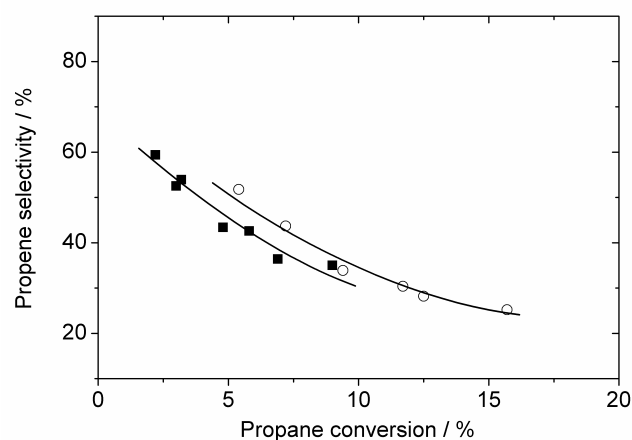


Figure 5-13: Comparison of single (■) and multi (○) channel design (hydroxypropyl cellulose as binder material, 450°C , $\text{C}_3\text{H}_8/\text{O}_2/\text{N}_2 = 2/1/4$, flow rate 30 to $240 \text{ ml}_n \text{ min}^{-1}$, catalyst mass 100 mg).

The multi channel design appears slightly better in terms of propene selectivity compared to the single channel design. However, these differences are small and might well be within the range of experimental error. The more complex multi channel design does not yield a significant superior catalytic performance.

5.3.6 Catalytic Long-term Performance

Since long-term stability is a major objective in a later phase of the development process, one of our microstructured reactors (single channel design, hydroxypropyl cellulose as binder material for pre-prepared $\text{VO}_x/\gamma\text{-Al}_2\text{O}_3$ particles, catalyst mass approx. 68 mg) was tested over 150 h under reaction conditions. The temperature was kept at 500 °C during the whole testing period, whereas the feed gas composition was changed from 100 $\text{ml}_\text{n} \text{ min}^{-1}$ $\text{C}_3\text{H}_8/\text{O}_2/\text{N}_2 = 2/1/4$ during working hours to 60 $\text{ml}_\text{n} \text{ min}^{-1}$ N_2 at night. Propene conversion, propene selectivity and propene yield are shown in Figure 5-14 as a function of time.

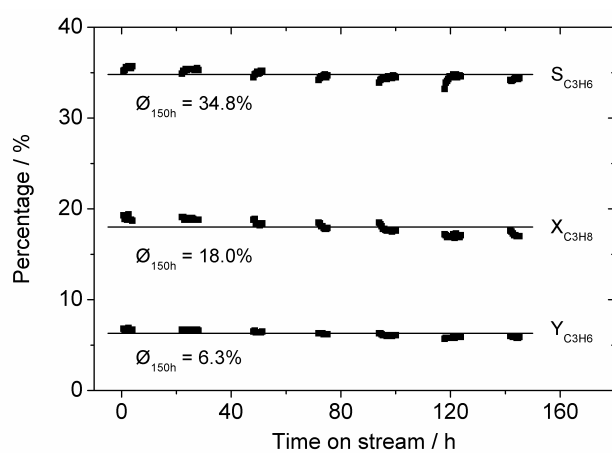


Figure 5-14: Long-term performance over 150 h (single channel design, hydroxypropyl cellulose as binder material, 500 °C, $\text{C}_3\text{H}_8/\text{O}_2/\text{N}_2 = 2/1/4$, flow rate 100 $\text{ml}_\text{n} \text{ min}^{-1}$, catalyst mass 68 mg).

It can be seen that all parameters slightly decrease over time. However, an average propene selectivity of 34.8% at a propane conversion of 18% can be sustained over 150 h. The decrease in catalytic activity and selectivity might be due to the deposition of small amounts of coke on the surface of the catalyst. Reaction conditions were chosen to work under full oxygen conversion in order to maximize propene yield. Therefore, the oxygen concentration towards the end of the catalytic bed steadily decreases to almost zero, which favors coke formation. However, the catalyst can easily be regenerated, if pure oxygen or air is fed to the reactor for the combustion of any carbon depositions. If oxygen conversion is adjusted to an intermediate degree, coke formation can be kept to a minimum.

6 Reactor Characterization and Kinetic Investigations

All catalytic coatings and microstructured reactors were fabricated according to the detailed descriptions in Chapter 5. The obtained reactor modules were tested with respect to reaction engineering aspects that might be useful to improve the overall process efficiency of the ODP. Especially, residence time distributions and catalytic behavior were investigated. Experimental results were compared to a kinetic model published by Frank et al. [112] in order to verify the potential of microstructured reactors for performing fast and strongly exothermic heterogeneously catalyzed gas phase reactions. In particular, the effectiveness of a distributed oxygen feed for increasing the selectivity towards propene was analyzed.

6.1 Reactor Designs

In addition to the microstructured reactor that was introduced in Chapter 5.1, a new design was applied in this part of the present study. Figure 6-1 (a) shows a schematic drawing of the reactor that was used to distribute oxygen over the catalyst bed. It is made of two different types of multi channel platelets with 22 channels each (channel geometry: length 54 mm, width 1 mm, depth 0.3 mm, volume per platelet 0.356 cm^3 , internal surface area per channel 11.9 cm^2 , see Figure 6-1 (b) and (c)). Specifically, one of the multi channel platelets was perforated with 22 equally spaced holes in each channel (average diameter 0.5 mm). With this reactor configuration, C_3H_8 and N_2 are fed to the catalyst coated channels whereas O_2 is fed separately through the perforated channels.

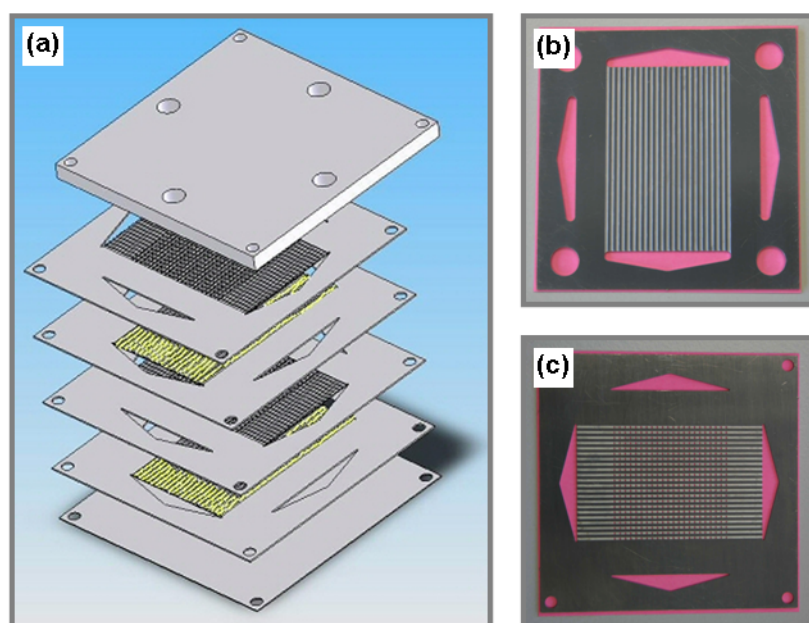


Figure 6-1: Schematic drawing of alternative reactor design for distributing O_2 over the catalyst bed (a) and photographs of both multi channel platelets (b,c).

6.2 Residence Time Distributions

Residence time behavior of the different reactor designs was recorded at room temperature using O₂/N₂ step injection experiments (flow rate 60 ml_n min⁻¹). For changing the flow from oxygen to nitrogen, a four-way cross flow valve was used. Signals were detected by a mass spectrometer (InProcess Instruments GAM200). The reactors were directly attached to the cross flow valve and the mass spectrometer via two connectors (1/8" at valve outlet and mass spectrometer inlet to 6 mm at reactor in- and outlet, respectively). For blind tests, the reactors were removed and the connectors were directly linked with each other. Thereby, the influence of the mass spectrometer and the tubing on the recorded residence time distribution can be separated from the influence of the microstructured reactors. For quantitative analysis of the residence time experiments, the axial dispersion model was combined with a PFTR and a cascade of CSTRs in order to fit experimental data and extract corresponding Bodenstein numbers for all examined reactor designs. The residence time distribution (RTD) function $E(\theta)$ and the cumulative RTD function $F(\theta)$ of the axial dispersion model are given according to Equation 6-1 and 6-2 [16]:

$$E(\theta) = \frac{1}{2} \sqrt{\frac{Bo}{\pi\theta}} \cdot \exp\left(-\frac{(1-\theta)^2 Bo}{4\theta}\right) \quad (6-1)$$

$$F(\theta) = \frac{1}{2} \left[1 - \operatorname{erf}\left((1-\theta) \sqrt{\frac{Bo}{4\theta}}\right) \right] \quad (6-2)$$

where $\theta = t / \tau_{MR}$ is the reduced residence time and $Bo = (u \cdot l) / D_{ax}$ is the dimensionless Bodenstein number. Furthermore, t is the effective residence time, τ_{MR} is the mean residence time of the microstructured reactor, D_{ax} is the axial dispersion coefficient, u is the linear flow velocity, and l the reactor length. The RTD function $E(\theta)$ and the cumulative RTD function $F(\theta)$ of a cascade of CSTRs are given in Equations 6-3 and 6-4 [16]:

$$E(\theta) = \frac{N(N\theta)^{N-1}}{(N-1)!} \cdot \exp(-N\theta) \quad (6-3)$$

$$F(\theta) = 1 - \exp(-N\theta) \cdot \left[\sum_{i=0}^{N-1} \frac{(N\theta)^i}{i!} \right] \quad (6-4)$$

where N is the number of CSTRs, and τ_{Cascade} is the mean residence time of the reactor cascade. The software package Berkeley Madonna (Version 8.0.1) was used to numerically fit model curves to experimental data.

The knowledge about residence time behavior of a reactor is crucial for any further reactor modeling. Parameter estimation from experimental data for standardized models, such as the axial dispersion model, is necessary to mathematically describe the behavior of non-ideal reactors. However, deriving model parameters from experimental data for microstructured devices turned out to be problematic, since adequate detectors and theoretical models are still under development [31,135-139]. Therefore, we do not aim for a highly accurate mathematical description of our reactors but for a sufficiently precise parameter estimate in order to evaluate residence time behavior and select a suitable reactor model. Figure 6-2 shows the cumulative RTD functions of all analyzed microstructured reactors.

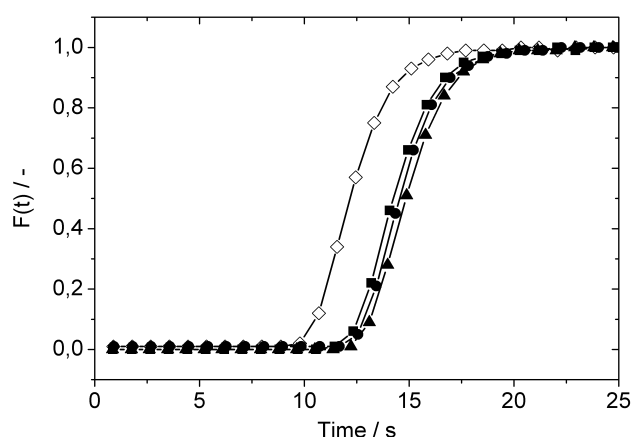


Figure 6-2: Response functions of mass spectrometer (\diamond), single channel designs (\blacksquare face-to-back, \bullet face-to-face) and multi channel design (\blacktriangle) to O_2/N_2 step injection experiments (flow rate $60 \text{ ml}_n \text{ min}^{-1}$).

Fitting the axial dispersion model to unadjusted experimental data in order to determine model parameters will result in highly inaccurate parameter estimates, since the mass spectrometer that was used for detecting the cumulative RTD functions also contributed to overall backmixing and residence time (as seen in Figure 6-2). Therefore, we combined the axial dispersion model for fitting the reactor behavior with an ideal PFTR to account for the influence of the tubing and the mass spectrometer as follows:

Step injection \rightarrow Microstructured reactor \rightarrow PFTR \rightarrow Detector

Model parameters (τ_{MR} , Bo , and τ_{PFTR}) were simultaneously varied by the software package Berkeley Madonna to fit the combined model to our experimental data. The residence time of the imaginary PFTR τ_{PFTR} was determined to be 9.9 s. Corresponding residence times $\tau_{MR,1}$ of the microstructured reactors varied between 4.6 and 5.2 s. Under these assumptions, all backmixing is assigned to the microstructured reactors, resulting in relatively low Bodenstein numbers Bo_1 of 15 to 19 and high residence times compared to hydrodynamic residence times ($\tau_{hyd} = \text{reactor volume} / \text{flow rate}$). However, step injection experiments without microstructured reactors showed that a significant proportion of the backmixing is due to the valve system of the mass spectrometer (see Figure 6-2). Therefore, our model was modified in order to account for the influence of the mass spectrometer by adding a cascade of CSTRs:

Step injection \rightarrow Microstructured reactor \rightarrow PFTR \rightarrow Cascade of CSTRs \rightarrow Detector

In the first step, parameters of the PFTR and the reactor cascaded were determined by fitting experimental data from blind tests (without microstructured reactors). The influence of the mass spectrometer can be described by a parameter combination of $\tau_{PFTR} = 9.5$ s, $\tau_{Cascade} = 2.9$ s and $N = 3$. These parameters were kept constant for consecutive fits in order to guarantee identical boundary conditions. In the second step, τ_{MR} and Bo were simultaneously varied to fit the combined model to the experimental data. The result of this method is shown in Figure 6-3, revealing a good agreement of experimental and model data.

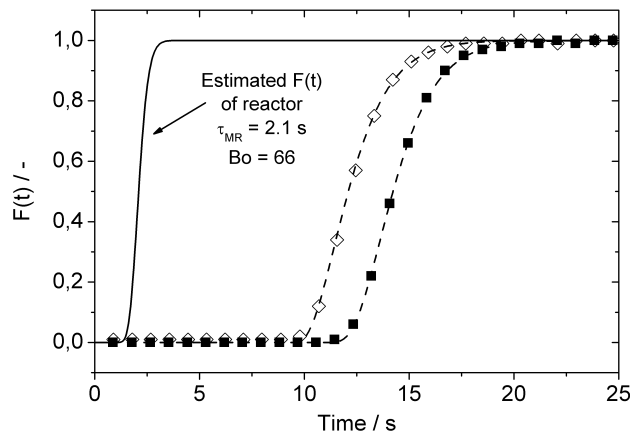


Figure 6-3: Fit of adjusted model (dashed lines) to experimental data (■ response function of microstructured reactor including mass spectrometer, ◇ response function of mass spectrometer individually) in order to estimate $\tau_{MR,2}$ and Bo_2 for microstructured reactor (solid line, flow rate $60 \text{ ml}_n \text{ min}^{-1}$).

By accounting for the influence of the mass spectrometer on the cumulative RTD function, significantly higher Bodenstein numbers Bo_2 were obtained for the microstructured reactors. Through this method, backmixing effects are proportionally assigned to the mass spectrometer and the microstructured reactors, respectively. Values of Bo_2 vary between 66 and 76, giving justified rise to the assumption that the residence time behavior of our microstructured reactors can be approximated with an ideal PFTR model [16]. In addition, experimental $\tau_{MR,2}$ values fall into the range of hydrodynamic residence times, which is in good accordance with assuming a PFTR model for the microstructured reactors.

Table 6-1: Residence times (τ_{hyd} , τ_{MR}) and Bodenstein numbers (Bo) of reactor designs determined from parameter estimation. Index 1 corresponds to adapted model with PFTR, index 2 to adapted model with PFTR/ CSTRs.

Reactor design	Face-to-back Single channel	Face-to-face Single channel	Face-to-back Multi channel
τ_{hyd} [s]	1.8	2.1	2.8
$\tau_{MR,1}$ [s]	4.6	4.9	5.2
Bo_1 [-]	15	17	19
$\tau_{MR,2}$ [s]	2.1	2.5	2.7
Bo_2 [-]	66	73	76

However, it has to be stressed that this method is not suitable for determining model parameters with high accuracy. This is mainly due to the substantial influence of the detector system on resulting cumulative RTD functions. Sensitivity of parameter estimation is high, making this method prone to misinterpretation. However, it serves the purpose to assess residence time behavior of microstructured devices and to choose a suitable reactor model.

6.3 Comparison of Kinetic Model and Experimental Results

The microstructured reactors were kept between 400 and 500 °C. The ratio of the $C_3H_8/O_2/N_2$ inlet flow was 2/1/4. Total volume flows were varied from 30 to 240 $ml_n \min^{-1}$. Since organic binder formulations showed least influence on the catalytic behavior of the coatings compared to the reference catalyst, results from inorganic binder formulations were excluded from this part of the present study. The thickness of the catalytic coatings varied between 5 and 25 μm . All measurements except for the oxygen distribution reactor were performed using microstructured reactors made from four structured single channel platelets and two

platelets for inserting the thermocouples. In case of the oxygen distribution reactor, four multi channel platelets and four perforated multi channel platelets were combined without including platelets for temperature control.

In order to analyze the catalytic behavior of the tested microstructured reactors, a kinetic model was chosen from the literature to evaluate the potential performance of our reactors in the ODP. Frank et al. suggested a power law approach for a low loaded $\text{VO}_x/\gamma\text{-Al}_2\text{O}_3$ catalyst to describe their experimental data and extract intrinsic kinetic parameters [112]:

$$r_{m,1} = \frac{dc_{\text{C}_3\text{H}_8}}{d\tau_{\text{mod}}} = k_{\infty,1} \exp\left(-\frac{E_{A,1}}{RT}\right) c_{\text{C}_3\text{H}_8}^{m_1} c_{\text{O}_2}^{n_1} \quad (6-5)$$

$$r_{m,2} = \frac{dc_{\text{C}_3\text{H}_6}}{d\tau_{\text{mod}}} = k_{\infty,2} \exp\left(-\frac{E_{A,2}}{RT}\right) c_{\text{C}_3\text{H}_6}^{m_2} c_{\text{O}_2}^{n_2} \quad (6-6)$$

$$r_{m,3} = \frac{dc_{\text{O}_2}}{d\tau_{\text{mod}}} = -0.5r_1 - 3.5r_2 \quad (6-7)$$

where $r_{m,1}$ and $r_{m,2}$ are the reaction rates for selective propane conversion and propene deep oxidation, and $r_{m,3}$ is the reaction rate for oxygen conversion, and τ_{mod} is the modified residence time (catalyst mass divided by volume flow of reactants). All model parameters were taken as published (i.e., activation energies and reaction orders), except $k_{\infty,1}$ and $k_{\infty,2}$, which were matched to experimental data as reported in Chapter 4.2 in order to adjust for specific catalyst characteristics, such as the surface density of VO_x species. In addition, the accuracy of activation energies was crosschecked with kinetic data from the literature and showed good agreement [88]. All parameters used in the kinetic model are summarized in Table 6-2.

Table 6-2: Kinetic parameters applied for modeling isothermal microstructured reactor.

	k_{∞}	E_A	m	n
Propane conversion (r_1)	$5.816 \cdot 10^5 \text{ mol}^{0.25} \text{ m}^{2.25} \text{ kg}^{-1} \text{ s}^{-1}$	111 kJ mol^{-1}	0.65	0.10
Propene combustion (r_2)	$5.672 \cdot 10^5 \text{ mol}^{0.7} \text{ m}^{5.1} \text{ kg}^{-1} \text{ s}^{-1}$	102 kJ mol^{-1}	0.70	1.00

In order to predict catalytic behavior of our microstructured reactors from intrinsic kinetics, an isothermal PFTR reactor model was chosen. The assumptions inherent to this model are as

follows: 1) Neither axial nor radial temperature gradients exist along the catalytic bed, 2) No axial backmixing but perfect radial mixing prevails in the reactor. Since residence time behavior experiments revealed Bodenstein numbers in the range of 70, the PFTR reactor type appears to be well-suited to mathematically describe the progress of the reaction in our microstructured reactors. In terms of isothermal reaction conditions, no temperature gradients were observed along the catalyst bed measured by three thermocouples that were placed close to the coated channels, justifying the assumptions of an isothermal reactor model.

In the first step, the mass balances given in Equations 6-5 to 6-7 were solved separately from the heat balance to verify, if the experimental data obtained from the microstructured reactors can be described by the assumed kinetics and the applied reactor model. Figure 6-4 (a) shows measured and simulated propane conversion vs. modified residence time, whereas Figure 6-4 (b) shows propene selectivity vs. propane conversion.

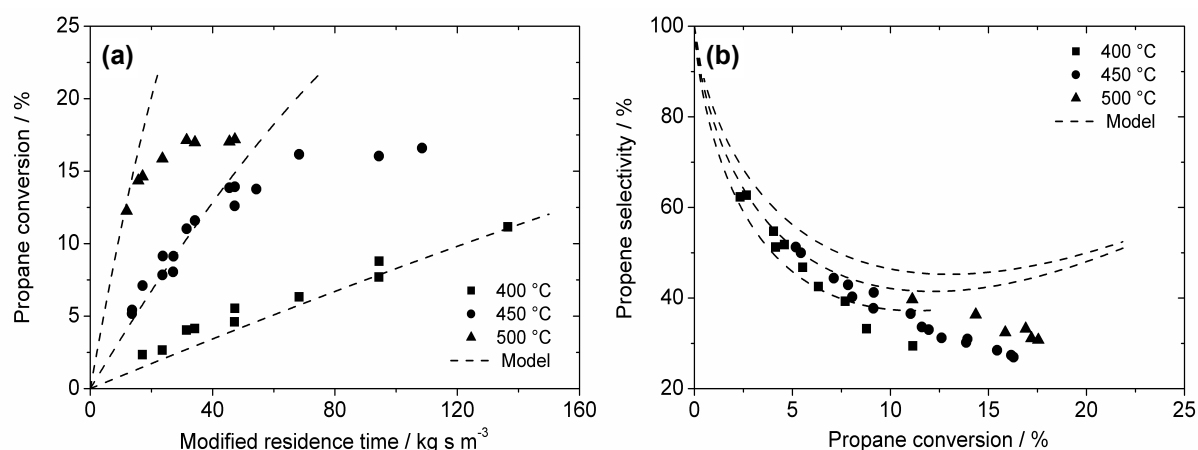


Figure 6-4: Comparison of predicted model data with experimental data for (a) propane conversion and (b) propene selectivity ($\text{C}_3\text{H}_8/\text{O}_2/\text{N}_2 = 2/1/4$, flow rate 30 to 240 ml_n min⁻¹).

It can be seen that activity behavior of the microstructured reactors can be simulated with good accuracy for propane conversion degrees < 12.5% at 400 and 450 °C. At 500 °C propane conversion could not be kept below 12.5% due to the high activity of the applied catalyst. However, the trend predicts that activity behavior at 500 °C will be described by the model for propane conversion degrees < 12.5%, too. Therefore, it can be concluded that the assumed kinetic model is suitable for describing our experimental data from the microstructured reactors. However, once propane conversion is further increased (> 12.5%), activity is dramatically overestimated by the model. Similarly, selectivity towards propene can be predicted with good accuracy for low propane conversion degrees but once propane conversion is increased beyond 12.5%, selectivity is greatly overestimated by the model.

The discrepancy between experimental and predicted model data might be due to several reasons. First of all it has to be verified that isothermal reaction conditions can be assumed for all measurements. As was noted before, no temperature gradients could be observed along the catalyst bed during our experimental studies. In addition, thermal behavior of the microstructured reactors was theoretically modeled by simultaneously solving the mass balances according to Equations 6-5 to 6-7 and the heat balance according to Equation 6-8:

$$\frac{dT}{d\tau_{\text{mod}}} = \frac{-r_{m,1} \cdot \Delta_r H_1 - r_{m,2} \cdot \Delta_r H_2}{c_0 c_p} - (T - T_w) \frac{k_w A_w}{V_r c_0 c_p \rho} \quad (6-8)$$

where $\Delta_r H_1 = -117.6 \text{ kJ mol}^{-1}$ and $\Delta_r H_2 = -1360.2 \text{ kJ mol}^{-1}$ are the reaction enthalpies of Reaction (1) and (2), c_0 is the initial total gas concentration, and c_p and ρ are the average heat capacity and density of the gases estimated from the literature [140]. Furthermore, T_w is the temperature of the reactor wall, k_w is the estimated overall heat transfer coefficient, A_w the heat transfer area, and V_r the reactor volume. Figure 6-5 shows the temperature gradient, propane and oxygen conversion along the catalyst bed in a microstructured reactor (single channel design) at 500 °C.

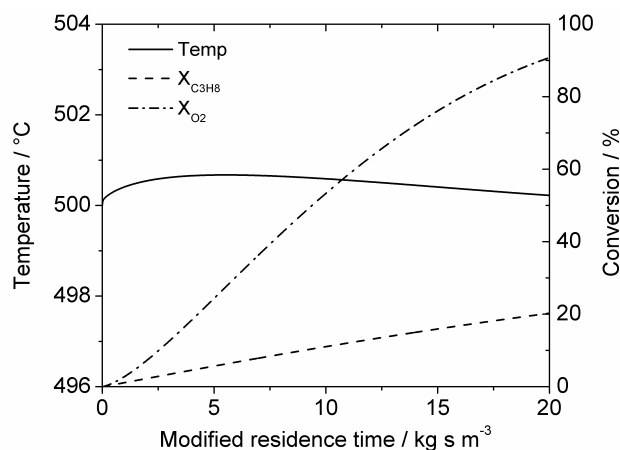


Figure 6-5: Simulated temperature gradient and conversion degrees of propane and oxygen along the catalytic bed in a microstructured reactor ($\text{C}_3\text{H}_8/\text{O}_2/\text{N}_2 = 2/1/4$, flow rate 30 to 240 $\text{ml}_n \text{ min}^{-1}$).

Applying conservative estimates for k_w ($50 \text{ W m}^{-2} \text{ K}^{-1}$) and A_w ($1.47 \cdot 10^{-3} \text{ m}^2$), the maximum temperature rise along the catalyst bed is less than 1 K at full oxygen conversion. Therefore, it can be concluded that isothermal reaction conditions prevail in all experimental series.

Another possible reason for overestimating the activity of the microstructured reactors might be the existence of mass transport limitations, decreasing experimentally determined propane conversion. In order to estimate the influence of possible mass transport limitations, two diagnostic criteria were applied. For evaluating external and internal mass transport limitations, the Mears criterion [16,141] according to Equation 6-9 and the Weisz-Prater criterion [16,142] according to Equation 6-10 adjusted for planar catalyst layers were used:

$$\frac{d_h \cdot (r_{\text{eff}})_s}{D_i \cdot c_0} < 0.05 \quad (6-9)$$

$$\frac{\delta_{\text{Cat}}^2 \cdot (r_{\text{eff}})_v}{D_e \cdot c_0} < 0.07 \quad (6-10)$$

where d_h is the hydraulic diameter of the channel, D_i is the molecular diffusion coefficient, D_e is the effective diffusion coefficient, δ_{Cat} is the thickness of the catalytic coating, $(r_{\text{eff}})_s$ is the effective reaction rate normalized to the catalyst surface, and $(r_{\text{eff}})_v$ is the effective reaction rate normalized to the reactor volume. The Mears and Weisz-Prater criteria were evaluated for reaction rate r_1 at 500 °C using parameters provided in Table 6-2 and a coating thickness of 25 μm . The left hand side of Equations 6-9 and 6-10 were calculated to be 9.8×10^{-6} and 8.7×10^{-4} , respectively. Both values are far below the given limits for an irreversible first order reaction. Therefore, it is unlikely that mass transport phenomena limit propane conversion in the microstructured reactors and are responsible for the discrepancies between experimental and simulated data.

Since the kinetic model by Frank et al. was developed exclusively from differential measurements of propane and propene conversion, it might well be possible that some of their model parameters are not representative for higher degrees of propane conversion. Especially, the overestimated activity might be due to a wrong reaction order for oxygen in Reaction (1). It was estimated to be 0.1, which limits the influence of oxygen concentration on the reaction rate. However, it is obvious that the consumption of propane strongly decreases with decreasing oxygen concentrations, which gives rise to the assumption that n_1 was underestimated in the applied kinetic model.

In addition to the discrepancies between experimental and simulated data for activity behavior of the microstructured reactors, also selectivity towards propene cannot be forecasted with satisfactory accuracy. As was shown in Figure 6-4 (b), selectivity is predicted to de-

crease to a minimum and subsequently increase at high degrees of propane conversion. This catalytic behavior was not observed during any experimental series while using our microstructured reactors. The prediction of the rising propene selectivity is based on the difference between reaction orders for oxygen in Reaction (1) and (2). Reaction order n_1 was estimated to be 0.1, whereas reaction order n_2 was estimated to be 1.0. This difference in reaction orders leads to a relatively high reaction rate r_1 in comparison to reaction rate r_2 at low oxygen concentrations. Therefore, selectivity towards propene is forecasted to increase at high degrees of propane conversion. In order to verify or falsify the assumption that n_1 and n_2 are different from each other, the microstructured reactor with the distributed oxygen feed was applied. If n_1 is smaller than n_2 , lowering the oxygen partial pressure at the catalytically active sites should increase propene selectivity. This behavior was also theoretically examined in the literature [106]. Figure 6-6 shows experimental data from a conventional co-feed reactor and the oxygen distribution reactor as well as corresponding simulated selectivity-conversion trajectories.

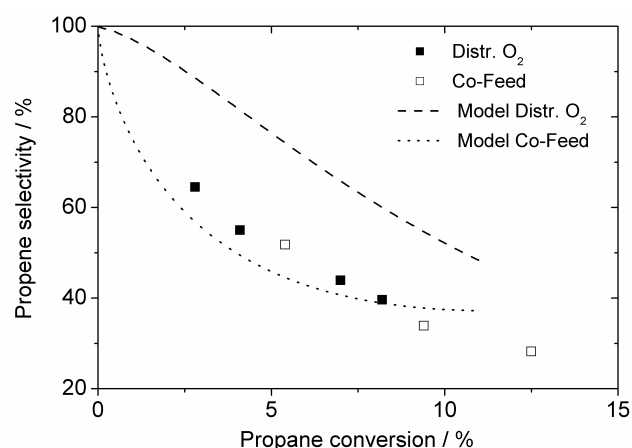


Figure 6-6: Comparison of predicted model data with experimental data for co-feed mode of reactants and distributed oxygen feed (450 °C, $C_3H_8/O_2/N_2 = 2/1/4$, total flow rate 30 to 240 ml_n min⁻¹).

It can be seen that experimental data from both reactor types are almost identical in terms of selectivity behavior. In contrast, propene selectivity predicted from the simulation of the oxygen distribution reactor is far higher than for the conventional co-feed reactor. Therefore, there are strong experimental and theoretical indications that oxygen reaction orders n_1 and n_2 are not as different as proposed by Frank et al. There are several reasons why their model is not able to predict concentrations for high degrees of propane conversion. In their experiments, propane and propene conversion degrees were kept to values < 2% and < 3%, re-

spectively. The main reason was the inability to control temperature gradients along the catalyst bed. In addition, simplifications such as the assumption of a constant CO : CO₂ ratio might not be justified. Most importantly, activation energies of both reactions were not determined in the same temperature range, whereas reaction orders were assumed to be independent from temperature. However, the model serves well for the purpose it was developed for but seems unsuitable for extrapolation. As was explained above, it appears most likely that oxygen reaction orders are rather similar. Therefore, another simulation was performed for values of $n_1 = n_2 = 1.0$ and zero, respectively, in order to check, if a better agreement with the experimental data can be achieved (in both cases, pre-exponential factors had to be slightly adjusted in order to correct for the change in reaction orders). Figure 6-7 (a) shows experimental and simulated propane conversion versus modified residence time at 450 °C for reaction orders $n_1 = n_2 = 1.0$ and zero ($k_{\infty,1} = 2.99 \times 10^5$, $k_{\infty,2} = 4.68 \times 10^5$ for $n = 1.0$ and $k_{\infty,1} = 2.93 \times 10^5$, $k_{\infty,2} = 4.17 \times 10^5$ for $n = \text{zero}$). In comparison, Figure 6-7 (b) shows experimental and simulated selectivity-conversion trajectories at 450 °C, also for reaction orders $n_1 = n_2 = 1.0$ and zero.

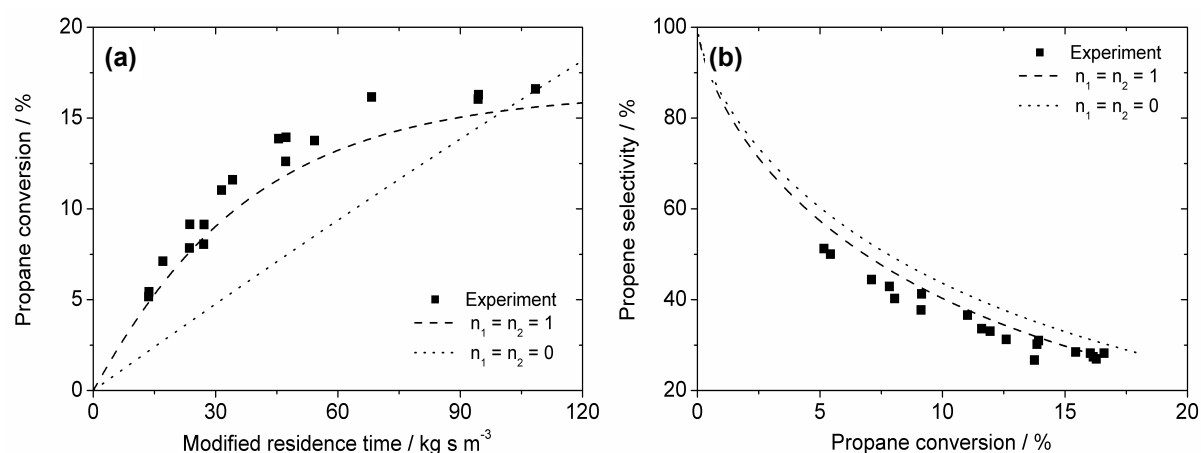


Figure 6-7: Theoretical propane conversion (a) and propene selectivity (b) for adjusted oxygen reaction orders compared to experimental data (450 °C, C₃H₈/O₂/N₂ = 2/1/4, flow rate 30 to 240 ml_n min⁻¹).

If both reaction orders are set to 1.0, activity behavior can be described more precisely than with the original model. The loss of activity at higher degrees of propane conversion is accounted for, since reaction rate r_1 experiences a higher dependency on oxygen concentration compared to the original model by Frank et al., where n_1 was determined to be 1.0. If both reaction orders are set to zero, the agreement between experimental and simulated data becomes worse, which is due to the same reason as above. The loss of activity due to the

unavailability of oxygen is not taken into account, since reaction rates are independent of the oxygen concentration. In case of selectivity behavior, both cases yield a more accurate prediction of experimental data. Selectivity-conversion trajectories monotonically decrease, without showing increasing propene selectivity at high degrees of propane conversion. However, it has to be noted that these insights have to be experimentally verified. So far, there are only strong indications that oxygen reaction orders have to be very similar. This result is also supported by the literature [96].

7 Conclusions and Outlook

In the present study, microstructured reactors containing $\text{VO}_x/\gamma\text{-Al}_2\text{O}_3$ wall catalysts were developed and optimized and subsequently tested in the oxidative dehydrogenation of propane to assess their catalytic performance.

Two sets of catalysts were prepared from wet saturation impregnation and ball-milling of $\gamma\text{-Al}_2\text{O}_3$ and crystalline V_2O_5 resulting in very similar physico-chemical and catalytic properties of the obtained materials. In both cases, temperature treatment during catalyst preparation leads to a distribution of monomeric and polymeric VO_x species as well as V_2O_5 crystallites on the support material surface. When correlating edge energies from UV-vis DRS experiments with catalytic performance, very similar dependencies for both examined materials can be observed although very different preparation methods were used. It appears that the differences in the characterization of both examined materials do not play a major role for the catalytic performance under reaction conditions. However, there is evidence that the catalytic behavior of VO_x surface species changes, if vanadium content is increased. It was shown that VO_x species with a higher degree of polymerization appear to be more active for propane conversion but less selective towards propene. Since E_g is related to the electronic structure of VO_x species, it is expected that the band gap decreases and total electrical conductivity of $\text{VO}_x/\gamma\text{-Al}_2\text{O}_3$ materials increases with a decrease in edge energy. Therefore, the transfer of free electrons from oxygen atoms to metal centers is facilitated in materials with lower edge energies. This leads to an easier C-H bond activation, which is the rate determining step for both, propane and propene conversion. However, with decreasing edge energies the rate for propene conversion increases stronger than the rate for propane conversion.

In order to deposit catalytic materials on the channel surfaces of microstructured reactors, a specific catalyst preparation method had to be developed. $\text{VO}_x/\gamma\text{-Al}_2\text{O}_3$ materials with different vanadium contents were obtained and thoroughly characterized to clearly separate effects related to a change of the catalyst characteristics from effects related to a change of the reactor geometry. The results from UV-vis DRS and Raman spectroscopy indicate that with increasing vanadium content the formation of polymerized vanadia species is enhanced whereas crystalline V_2O_5 is observed at higher vanadium contents (i.e., starting from 5.3 wt.-% $\text{V}/\gamma\text{-Al}_2\text{O}_3$). Catalytic tests in conventional tubular reactors showed higher selectivity with decreasing vanadium content and higher activity with increasing vanadium content. These results are in good agreement with findings from Chapter 4.1.

Catalytic materials from the third preparation method were applied in microstructured reactors, which are well-suited for performing strongly exothermic heterogeneously catalyzed gas

phase reactions. So far, these devices have been relatively expensive due to the lack of an adequate low-cost manufacturing concept. Therefore, a new and flexible production method has been developed in order to make the application of microstructured reactors more feasible for small and medium scale industrial processes. A Ni-Ag-Sn soldering system was applied for manufacturing the reactor modules. Three different techniques for coating the micro channel surfaces with catalytic materials were investigated. The obtained reactors containing the active coatings turned out to be sufficiently stable under reaction conditions of the oxidative dehydrogenation of propane. In order to stabilize the ceramic catalyst coatings on the metallic reactor material, different binder formulations were applied. It was shown that inorganic binder materials substantially decrease catalytic activity and selectivity, whereas organic binders do not influence catalytic behavior. Due to the various preparation methods, chemical binder systems, and channel geometries that were investigated, a highly flexible toolbox for manufacturing low-cost microstructured reactors is available. Catalyst support and active component can be adapted to alternative reactions with minor effort. In addition, all manufacturing methods were chosen to be easily scaled-up for the production of larger reactor modules.

The obtained microstructured reactors were characterized in more detail, especially with respect to residence time distributions, thermal, and catalytic behavior. It was shown that this type of reactor exhibits only minor backmixing, since Bodenstein numbers are in the range of 70. Furthermore, it could be experimentally and theoretically verified that isothermal reaction conditions can be achieved over a wide temperature range, making microstructured reactors excellent tools for controlling strongly exothermic reactions. In comparison to conventional reactor technologies, they are advantageous with respect to their superior heat transfer properties. In order to assess the prospective catalytic performance of our microstructured reactors, a kinetic model from the literature was applied to predict propane conversion and propene selectivity. It was shown that the full kinetic potential can be exploited due to the well controllable reactor behavior. However, it was also found that the applied kinetic model is not suitable for extrapolation mainly due to the inability to correctly predict activity and selectivity for high degrees of propane conversion. Furthermore, it was shown that a distributed oxygen feed in the oxidative dehydrogenation of propane is not beneficial, since oxygen reaction orders appear to be very similar for both consecutive reactions. With this study, the basis for a detailed kinetic investigation of the chosen model reaction was established, since microstructured reactors are well suited to analyze strongly exothermic heterogeneously catalyzed gas phase reactions under isothermal reaction conditions in a wide range of concentrations and temperatures. Typical problems with challenging reactions such as inefficient heat transfer can be avoided, resulting in more accurate kinetic parameters.

The commonly cited potential of micro reaction technology for heterogeneously catalyzed gas phase reactions was proven in the present study. Principally, the obtained results can be transferred to industrial-scale microstructured reactors as was shown before in the DEMiS project [65]. Therefore, the application of these reactors in the development process of challenging heterogeneously catalyzed gas phase reactions appears reasonable, since the principal option for applying microstructured reactors in industrial-scale production processes is available. However, realistic chances for the oxidative dehydrogenation of propane to be industrially applied in the near future are questionable. Comparative studies of different production routes and recent reviews of the relevant literature clarified that even state-of-the-art catalyst performance is relatively far from economic feasibility [74,75,143]. The only practical way towards a substantial increase of propene selectivity might be a systematic evaluation of all information available from the literature to identify and combine the most promising approaches in terms of catalyst formulation, choice of oxidant, and reactor system as recently proposed by Corberán [144]. By applying innovative reaction engineering concepts (e.g., distributed oxygen feed [111], advanced membrane type reactors [107,108,110], or auto-thermal reactor concepts combining endothermal non-oxidative with exothermal oxidative dehydrogenation [145-147]), mechanistic and kinetic characteristics of the ODP could be exploited, resulting in a higher propene selectivity.

Independently of the predictions for the oxidative dehydrogenation of propane, micro reaction technology and chemical micro processing face a more optimistic future. The potentials and chances of this new technology in research and development activities have been shown many times since the 1990s [36]. Even some applications in (semi-)industrial-scale production processes have been reported lately, mainly in the field of pharmaceuticals and fine-chemistry [60-65]. The availability of lab-scale components has reached a high level of diversification [7-9], opening-up the field for many future applications. However, the development and availability of industrial-scale components is not yet satisfactory, inhibiting the successful introduction in chemical production processes.

With growing maturity of micro reaction technology, studies on the market potential [148,149], economic feasibility [61,150], and ecologic impact [151] of chemical micro systems start to focus on more quantitative aspects. However, fundamental doubts about the possible range of applications still prevail [35].

The major obstacle to a broad introduction of chemical micro processing to industrial practice is due to the shift of paradigm that is normally connected to this technology. While many processes in pharmaceutical and fine chemistry companies are performed in batch reactors,

micro reaction technology is based on continuous flow regimes, which is not easily accepted by potential users. Yet with increasing efforts to include micro reaction technology and chemical micro processing into the academic education of young engineers [16,152-154], this difficulty will slowly be overcome. In addition, awareness for this new technology advances through many funded research projects enhancing the co-operation between academia and industry [59,155,156].

Apart from all positive perspectives, chemical micro processing and micro reaction technology will have to compete with well-established, conventional strategies in all fields of chemical engineering. It is safe to say that this new technology will only be applied where advantages in comparison to conventional techniques are evident. However, since cost pressure and demand for environmentally benign processes constantly increase, faster and more efficient development and production systems will be required, making microstructured components attractive tools for many future applications. No matter what, micro reaction technology and chemical micro processing will be established in all fields of chemical research, development, and production activities.

8 Literature

- [1] K.-P. Jäckel, in *Microsystem Technology for Chemical and Biological Microreactors - DECHEMA Monographs Vol. 132*, (W. Ehrfeld), pp. 29-50, Dechema e.V., Weinheim, 1996.
- [2] W. Ehrfeld, V. Hessel, H. Lehr, in *Microsystem Technology in Chemistry and Life Science*, (A. Manz, H. Becker), pp. 233-252, Springer-Verlag, Berlin, 1998.
- [3] W. Ehrfeld, V. Hessel, H. Löwe, *Microreactors*, Wiley-VCH, Weinheim, 2000.
- [4] W. Ehrfeld, V. Hessel, V. Haverkamp, in *Ullmann's Encyclopedia of Industrial Chemistry*, Electronic Release, Wiley-VCH, Weinheim, 2002.
- [5] E. Klemm, M. Rudek, G. Markowz, R. Schütte, in *Winnacker/ Küchler - Chemische Technik, Band 2: Neue Technologien* (R. Dittmeyer, W. Keim, G. Kreysa, A. Oberholz), 5th edition, pp. 759-819, Wiley-VCH, Weinheim, 2004.
- [6] A. Gavriilidis, P. Angeli, E. Cao, K.K. Yeong, Y.S.S. Wan, *Chem. Eng. Res. Des.* 80 (2002) 3-30.
- [7] V. Hessel, H. Löwe, *Chem. Eng. Technol.* 26 (2003) 13-24.
- [8] V. Hessel, H. Löwe, *Chem. Eng. Technol.* 26 (2003) 391-408.
- [9] V. Hessel, H. Löwe, *Chem. Eng. Technol.* 26 (2003) 531-544.
- [10] K. Jähnisch, V. Hessel, H. Löwe, M. Baerns, *Angew. Chem.* 116 (2004) 410-451.
- [11] D. Kirschneck, R. Marr, *Chem. Ing. Tech.* 78 (2006) 29-38.
- [12] V. Hessel, H. Löwe, F. Schönfeld, *Chem. Eng. Sci.* 60 (2005) 2479-2501.
- [13] B. Pentth, WO/2000/061275.
- [14] Z. Yang, S. Matsumoto, H. Goto, M. Matsumoto, R. Maeda, *Sensor. Actuat. A: Physical* 93 (2001) 266-272.
- [15] J.J. Brandner, Dechema - Weiterbildungskurs Mikroverfahrenstechnik, Frankfurt a.M., 2007.
- [16] G. Emig, E. Klemm, *Technische Chemie - Einführung in die Chemische Reaktionstechnik*, 5th edition, pp. 444-467, Springer-Verlag, Berlin, 2005.
- [17] K. Benz, K.-P. Jäckel, K.-J. Regenauer, J. Schiewe, K. Drese, W. Ehrfeld, V. Hessel, H. Löwe, *Chem. Eng. Technol.* 24 (2001) 11-17.
- [18] H. Fink, M.J. Hampe, in *Microreaction Technology: Proceedings of the Third International Conference on Microreaction Technology, IMRET 3*, (W. Ehrfeld), pp. 664-673, Springer-Verlag, Berlin, 2000.
- [19] K. Jähnisch, M. Baerns, V. Hessel, W. Ehrfeld, V. Haverkamp, H. Löwe, C. Wille, A. Guber, *J. Fluorine Chem.* 105 (2000) 117-128.
- [20] M. Schmidt, G. Kreisel, *Chem. Ing. Tech.* 71 (1999) 111-117.

-
- [21] H. Lu, M.A. Schmidt, K.F. Jensen, Lab Chip 1 (2001) 22-28.
- [22] G. Kreisel, S. Meyer, D. Tietze, T. Fidler, R. Gorges, A. Kirsch, B. Schäfer, S. Rau, Chem. Ing. Tech. 79 (2007) 153-159.
- [23] A. Rouge, B. Spoetzi, K. Gebauer, R. Schenk, A. Renken, Chem. Eng. Sci. 56 (2001) 1419-1427.
- [24] C.M. Knösche, Chem. Ing. Tech. 77 (2005) 1715-1722.
- [25] M. Matlosz, Chem. Ing. Tech. 77 (2005) 1393-1398.
- [26] A. Hüther, A. Geißelmann, H. Hahn, Chem. Ing. Tech. 77 (2005) 1829-1837.
- [27] J.-M. Commenge, L. Falk, J.-P. Corriou, M. Matlosz, Chem. Eng. Technol. 28 (2005) 446-458.
- [28] E. Klemm, H. Döring, A. Geißelmann, S. Schirrmeister, Chem. Ing. Tech. 79 (2007) 697-706.
- [29] M.T. Janicke, H. Kestenbaum, U. Hagendorf, F. Schüth, M. Fichtner, K. Schubert, J. Catal. 191 (2000) 282-293.
- [30] G. Vesper, Chem. Eng. Sci. 56 (2001) 1265-1273.
- [31] P. Pfeifer, L. Bohn, O. Görke, K. Haas-Santo, U. Schygulla, K. Schubert, Chem. Ing. Tech. 76 (2004) 607-613.
- [32] S. Chattopadhyay, G. Vesper, AIChE J. 52 (2006) 2217-2229.
- [33] M. Jucys, Dechema - Weiterbildungskurs Mikroverfahrenstechnik, Frankfurt a.M., 2007.
- [34] C. Liebner (BAM - Bundesanstalt für Materialforschung und -prüfung), Personal Communication, Würzburg, 2008.
- [35] O. Wörz, Chemie in unserer Zeit 34 (2000) 24-29.
- [36] O. Wörz, K.-P. Jäckel, T. Richter, A. Wolf, Chem. Ing. Tech. 72 (2000) 460-463.
- [37] J.J. Lerou, M.P. Harold, J. Ryley, J. Ashmead, T.C. O'Brien, M. Johnson, J. Perrotto, C.T. Blaisdell, T.A. Rensi, J. Nyquist, in *Microsystem Technology for Chemical and Biological Microreactors - DECHEMA Monographs Vol. 132*, (W. Ehrfeld), pp. 51-70, Dechema e.V., Weinheim, 1996.
- [38] F. Herbstritt, Dechema - Weiterbildungskurs Mikroverfahrenstechnik, Frankfurt a.M., 2007.
- [39] O. Kurtz, R. Herber, K. Crämer, H. Meyer, N. Kanani, Galvanotechnik 94 (2003) 92-97.
- [40] Atotech Deutschland GmbH, EP 1 829 608 B1.
- [41] S. Schimpf, P. Claus, Dechema - Weiterbildungskurs Mikroverfahrenstechnik, Frankfurt a.M., 2007.
- [42] D. Hönicke, Appl. Catal. 5 (1983) 179-198.
-

-
- [43] G. Wießmeier, D. Hönicke, J. Micromech. Microeng. 6 (1996) 285-289.
- [44] R. Wunsch, M. Fichtner, O. Görke, K. Haas-Santo, K. Schubert, Chem. Eng. Technol. 25 (2002) 700-703.
- [45] G. Wießmeier, Diploma Thesis, Karlsruhe, 1992.
- [46] M. Fichtner, J. Mayer, D. Wolf, A. Schubert, Ind. Eng. Chem. Res. 40 (2001) 3475-3483.
- [47] H. Kestenbaum, A.L. de Oliveira, W. Schmidt, F. Schüth, W. Ehrfeld, K. Gebauer, H. Löwe, T. Richter, D. Lebiez, I. Untiedt, H. Züchner, Ind. Eng. Chem. Res. 41 (2002) 710-719.
- [48] A. Kursawe, D. Hönicke, in *Microreaction Technology: Proceedings of the Fifth International Conference on Microreaction Technology, IMRET 5*, (M. Matlosz, W. Ehrfeld, J.P. Baselt), pp. 240-251, Springer-Verlag, Berlin, 2002.
- [49] K. Haas-Santo, M. Fichtner, K. Schubert, Appl. Catal. A: Gen. 220 (2001) 79-92.
- [50] R. Zapf, C. Becker-Willinger, K. Berresheim, H. Bolz, H. Gnaser, V. Hessel, G. Kolb, P. Lob, A.K. Pannwitt, A. Ziogas, Chem. Eng. Res. Des. 81 (2003) 721-729.
- [51] R. Zapf, V. Hessel, Chem. Ing. Tech. 76 (2004) 513-514.
- [52] P. Pfeifer, K. Schubert, M.A. Liauw, G. Emig, Appl. Catal. A: Gen. 270 (2004) 165-175.
- [53] P. Pfeifer, K. Schubert, G. Emig, Appl. Catal. A: Gen. 286 (2005) 175-185.
- [54] R. Schenk, V. Hessel, C. Hofmann, J. Kiss, H. Löwe, A. Ziogas, Chem. Eng. J. 101 (2004) 421-429.
- [55] K.F. Jensen, Chem. Eng. Sci. 56 (2001) 293-303.
- [56] J.M. Commenge, L. Falk, J.P. Corriou, M. Matlosz, AIChE J. 48 (2002) 345-358.
- [57] A. Tonkovich, D. Kuhlmann, A. Rogers, J. McDaniel, S. Fitzgerald, R. Arora, T. Yuschak, Chem. Eng. Res. Des. 83 (2005) 634-639.
- [58] O. Tonomura, T. Tominari, M. Kano, S. Hasebe, Chem. Eng. J. 135 (2008) S131-S137.
- [59] T. Bayer, J. Jenck, M. Matlosz, Chem. Eng. Technol. 28 (2005) 431-438.
- [60] D.M. Roberge, Org. Proc. Res. Dev. 8 (2004) 1049-1053.
- [61] D.M. Roberge, L. Ducry, N. Bieler, P. Cretton, B. Zimmermann, Chem. Eng. Technol. 28 (2005) 318-323.
- [62] H. Krummradt, U. Koop, J. Stoldt, in *Microreaction Technology: Proceedings of the Third International Conference on Microreaction Technology, IMRET 3*, (W. Ehrfeld), pp. 181-186, Springer-Verlag, Berlin, 1999.
- [63] C. Wille, H.-P. Gabski, T. Haller, H. Kim, L. Unverdorben, R. Winter, Chem. Eng. J. 101 (2004) 179-185.
-

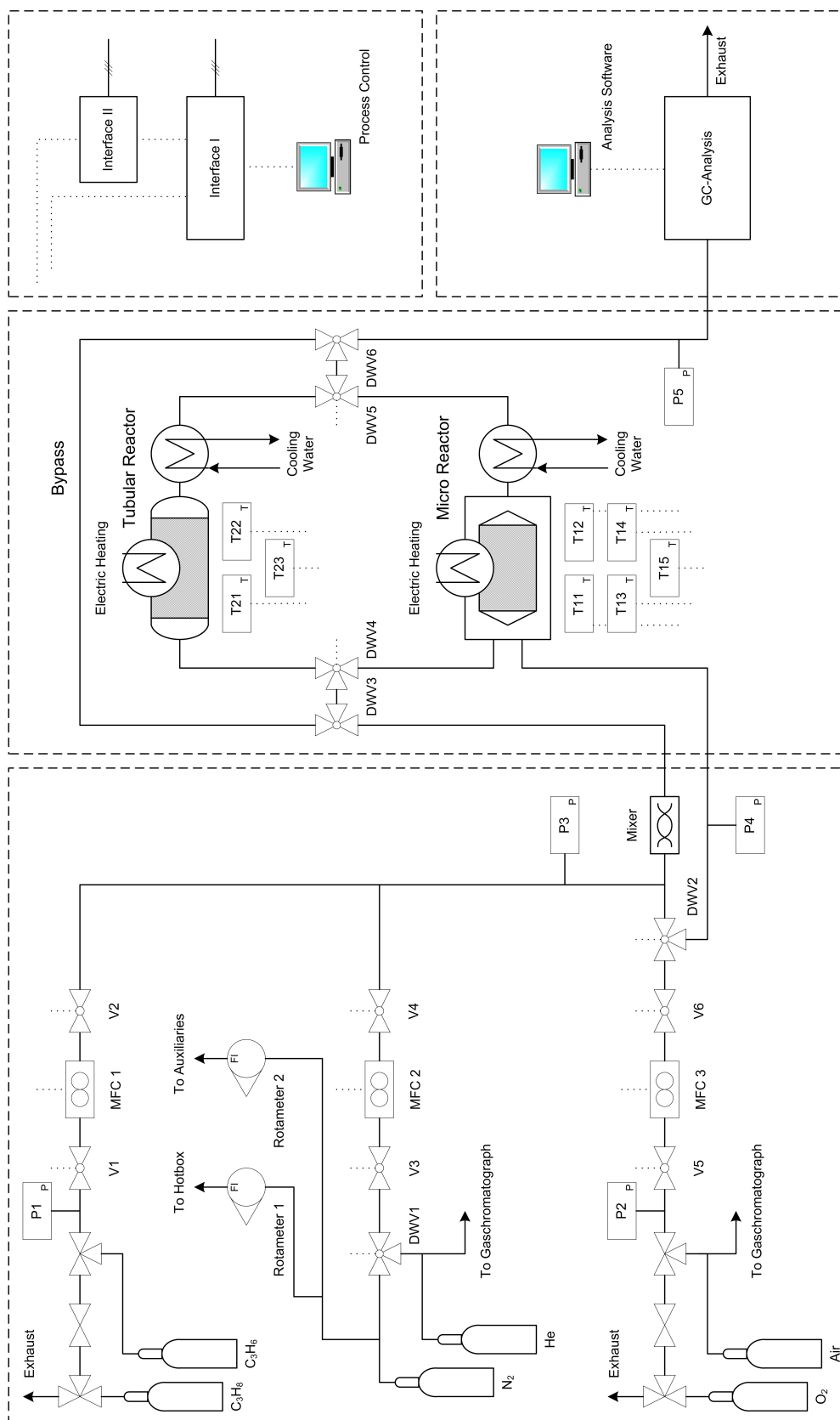
-
- [64] Forschungszentrum Karlsruhe, Presseerklärung 13/2005.
- [65] G. Markowz, S. Schirrmeister, J. Albrecht, F. Becker, R. Schütte, K.J. Caspary, E. Klemm, Chem. Ing. Tech. 76 (2004) 620-625.
- [66] P. Eisele, R. Killpack, in *Ullmann's Encyclopedia of Industrial Chemistry*, Electronic Release, Wiley-VCH, Weinheim, 2002.
- [67] U. Onken, A. Behr, Chemische Prozeßkunde - Lehrbuch der Technischen Chemie - Band 3, (M. Baerns, J. Falbe, F. Fetting, H. Hofmann, W. Keim, U. Onken), Georg Thieme Verlag, Stuttgart, 1996.
- [68] E.A. Mamedov, V.C. Corberán, Appl. Catal. A: Gen. 127 (1995) 1-40.
- [69] I.E. Wachs, B.M. Weckhuysen, Appl. Catal. A: Gen. 157 (1997) 67-90.
- [70] T. Blasco, J.M. López Nieto, Appl. Catal. A: Gen. 157 (1997) 117-142.
- [71] M. Baerns, O. Buyevskaya, Catal. Today 45 (1998) 13-22.
- [72] B.M. Weckhuysen, D.E. Keller, Catal. Today 78 (2003) 25-46.
- [73] M. Baerns, G. Grubert, E.V. Kondratenko, D. Linke, U. Rodemerk, Oil Gas-Eur. Mag. 29 (2003) 36.
- [74] J.F. Brazdil, Top. Catal. 38 (2006) 289-294.
- [75] F. Cavani, N. Ballarini, A. Cericola, Catal. Today 127 (2007) 113-131.
- [76] O.V. Buyevskaya, M. Baerns, Catal. Today 42 (1998) 315-323.
- [77] K. Chen, A.T. Bell, E. Iglesia, J. Catal. 209 (2002) 35-42.
- [78] Z. Zhao, X. Gao, I.E. Wachs, J. Phys. Chem. B 107 (2003) 6333-6342.
- [79] J.B. Stelzer, H. Kosslick, J. Caro, D. Habel, E. Feike, H. Schubert, Chem. Ing. Tech. 75 (2003) 872-877.
- [80] J.B. Stelzer, D. Habel, M.-M. Pohl, H. Kosslick, E. Feike, J. Caro, H. Schubert, Chem. Ing. Tech. 75 (2003) 1656-1660.
- [81] J.B. Stelzer, A. Feldhoff, J. Caro, M. Fait, D. Habel, E. Feike, H. Schubert, Chem. Ing. Tech. 76 (2004) 1086-1092.
- [82] J. Le Bars, A. Auroux, M. Forissier, J.C. Vedrine, J. Catal. 162 (1996) 250-259.
- [83] A. Khodakov, B. Olthof, A.T. Bell, E. Iglesia, J. Catal. 181 (1999) 205-216.
- [84] J.M. López Nieto, J. Soler, P. Concepción, J. Herguido, M. Menéndez, J. Santamaría, J. Catal. 185 (1999) 324-332.
- [85] J.L. Male, H.G. Niessen, A.T. Bell, T. Don Tilley, J. Catal. 194 (2000) 431-444.
- [86] E.V. Kondratenko, O.V. Buyevskaya, M. Baerns, Top. Catal. 15 (2001) 175-180.
- [87] C. Pak, A.T. Bell, T.D. Tilley, J. Catal. 206 (2002) 49-59.
- [88] M.D. Argyle, K. Chen, A.T. Bell, E. Iglesia, J. Catal. 208 (2002) 139-149.
- [89] N. Steinfeldt, D. Müller, H. Berndt, Appl. Catal. A: Gen. 272 (2004) 201-213.
- [90] O.R. Evans, A.T. Bell, T.D. Tilley, J. Catal. 226 (2004) 292-300.
-

-
- [91] E.V. Kondratenko, M. Baerns, *Appl. Catal. A: Gen.* 222 (2001) 133-143.
- [92] K. Routray, K.R.S.K. Reddy, G. Deo, *Appl. Catal. A: Gen.* 265 (2004) 103-113.
- [93] E.V. Kondratenko, M. Cherian, M. Baerns, D. Su, R. Schlögl, X. Wang, I.E. Wachs, *J. Catal.* 234 (2005) 131-142.
- [94] D. Creaser, B. Andersson, *Appl. Catal. A: Gen.* 141 (1996) 131-152.
- [95] K. Chen, A.T. Bell, E. Iglesia, *J. Phys. Chem. B* 104 (2000) 1292-1299.
- [96] A. Bottino, G. Capannelli, A. Comite, S. Storace, R. Di Felice, *Chem. Eng. J.* 94 (2003) 11-18.
- [97] P. Mars, D.W. van Krevelen, *Chem. Eng. Sci. Special Supplement* 3 (1954) 41-59.
- [98] M.A. Vannice, *Catal. Today* 123 (2007) 18-22.
- [99] D. Creaser, B. Andersson, R.R. Hudgins, P.L. Silveston, *Appl. Catal. A: Gen.* 187 (1999) 147-160.
- [100] K. Chen, A. Khodakov, J. Yang, A.T. Bell, E. Iglesia, *J. Catal.* 186 (1999) 325-333.
- [101] K. Chen, E. Iglesia, A.T. Bell, *J. Catal.* 192 (2000) 197-203.
- [102] E.V. Kondratenko, N. Steinfeldt, M. Baerns, *Phys. Chem. Chem. Phys.* 8 (2006) 1624-1633.
- [103] O. Ovsitser, M. Cherian, E.V. Kondratenko, *J. Phys. Chem. C* 111 (2007) 8594-8602.
- [104] N. Steinfeldt, O.V. Buyevskaya, D. Wolf, M. Baerns, *Stud. Surf. Sci. Catal.* 136 (2001) 185-190.
- [105] N. Steinfeldt, N. Dropka, D. Wolf, M. Baerns, *Chem. Eng. Res. Des.* 81 (2003) 735-743.
- [106] C. Hamel, S. Thomas, K. Schädlich, A. Seidel-Morgenstern, *Chem. Eng. Sci.* 58 (2003) 4483-4492.
- [107] F. Klose, T. Wolff, S. Thomas, A. Seidel-Morgenstern, *Catal. Today* 82 (2003) 25-40.
- [108] F. Klose, T. Wolff, S. Thomas, A. Seidel-Morgenstern, *Appl. Catal. A: Gen.* 257 (2004) 193-199.
- [109] N. Steinfeldt, U. Dingerdissen, M. Baerns, *Chem. Eng. Technol.* 28 (2005) 421-425.
- [110] D. Ahchieva, M. Peglow, S. Heinrich, L. Mörl, T. Wolff, F. Klose, *Appl. Catal. A: Gen.* 296 (2005) 176-185.
- [111] Velocys Inc., WO 03/106386 A2.
- [112] B. Frank, A. Dinse, O. Ovsitser, E.V. Kondratenko, R. Schomäcker, *Appl. Catal. A: Gen.* 323 (2007) 66-76.
- [113] S. Brunauer, P.H. Emmett, E. Teller, *J. Am. Chem. Soc.* 60 (1938) 309-319.
- [114] M.M. Koranne, J.G. Goodwin, G. Marcelin, *J. Catal.* 148 (1994) 369-377.
- [115] A. Khodakov, J. Yang, S. Su, E. Iglesia, A.T. Bell, *J. Catal.* 177 (1998) 343-351.
- [116] E.P. Reddy, R.S. Varma, *J. Catal.* 221 (2004) 93-101.
-

-
- [117] G. Centi, Appl. Catal. A: Gen. 147 (1996) 267-298.
- [118] Z. Wu, H.-S. Kim, P.C. Stair, S. Rugmini, S.D. Jackson, J. Phys. Chem. B 109 (2005) 2793-2800.
- [119] S. Xie, E. Iglesia, A.T. Bell, Langmuir 16 (2000) 7162-7167.
- [120] M.A. Vuurman, I.E. Wachs, J. Phys. Chem. 96 (1992) 5008-5016.
- [121] X. Gao, M.A. Bañares, I.E. Wachs, J. Catal. 188 (1999) 325-331.
- [122] J. Tauc, Amorphous and Liquid Semiconductors, (J. Tauc), Plenum Press, London, 1974.
- [123] F. Klose, T. Wolff, H. Lorenz, A. Seidel-Morgenstern, Y. Suchorski, M. Piórkowska, H. Weiss, J. Catal. 247 (2007) 176-193.
- [124] M.V. Martínez-Huerta, X. Gao, H. Tian, I.E. Wachs, J.L.G. Fierro, M.A. Bañares, Catal. Today 118 (2006) 279-287.
- [125] H. Bosch, B.J. Kip, J.G. van Ommen, P.J. Gellings, J. Chem. Soc., Faraday Trans. 1 80 (1984) 2479-2488.
- [126] T. Kim, I.E. Wachs, J. Catal. 255 (2008) 197-205.
- [127] H. Tian, E.I. Ross, I.E. Wachs, J. Phys. Chem. B 110 (2006) 9593-9600.
- [128] V.R. Choudhary, V.H. Rane, A.M. Rajput, AIChE J. 44 (1998) 2293-2301.
- [129] S. Schimpf, M. Lucas, C. Mohr, U. Rodemerck, A. Bruckner, J. Radnik, H. Hofmeister, P. Claus, Catal. Today 72 (2002) 63-78.
- [130] G. Martra, F. Arena, S. Coluccia, F. Frusteri, A. Parmaliana, Catal. Today 63 (2000) 197-207.
- [131] A. Dinse, B. Frank, C. Hess, D. Habel, R. Schomäcker, J. Mol. Catal. A: Chemical 289 (2008) 28-37.
- [132] T.A. Nijhuis, A.E.W. Beers, T. Vergunst, I. Hoeck, F. Kapteijn, J.A. Moulijn, Catal. Rev. Sci. Eng. 43 (2001) 345-380.
- [133] G. Groppi, G. Aioldi, C. Cristiani, E. Tronconi, Catal. Today 60 (2000) 57-62.
- [134] H. Pennemann, V. Hessel, G. Kolb, H. Löwe, R. Zapf, Chem. Eng. J. 135 (2008) S66-S73.
- [135] J.-M. Commenge, L. Falk, J.-P. Corriou, M. Matlosz, in *Microreaction Technology: Proceedings of the Fifth International Conference on Microreaction Technology, IM-RET 5*, (M. Matlosz, W. Ehrfeld, J.P. Baselt), pp. 131-140, Springer-Verlag, Berlin, 2002.
- [136] F. Trachsel, A. Günther, S. Khan, K.F. Jensen, Chem. Eng. Sci. 60 (2005) 5729-5737.
- [137] M. Hoffmann, M. Schlüter, N. Rübiger, Chem. Ing. Tech. 79 (2007) 1067-1075.
- [138] S. Lohse, M. Arnold, J. Franzke, D.W. Agar, Chem. Ing. Tech. 79 (2007) 1296.
-

-
- [139] T. Stief, U. Schygulla, H. Geider, O.-U. Langer, E. Anurjew, J. Brandner, Chem. Eng. J. 135 (2008) 191-198.
- [140] Handbook of Chemistry and Physics, (R.C. Weast, G.L. Tuve), 48th edition, The Chemical Rubber Co., Cleveland (Ohio), 1967.
- [141] D.E. Mears, Ind. Eng. Chem. Proc. Des. Dev. 10 (1971) 541-547.
- [142] P.B. Weisz, Z. Phys. Chem. 11 (1957) 1.
- [143] D. Wolf, N. Dropka, Q. Smejkal, O. Buyevskaya, Chem. Eng. Sci. 56 (2001) 713-719.
- [144] V.C. Corberán, Catal. Today 99 (2005) 33-41.
- [145] M. van Sint Annaland, H.A.R. Scholts, J.A.M. Kuipers, W.P.M. van Swaaij, Chem. Eng. Sci. 57 (2002) 833-854.
- [146] M. van Sint Annaland, H.A.R. Scholts, J.A.M. Kuipers, W.P.M. van Swaaij, Chem. Eng. Sci. 57 (2002) 855-872.
- [147] M. van Sint Annaland, R.C. Nijssen, Chem. Eng. Sci. 57 (2002) 4967-4985.
- [148] T. Stange, S. Kieselwaller, K. Russow, V. Hessel, M. Provence, C. Balsalobre, P. Boulon, E. Mounier, PAMIR - Potential and Applications of MicroReaction technology - A Market Survey, Institut für Mikrotechnik Mainz, Mainz, 2002.
- [149] D. Schmalz, M. Häberl, N. Oldenburg, M. Grund, H. Muntermann, U. Kunz, Chem. Ing. Tech. 77 (2005) 859-866.
- [150] U. Krtischil, V. Hessel, D. Kralisch, G. Kreisel, M. Küpper, R. Schenk, Chimia 60 (2006) 611-617.
- [151] D. Kralisch, G. Kreisel, Chem. Ing. Tech. 77 (2005) 784-791.
- [152] T.R. Dietrich, M.A. Liauw, Chem. Ing. Tech. 76 (2004) 517-519.
- [153] R. Gorges, W. Klemm, G. Kreisel, B. Ondruschka, P. Scholz, T. Taubert, Chem. Ing. Tech. 76 (2004) 519-522.
- [154] M. Günther, J.M. Köhler, Chem. Ing. Tech. 76 (2004) 522-526.
- [155] A. Bazzanella, Chem. Ing. Tech. 76 (2004) 511-513.
- [156] U. Ackermann, Chem. Ing. Tech. 76 (2004) 508-511.

Appendix A: Flow chart



Appendix B: List of Publications

Articles in Reviewed Journals

O. SCHWARZ, G. SCHÄFER, R. SCHOMÄCKER

Microstructured reactors on their way to academic teaching at the TU Berlin

Chemical Engineering and Technology, manuscript in preparation

D. HABEL, O. GÖRKE, M. TOVAR, M. WILLINGER, M. ZIEMANN, O. SCHWARZ, R. SCHOMÄCKER, H. SCHUBERT

Micro straining in titania-, alumina- and silica-supported V_2O_5 -catalysts

Journal of the European Ceramic Society, accepted manuscript

O. SCHWARZ, P.-Q. DUONG, G. SCHÄFER, R. SCHOMÄCKER

Development of a microstructured reactor for heterogeneously gas phase reactions -

Part II: Reactor characterization and kinetic investigations

Chemical Engineering Journal 145 (2009) 429-435

O. SCHWARZ, P.-Q. DUONG, G. SCHÄFER, R. SCHOMÄCKER

Development of a microstructured reactor for heterogeneously gas phase reactions -

Part I: Reactor fabrication and catalytic coatings

Chemical Engineering Journal 145 (2009) 420-428

O. SCHWARZ, D. HABEL, O. OVSITSER, E.V. KONDRATENKO, C. HESS, R. SCHOMÄCKER, H. SCHUBERT

Impact of preparation method on physico-chemical and catalytic properties of $VO_x/\gamma-Al_2O_3$ materials

Journal of Molecular Catalysis A: Chemical 293 (2008) 45-52

O. SCHWARZ, B. FRANK, C. HESS, R. SCHOMÄCKER

Characterisation and catalytic testing of VO_x/Al_2O_3 catalysts for microstructured reactors

Catalysis Communications 9 (2008) 229-233

Conference Contributions

O. SCHWARZ, A. DINSE, B. FRANK, E.V. KONDRATENKO, R. SCHLÖGL, R. SCHOMÄCKER
Die oxidative Dehydrierung von Propan - Maßnahmen zur Steigerung der Selektivität
Oral Presentation, ProcessNet Jahrestagung, Karlsruhe, 07.-09.10.2008
Abstract published in *Chemie Ingenieur Technik* 80 (2008) 1246

O. SCHWARZ, P.-Q. DUONG, G. SCHÄFER, R. SCHOMÄCKER
Entwicklung und Optimierung eines mikrostrukturierten Reaktors für die partielle Oxidation von Propan
Poster Presentation, Jahrestreffen Reaktionstechnik, Würzburg, 18.-20.05.2008

O. SCHWARZ, P.-Q. DUONG, G. SCHÄFER, R. SCHOMÄCKER
Development and Optimization of a Microstructured Reactor for the Partial Oxidization of Propane
Oral Presentation, IMRET 10 at AIChE Spring National Meeting, New Orleans, 06.-10.04.2008
Abstract published on CD-ROM, ISBN: 978-0-8169-1023-6

O. SCHWARZ, P.-Q. DUONG, G. SCHÄFER, R. SCHOMÄCKER
Mikrostrukturierte Reaktoren für den Einsatz in der heterogenen Katalyse am Beispiel der ODP
S. KHENNACHE, O. SCHWARZ, C. HESS, E.V. KONDRATENKO, D. HABEL, H. SCHUBERT, R. SCHOMÄCKER
Preparation, characterization, and selectivity studies of $\text{VO}_x/\text{Al}_2\text{O}_3$ catalyst for the ODP
Poster Presentations, 41. Jahrestreffen Deutscher Katalytiker, Weimar, 27.-29.02.2008

O. SCHWARZ, A. DINSE, G. SCHÄFER, R. SCHOMÄCKER
Die partielle Oxidation von Propan an einem $\text{VO}_x/\text{Al}_2\text{O}_3$ Katalysator im Mikroreaktor
Poster Presentation, ProcessNet Jahrestagung, Aachen, 16.-18.10.2007
Abstract published in *Chemie Ingenieur Technik* 79 (2007) 1480

O. SCHWARZ, B. FRANK, A. DINSE, H. HÜBNER, G. SCHÄFER, R. SCHOMÄCKER
Entwicklung eines mikrostrukturierten Reaktors für die kinetische Untersuchung der oxidativen Dehydrierung von Propan an einem $\text{V}_2\text{O}_5/\text{Al}_2\text{O}_3$ -Katalysator
Poster Presentation, 40. Jahrestreffen Deutscher Katalytiker, Weimar, 14.-16.03.2007

Appendix C: Curriculum Vitae



Personal Information

Name	Oliver Schwarz
Date/ Place of Birth	14.06.1979, Pinneberg
Email	oliver.schwarz@alumni.tu-berlin.de

Academic Education

10/2005 – 09/2008	<p>PhD thesis at Institute of Chemistry, TU Berlin (in cooperation with Atotech Deutschland GmbH, Berlin)</p> <p><i>“Development of a Microstructured Reactor for Heterogeneously Catalyzed Gas Phase Reactions and its Application in the Oxidative Dehydrogenation of Propane”</i></p> <p>NaFöG-Scholarship granted by State of Berlin</p>
02/2005 – 06/2005	<p>Diploma thesis at Schering AG, Berlin</p> <p><i>“Modellierung und Simulation des Produktionsprozesses einer mehrstufigen Wirkstoffsynthese in der Entwicklungsphase mit Hilfe ausgewählter Softwaresysteme”</i></p>
03/2003 – 11/2003	<p>Study abroad program at University of Queensland, Australia</p> <p>Scholarship granted by TU Berlin and University of Queensland</p>
04/2000 – 06/2005	<p>Study of Chemical Engineering and Management at TU Berlin</p> <p>Special focus on Technical Chemistry, Chemical Reaction Engineering, Corporate Finance, Portfolio Management</p>

Military Service

07/1999 – 04/2000	Basic military service at Luftwaffe der Bundeswehr, Husum
-------------------	---

Secondary School

08/1990 – 06/1999	Abitur at Wolfgang-Borchert-Gymnasium, Halstenbek
-------------------	---
